universität
wien

MASTERARBEIT

Titel der Masterarbeit

„Development of a Heterologous Model System for Agrin-Lrp4-MuSK Signaling
and
Analysis of Muscle-Specific Kinase Endocytosis"

verfasst von

Andreas Höbartner, BSc

angestrebter akademischer Grad

Master of Science (MSc)

Wien, 2015

Table of Contents

1   Introduction

1.1 The Neuromuscular Junction

The neuromuscular junction (NMJ) emerges at the contact site between a motor neuron and a muscle fiber (Fig. 1a). This chemical synapse is important in transducing brain-derived signals to the muscle and thus allowing precise body movements. As a chemical synapse it is composed of several specific proteins and shows a unique three-dimensional structure. Distinct fundamental events from synaptogenesis to synapse maturation and maintenance have to take place in order to generate a functional NMJ.

Compared to synapses in the central nervous system, the NMJ is large in its size, has a relative simplicity and is easily accessible (Fig. 1b) (Sanes and Lichtmann, 2001; Sanes and Lichtmann, 1999). These aspects allow the NMJ to be easily investigated and so it has been depicted as a marvelous model system to study the fundamental nature of synapses.
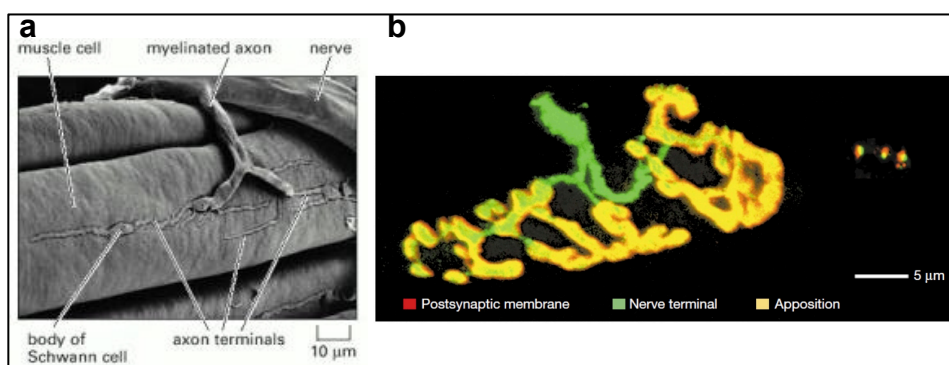
Figure 1 The Neuromuscular Junction
a. A scanning electron micrograph of a NMJ in a frog, showing the contact between a myelinated alpha motor neuron and a skeletal muscle fiber (Molecular Biology of the Cell, 2008). **b.** The NMJ of an adult mouse (left) and three synapses on cultured mouse hippocampal neurons (right) are shown (Sanes and Lichtman, 2001).

1.1.1   The Neuromuscular Junction as a Chemical Synapse

The fundamental function executed by the NMJ is the transmission of an electric signal from an alpha motor neuron to a contractile event in a muscle fiber. The cell

bodies of alpha motor neurons are located in the ventral horn of the spinal cord and in the brainstem (cranial nerves). These neurons are activated by the motor cortex and brainstem centers and are regulated or modulated directly or indirectly by the cerebellum, the basal ganglia and by descending systems from higher brain regions. An alpha motor neuron axon exits the spinal cord through the ventral root and directly innervates a subset of muscle fibers in a single skeletal muscle. This is called a motor unit (Fig. 2a) (Hartline and Maynard, 1975; Marder and Calabrese, 1996; Selverston et al., 1976).

Upon stimulation of an alpha motor neuron an action potential is generated and travels along the axon to the nerve terminal. At the NMJ, the local depolarization induces the opening of voltage-gated Ca^{2+} channels on the presynaptic membrane (Fig. 2b). The following Ca^{2+} influx induces the fusion of synaptic vesicles with the membrane at the active zones and in turn the release of the neurotransmitter acetylcholine (ACh) into the synaptic cleft. ACh reversibly binds to ionotrop acetylcholine receptors (AChRs), which are located at the postsynaptic membrane of the muscle fiber. Neurotransmitter bound AChRs become permeable to Na^+ influx and K^+ efflux, which in turn depolarize the postsynaptic membrane and lead to the opening of voltage-gated Na^+ channels. This initiates an action potential at the muscle membrane and T-tubules and thus allows Ca^{2+} release from the sarcoplasmatic reticulum into the cytosol. Ca^{2+} binds to troponin-C of the troponin complex, which is closely located to the myofibril. Resulting conformational changes in the troponin complex disable the binding of tropomyosin to actin and allow muscle contractions by the movement of myosin motor proteins along actin (Fig. 2c). Nerve-derived acetylcholinesterase, located in the basal lamina, hydrolyses released ACh into choline and acetic acid to rapidly stop transmission and muscle contraction. Choline is then transported back into the nerve terminal by a choline transporter and is re-used or degraded (Ferraro et al., 2012).
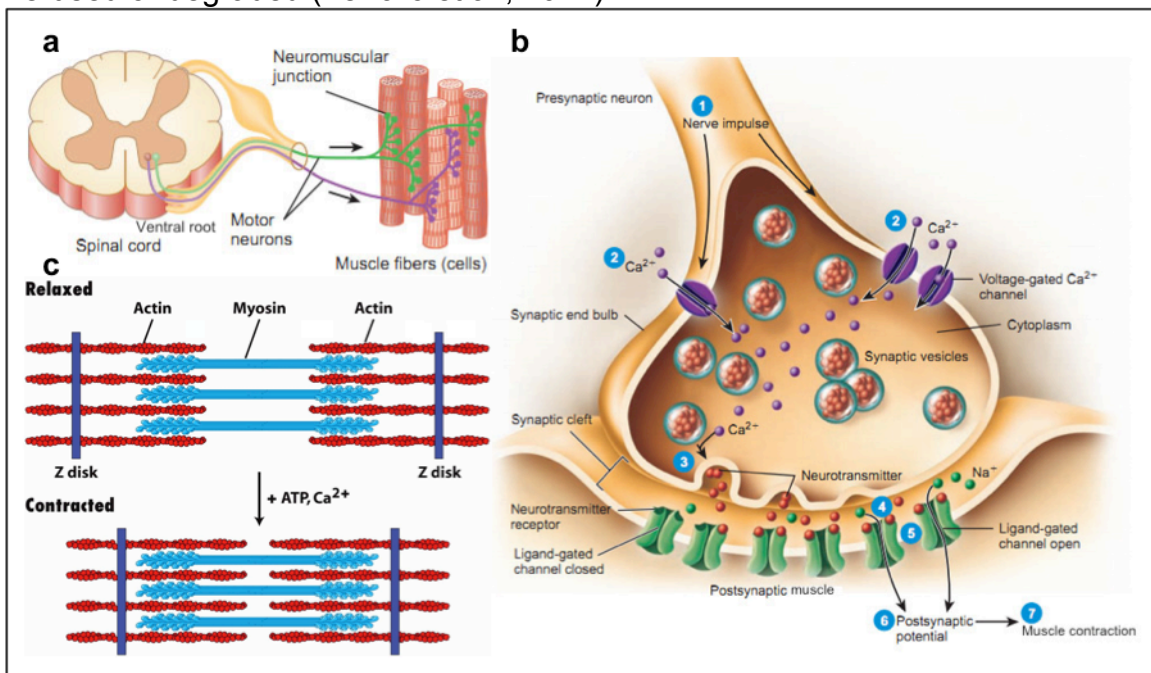
Figure 2 From Action Potential to Contraction
a. Axons of alpha motor neurons exit the spinal cord through the ventral horn and innervate muscle fibers

(antranik.org, 2014). **b.** A diagram of a chemical synapse shows the transmission of a nerve impulse into muscle contraction. Upon action potential arrival at the nerve terminal (1), voltage-gated Ca^{2+} channels open (2). The following Ca^{2+} influx induces the fusion of synaptic vesicles with the plasma membrane at the synaptic cleft and the release of the neurotransmitter ACh (3). ACh reversibly binds to AChRs at the muscle membrane (4), which become permeable to Na^+ influx and K^+ efflux (5). This depolarizes the postsynaptic membrane (6), which further leads to muscle contraction (7). ACh removal from the synaptic cleft is not shown (antranik.org, 2014). **c.** Muscle contraction is dependent on Ca^{2+} influx from the sarcoplasmatic reticulum and binding to the troponin complex. Thus myosin heads can dock on exposed actin filaments and head movement by the use of ATP results in muscle contraction (Molecular Cell Biology, 2008).

1.1.2 The Formation, Maturation and Maintenance of Neuromuscular Junctions

The formation of a NMJ is a highly complex process and requires several steps during embryonic and postnatal development. Differentiation of neural progenitor cells into postmitotic alpha motor neurons starts at mouse embryonic day (E) 9.5 in the neural tube and is followed by dendrite and axon growth and guidance to their specific targets (Alaynick et al., 2011). On the other hand, muscle formation starts by differentiation and fusion of muscle precursor cells (also called myoblasts) into multinucleated myotubes and myofibers around E12 to E14 (Witzemann, 2006; Ontell and Kozeka, 1984). Axon invasion of the muscle and arborization start after E12.5 (Koo and Pfaff, 2002). Still prior to this initial nerve-muscle contact, AChRs become concentrated in the central regions of myofibers (Fig. 3a,b) (Kummer et al., 2006). This aneural process is called "muscle pre-patterning" and is not understood so far (Witzemann, 2006; Ferraro et al., 2012; Bevan and Steinbach, 1977; Braithwaite and Harris, 1979; Ziskind-Conhaim and Bennett, 1982; Yang et al., 2001; Lin et al., 2001; Yang et al., 2000). When nerve innervation occurs, some axon terminals overlap with pre-patterned AChR clusters, resulting in enlargement and stabilization of innervated and disappearance of non-innervated AChR clusters by E18.5 (Yang et al., 2001; Lin et al., 2001; Young and Poo, 1983; Fambrough, 1979). Other studies favor a neurogenic model for NMJ formation, predicting AChR clustering induced by motorneurons only (Anderson and Cohen, 1977; Frank and Fischbach, 1979; Burden, 2011; Wu et al., 2010).
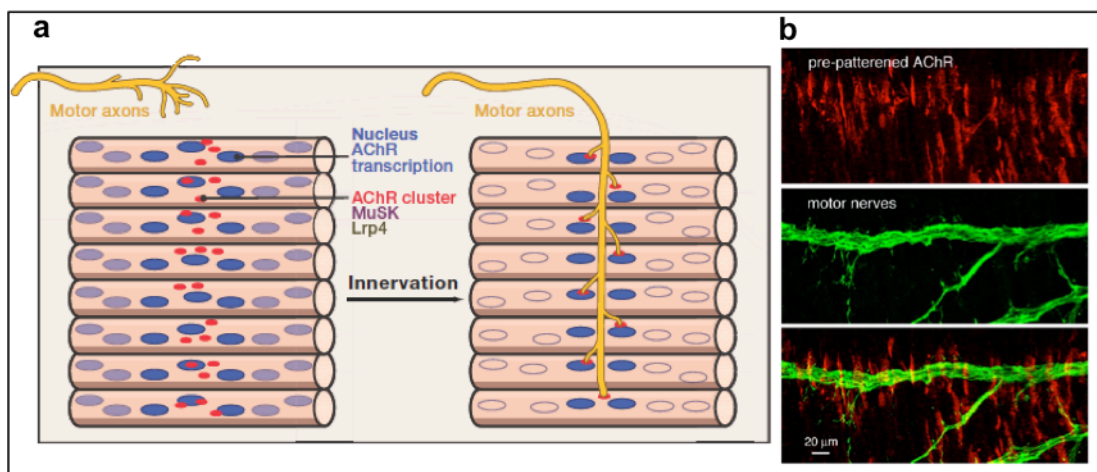
Figure 3 Acetylcholine Receptor Pre-Patterning and Nerve Innervation
a. AChRs (red) are pre-patterned at the central regions of the myofiber, where synaptic nuclei (blue) are specialized. Upon motor neuron innervation, some axon terminals overlap with pre-patterned AChR clusters, while non-innervated AChR clusters disappear (Burden, 2011). **b.** Pre-patterned AChRs are shown by rhodamine-

labeled alpha-bungarotoxin staining (red) in the mouse diaphragm at E14, as well as the phrenic nerve is visualized by anti-neurofilament antibodies (green). The overlay shows branches of the nerve contacting pre-patterned AChR clusters (Witzemann, 2006).

As soon as first primitive synapses are established, ACh is released into the synaptic cleft and binds to AChRs on the muscle membrane. This triggers muscle depolarization, inhibition of AChR transcription in extrasynaptic nuclei and induction of AChR transcription in synaptic nuclei (Fig. 4a) (Ferraro et al., 2012). At the same time, the motor nerve terminal secretes the large heparan sulphate proteoglycan agrin into the synaptic basal lamina (McMahan, 1990; Ruegg and Bixby, 1998). Agrin acting via the muscle-specific kinase (MuSK) signaling pathway, triggers and strengthens embryonic NMJ formation as well as additional maturation events in postnatal life (Ferraro et al., 2012; Sanes and Lichtmann, 2001). AChR plaques from mouse postnatal day (P) 0 are perforated to mature pretzel-like shapes (Fig. 4a), together with the formation of invaginations (Fig. 4b) (Marques et al., 2000; Steinbach, 1981). These so called junctional folds show a strictly organized protein expression pattern in the mature state with highly enriched AChR numbers ($<10000/\mu m^2$) at the crests and voltage-gated Na^+ channels concentrated in the depths (Fig. 4c) (Fambrough, 1979; Flucher and Daniels, 1989; Caldwell, 2000). Elimination of poly-innervated pretzels and alignment of the axon terminal with the AChR clusters are further steps during postnatal maturation (Fig. 4d) (Slater, 1982; Balice-Gordon and Lichtmann, 1993). Additionally, a subunit exchange from embryonic $\alpha 2\beta\gamma\delta$ AChRs into adult $\alpha 2\beta\epsilon\delta$ AChRs occurs during postnatal NMJ maturation. This leads to an increased ACh-induced muscle activity, shorter channel opening times, higher Ca^{2+} permeability and an increased half-life of AChR from 1 to 8-14 days (Duclert and Changeux, 1995; Villarroel and Sakmann, 1996; Fambrough, 1979). These modifications contribute to NMJ maturation (Ferraro et al., 2012; Sanes and Lichtmann, 2001; Witzemann, 2006).

Adult NMJs own the possibility to be maintained for the lifetime of the organism. This can be accomplished by constant remodeling, expanding and shrinking, as well as by reacting to axonal changes (Balice-Gordon et al., 1990; Balice-Gordon and Lichtmann, 1993).
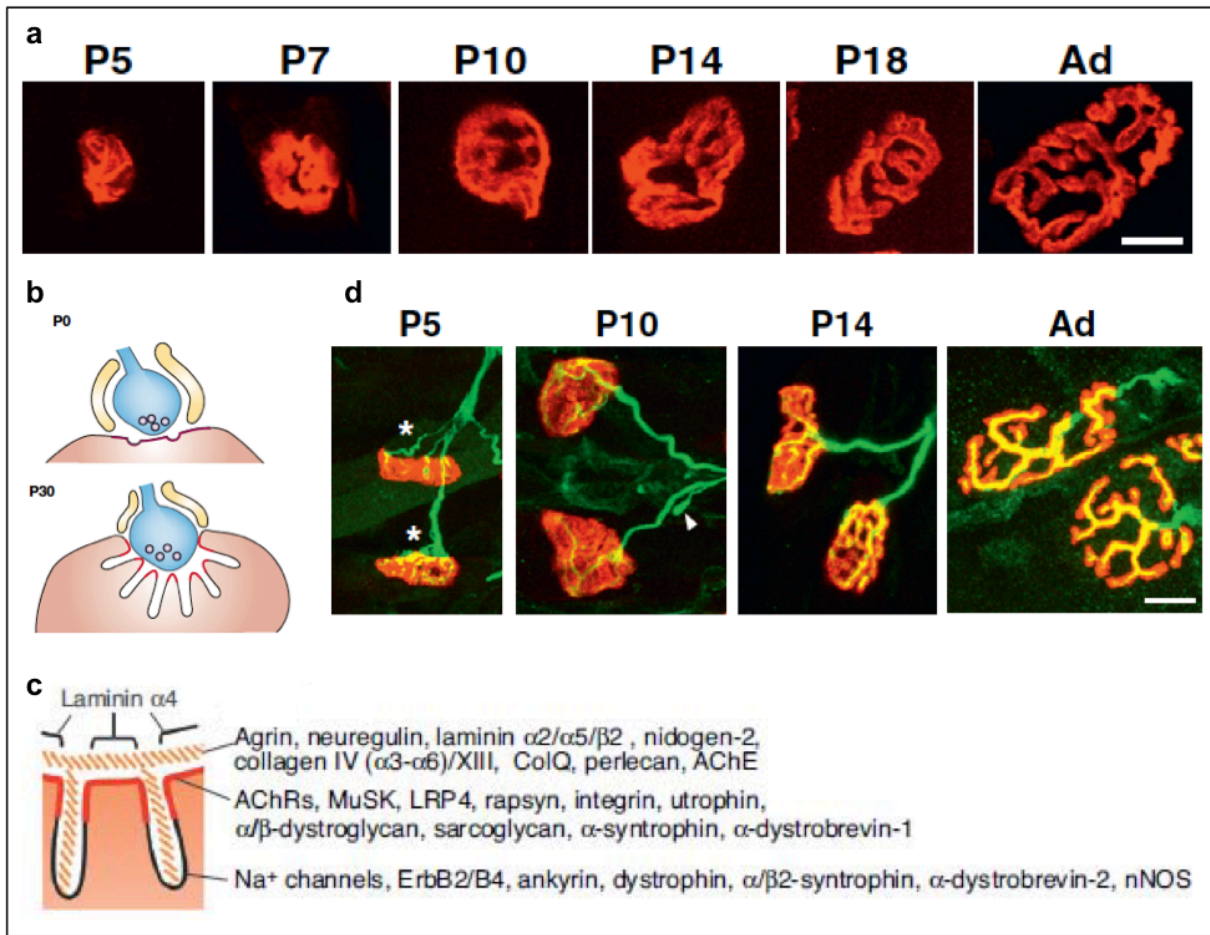
Figure 4 From Plaque to Mature NMJ
a. Oval-shaped plaques are changed into pretzel-like shaped AChR arrays (Shi et al., 2012). **b.** Junctional folds are invaginated into the postsynaptic muscle membrane after birth (Sanes and Lichtmann, 2001). **c.** Molecules expressed at the crests and depths of junctional folds, as well as in the synaptic basal lamina are shown (Shi et al., 2012). **d.** Poly-innervated pretzels are eliminated in the first postnatal days (Shi et al., 2012). P, postnatal day; Ad, adult; Scale bars, 10 µm.

1.1.3 Lrp4, MuSK and Dok-7 Control Molecular Mechanisms Underlying Agrin-Mediated Signaling at the Neuromuscular Junction

Agrin-mediated signaling at the postsynaptic site of the muscle membrane starts immediately after nerve innervation. Nerve-derived agrin is released at the motor axon terminal and binds to the extracellular domain of the low density lipoprotein receptor related protein 4 (Lrp4) located at the muscle membrane. This association leads to the binding of the agrin-Lrp4 complex to MuSK and increases MuSK kinase activity. Subsequently, several autophosphorylation events in the MuSK kinase domain strengthen MuSK dimerization and further phosphorylation. Phosphorylated Y553 in the juxtamembrane region of MuSK recruits docking protein-7 (Dok-7) and tyrosines of Dok-7 become phosphorylated. This leads to Dok-7 dimerization and further stimulation of MuSK kinase activity. Recruitment of CT10 regulator of kinase (Crk) and Crk-L to the MuSK signaling complex activates Rho GTPases, dishevelled (Dvl) and other kinases and proteins, which enhance the formation of AChR clusters via Rac/Rho-dependent and Rapsyn-dependent pathways. Transcriptional activation

5

of NMJ specific genes likely involves JNK-dependent signaling. Together, these fundamental events regulate the formation, maturation and maintenance of the NMJ (Fig. 5a,b) (Burden, 2011). Knockout mice lacking agrin, Lrp4, MuSK or Dok-7 are unable to form functional NMJs (Gautam et al., 1996; Okada et al., 2006; DeChiara et al., 1996; Weatherbee et al., 2006). Therefore these key proteins will be discussed in more detail in the next chapters.

In addition, different studies revealed alternative ways of forming and strengthening NMJs. Laminin-induced AChR clustering functions completely independent of the agrin-Lrp4-MuSK pathway (Sugiyama et al., 1997). On the other hand, it is known that MuSK has an extracellular cysteine-rich domain that can bind Wnts. This binding leads to agrin independent MuSK activation and contributes to pre- and postsynaptic development (Luo et al., 2002; Burden, 2000; Wu et al., 2010).
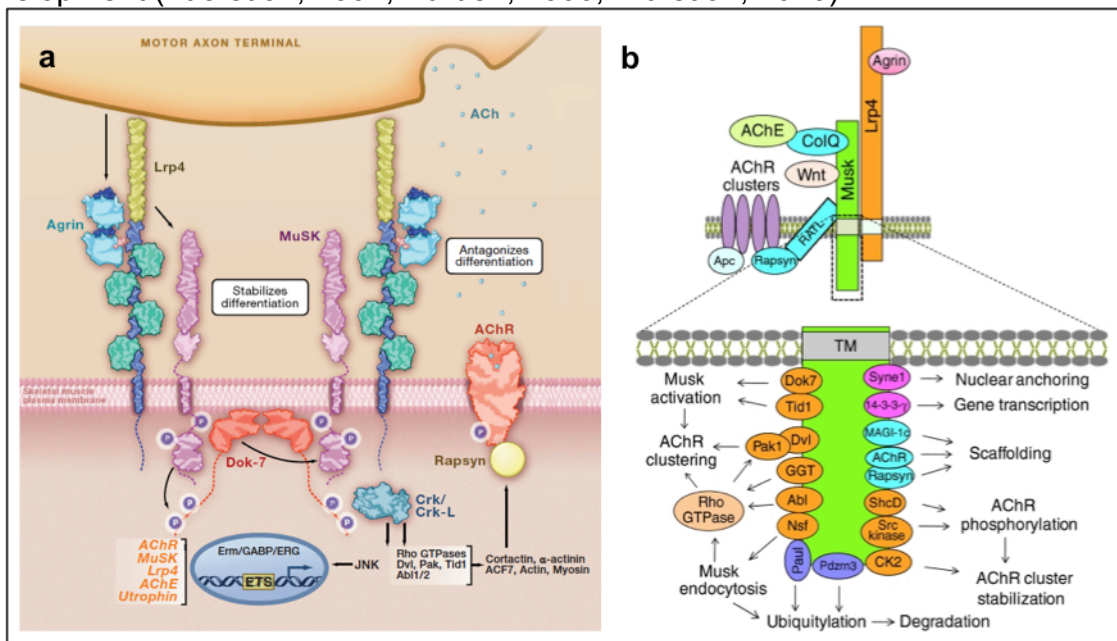
Figure 5 Agrin-Induced MuSK Signaling Pathway
a. This 'Snap Shot' shows the major molecular key players of NMJ development (Burden, 2011). **b.** This diagram illustrates different functions of agrin-Lrp4 activated MuSK. Proteins necessary for MuSK activity and downstream signaling are marked in orange. Proteins controlling agrin/MuSK signaling by ubiquitylation are highlighted in purple. Scaffolding proteins in blue and gene expression regulating proteins in pink are also important for NMJ formation and maintenance (Wu et al., 2010).

1.2 Agrin

Agrin is an extracellular matrix protein that activates MuSK signaling in the muscle after binding to Lrp4. It was originally purified from the basal lamina of the electric organ of the pacific electric ray *Torpedo californica* (Nitkin et al., 1987).

The agrin gene encodes a >2000 amino acid (AA) protein with a predicted molecular mass of 225 kilodalton (kDa) (Bezakova and Ruegg, 2003). Glycosylation of the aminoterminal half of the protein, important for docking of heparin sulphate glycosaminoglycan side chains, increases the molecular mass up to 600kDa (Tsen et al., 1995). Agrin is expressed in different cell types including nerve cells in the central and peripheral nervous system, skeletal muscle cells, Schwann cells and glia cells

(Wu et al., 2010; Bezakova and Ruegg, 2003). However, only the neural agrin isoform is capable of inducing AChR clusters at the NMJ (Fig. 6) (Burgess et al., 1999). mRNA splicing gives raise to two major isoforms (1) a secreted extracellular matrix attached form, which is found at the NMJ and (2) a transmembrane form that is exclusively expressed in the brain. Both can be further spliced at the carboxyterminal laminin-globular domains at two sites y and z. At the y site, splicing can produce isoforms with 0 or 4 additional AAs. On the other hand, splicing at the z position can generate isoforms containing 0, 8, 11 or 19 additional AAs (Gesemann et al., 1996; Kim et al., 2008b; Burgess et al., 1999). Neuronal agrin is characterized by a 4 AA insert at the y site and 8, 11 or 19 AA inserts at the z site and thus commonly termed z$^+$agrin (Ferns et al., 1993). z$^+$agrin is capable to stimulate AChR clustering 1000 fold stronger than non-nerve-derived agrin (Gesemann et al., 1995; Hoch et al., 1994; Bezakova et al., 2001). Agrin knockout mice fail to form functional NMJs and die after birth due to breathing failure (Gautam et al., 1996).
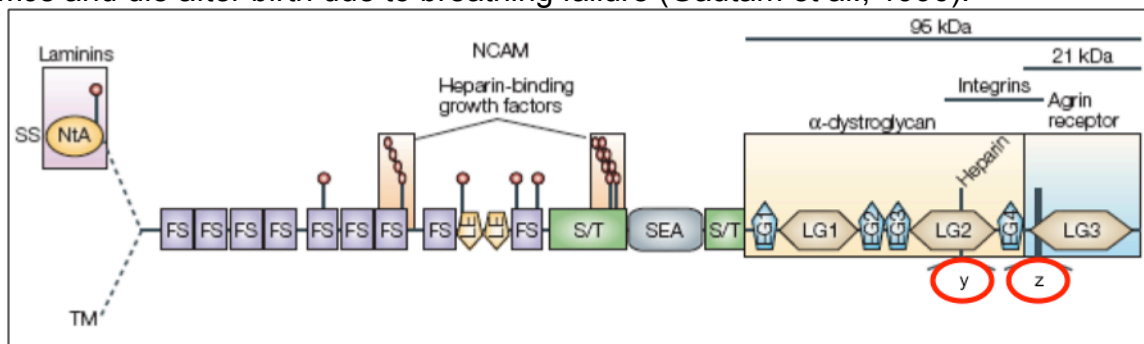
Figure 6 Structural Domains of Agrin
Important structural domains of agrin are shown. Neural agrin consists of the signal sequence (SS) and an aminoterminal agrin domain (NtA), while the alternatively spliced agrin isoform has a transmembrane segment (TM) at this position. The aminoterminal half of the protein is highly glycosylated. The carboxyterminal half starts at the first epidermal growth factor (EGF)-like domain (EG) and contains the alternative splicing sites y and z (red circles) (Bezakova and Ruegg, 2003). FS, follistatin-like domain; LE, laminin EGF-like domain; LG, laminin globular domain; SEA, sperm protein, enterokinase and agrin domain.

1.3 Lrp4

Lrp4 is a transmembrane protein expressed by muscle cells and acts as a receptor to secreted agrin. Ligand bound Lrp4 then binds to MuSK, which leads to the activation of the MuSK signaling pathway.
Lrp4 is a member of the low density lipoprotein receptor family, which plays a major role in diverse biological functions as surface receptors (Nykjaer and Willnow, 2002; Herz, 2001). Lrp4 has a large aminoterminal domain projecting into the extracellular synaptic cleft for ligand-binding (Fig. 7). The intracellular carboxyterminal domain is rather short and plays a minor role (Kim et al., 2008b; Zhang et al., 2001). In agrin-unbound state Lrp4 interacts with MuSK at low extent, likely being responsible for basal MuSK activity and in part for AChR pre-patterning (Kim et al., 2008b; Zhang et al., 2001). The extracellular domain of Lrp4 is also capable to bind to the presynaptic nerve terminal by interactions with a so far uncharacterized Lrp4 binding protein (Yumoto et al., 2012). This binding functions as a retrograde signal from the muscle

to the nerve for presynaptic differentiation. Lrp4 knockout mice not only fail to form functional NMJs, they also have malformed digits and face abnormalities in lung and kidney development (Weatherbee et al., 2006).
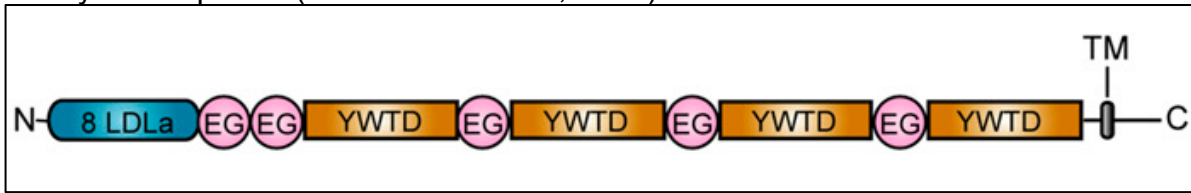
Figure 7 Structural Domains of Lrp4
Important structural domains of Lrp4 are shown. Lrp4 consists of 8 low density lipoprotein class A repeats (LDLa) at the aminoterminal end and 4 YWTD repeat-containing beta propellers (YWTD), which are separated by epidermal growth factor like domains (EG). A transmembrane domain (TM) anchors the protein in the muscle membrane, while the carboxyterminal domain is projecting into the cytoplasm (Zong et al., 2012).

1.4 MuSK

MuSK is a member of the receptor tyrosine kinase (RTK) family. It is expressed at high levels at the NMJ and phosphorylates downstream signaling molecules after activation by agrin-Lrp4 complex binding (Ghazanfari et al., 2010).

As it is common for all RTKs, MuSK has an extracellular ligand binding domain, an alpha helix spanning the plasma membrane and an intracellular tyrosine kinase domain (Lemmon and Schlessinger, 2010).

In the extracellular portion, MuSK has 3 immunoglobulin-like (Ig) domains and a cysteine rich domain (CRD) (Burden et al., 2013). Ig1 and Ig2 are important in agrin-bound Lrp4 binding (Fig. 8) (Zong and Jin, 2013). The CRD is related to Frizzled receptors, explaining why Wnts play a role in alternative MuSK activation (Valenzuela et al., 1995; Luo et al., 2002; Wu et al., 2010; Burden, 2000). After binding of Lrp4, tyrosine residue Y553 of a special NPXY motif in the intracellular juxtamembrane domain (JM) becomes autophosphorylated (Till et al., 2002; Herbst and Burden, 2000; Hubbard, 2004). This leads to recruitment of docking protein-7 (Dok-7), dimerization of the same and crosslinking of two MuSK molecules (Bergamin et al., 2010). This interaction leads to the release of the autoinhibition in the tyrosine kinase (TK) activation loop by phosphorylation of another 3 tyrosine residues Y750, Y754 and Y755 (Till et al., 2002). Further MuSK phosphorylation events implement its function in NMJ signaling cascades (Herbst and Burden, 2000; Dürnberger et al., 2014; Watty et al., 2000).

An important aspect of activated MuSK is its internalization. An E3 ubiquitin ligase can bind to the carboxyterminal end of rodent and human MuSK. In addition, caveolin-3 and N-ethylmalemide Sensitive Factor (NSF) are also able to bind (Lu et al., 2007; Zhu et al., 2008). These proteins are associated with MuSK endocytosis, suggesting a coupling of MuSK internalization and its activation. As RTKs can still be active in several endosomal compartments, this might play a critical role in NMJ formation and maintenance (Ghazanfari et al., 2010).
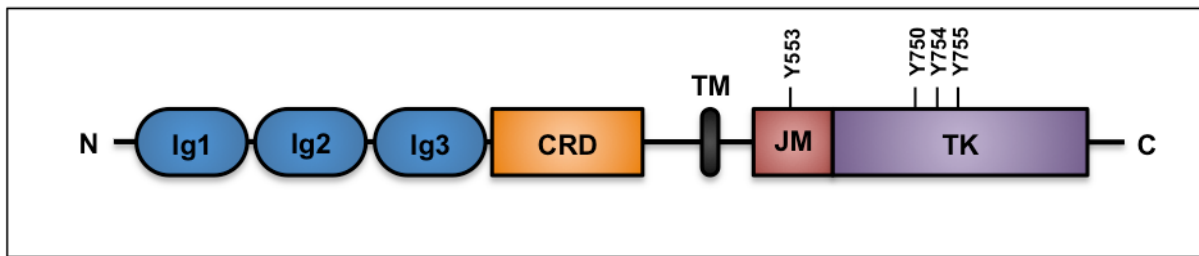
Figure 8 Structural Domains of MuSK
Important structural domains of MuSK are shown. MuSK has 3 extracellular immunoglobulin-like domains (Ig1-3) and an extracellular cysteine-rich domain (CRD) related to Frizzled receptors. A single alpha helical transmembrane domain anchors MuSK in the membrane of skeletal muscles. At the intracellular portion of MuSK, tyrosine 553 (Y553) at the juxtamembrane domain (JM) is phosphorylated upon Lrp4 binding, leading to Dok-7 recruitment and phosphorylation of Y750, Y754 and Y755 in the activation loop of the tyrosine kinase (TK).

1.5 Dok-7

Dok-7 is a cytosolic adaptor protein expressed by muscle cells. It is recruited to phosphorylated MuSK and enhances MuSK phosphorylation and downstream signaling.

Dok-7 is a member of adapter proteins with an aminoterminal pleckstrin homology (PH) domain and a phosphotyrosine binding (PTB) domain, as well as carboxyterminal located tyrosine phosphorylation sites (Fig. 9). Upon MuSK autophosphorylation of tyrosine 553 in the NPXY motif, the PTB domain of Dok-7 binds to phosphorylated tyrosine 553 (Okada et al., 2006; Inoue et al., 2009; Hamuro et al., 2008). This binding results in a dimeric structural unit of the Dok-7 PH domain, causing
dimerization, phosphorylation of carboxyterminal located tyrosines and thus activation of MuSK (Bergamin et al., 2010).
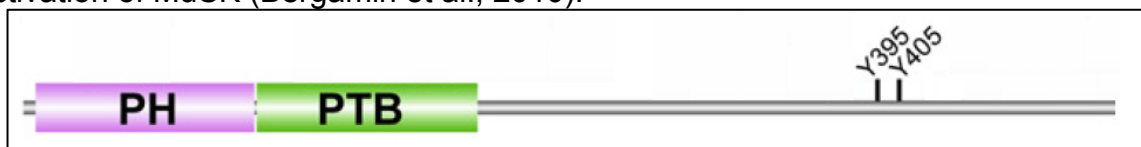
Figure 9 Structural Domains of Dok-7
Important structural domains of Dok-7 are shown. Dok-7 has an aminoterminal pleckstrin homology domain (PH) and a phosphotyrosine binding domain (PTB) next to it. Tyrosine phosphorylation sites are shown near the carboxyterminal end (Bergamin et al., 2010).

1.6 Acetylcholine Receptor

The AChR at the NMJ is a pentameric transmembrane protein and responds to the binding of the neurotransmitter ACh and of other extracellular ligands.

Two types of AChRs are known: muscarinic (mAChR) and nicotinic (nAChR). mAChRs are found in the central and peripheral nervous system and are coupled to G proteins (Hirota, 2001). Amongst others, these receptors play a role in psychotic disorders or REM sleep and several ligands are known (e.g. atropine, scopolamine) (Bridges et al., 2010; Nissen et al., 2006). nAChRs are found in the central and

peripheral nervous system and at the NMJ. These receptors play a role in many functions (nicotine addiction e.g.) and respond to ligands including nicotine or muscarine (Miyazawa et al., 2003).

nAChRs are ligand-gated ion channels and members of the cys-loop ligand gated ion channel superfamily, which respond to the binding of a ligand by channel opening and a subtype specific ion flow into the cell (Doyle, 2004). There are 17 homologous subunits divided into 5 subtypes α, β, γ, δ and ε (Millar, 2009). Each subtype consists of 4 transmembrane alpha helices contributing to the ion pore, a large extracellular aminoterminal domain being responsible for ligand binding and an intracellular domain determining ion specifity (Fig. 10) (Unwin, 2005). One nAChR is constructed from 5 subunits, which can be differently combined (Miyazawa et al., 2003).

The mature nAChR at the NMJ is composed of α2βγε subunits, while the fetal receptor has a α2βγδ subunit composition. This leads to a better reaction upon ACh binding in mature muscles (Duclert and Changeux, 1995; Villarroel and Sakmann, 1996; Fambrough, 1979). ACh can bind to sites at the two α subunits resulting in an allosteric change of the pore and allowing Na^+ and K^+ ions to pass (Miyazawa et al., 2003).
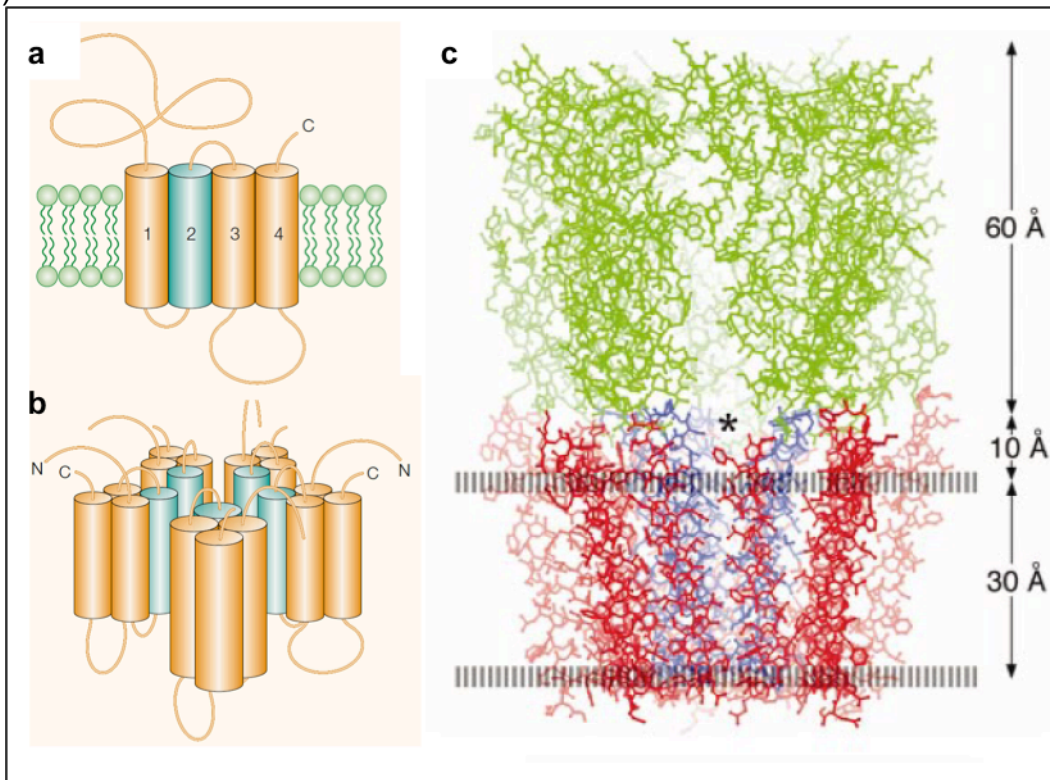
Figure 10 Structural Domains of the nAChR
a. One subunit of a nAChR consists of a large extracellular domain, a 4 alpha helices transmembrane domain and an intracellular domain (Fambrough, 1979; Unwin, 2005). **b.** One nAChR is constructed out of 5 single subunits. (mature: α2βγε; fetal: α2βγδ) (Fambrough, 1979). **c.** The pentameric structure of the alpha helical pore of nAChR (blue, pore-facing; red, lipid-facing helices) is shown in relation to the plasma membrane (broken lines) and the ligand binding domain (green) (Miyazawa et al., 2003).

1.7 Structural Interactions between the Agrin, Lrp4, MuSK and Dok-7 Complex

X-ray chrystallography, NMR and solid-phase binding assays generated a deeper understanding of the fundamental interactions within the agrin, Lrp4, MuSK and Dok-7 complex (Zong and Jin, 2013). Figure 11 summarizes important interaction regions.
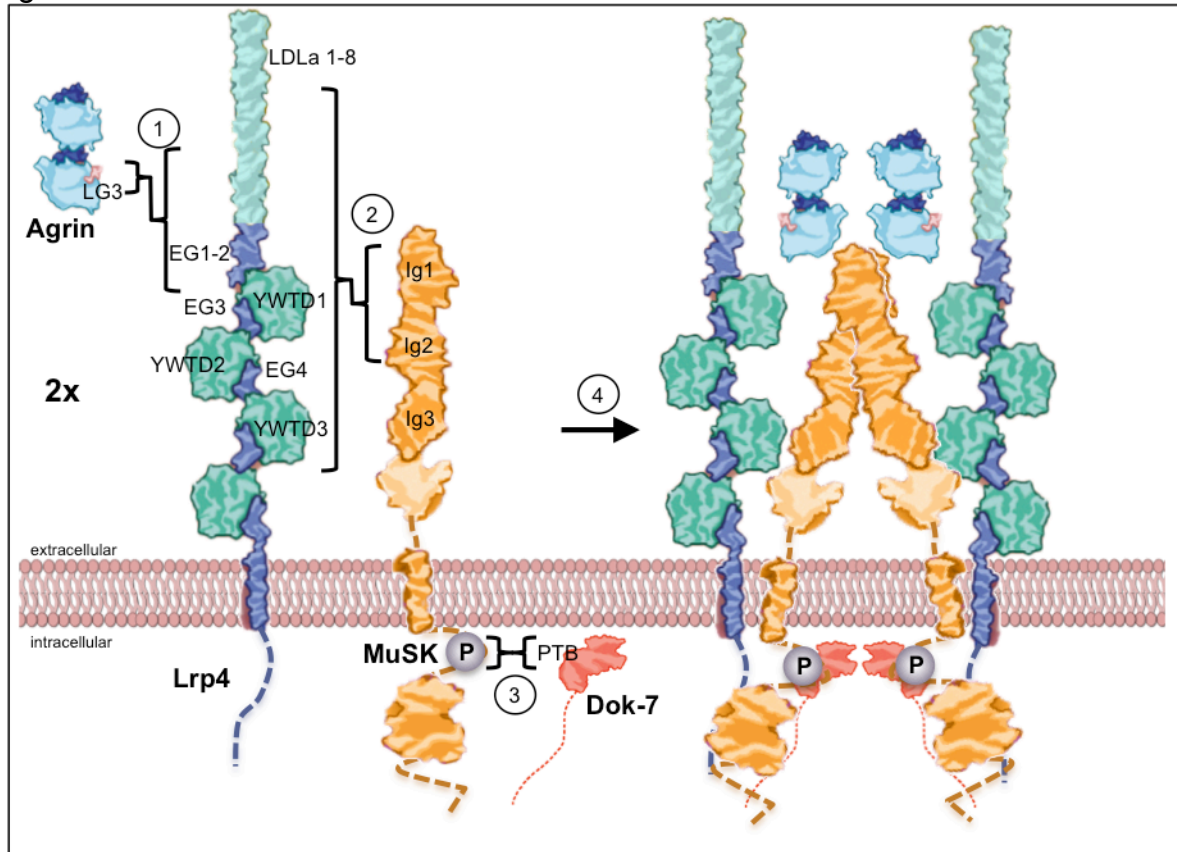
Figure 11 Summary of Interactions in the Agrin, Lrp4, MuSK and Dok-7 Complex
1-3. Regions which are important in protein association are shown. **4**. Stepwise association of all mentioned proteins leads to a large complex with activated MuSK at its center (adopted from Burden, 2011).

1.7.1 Interaction between Agrin and Lrp4

The carboxyterminal region of neural agrin (LG1-3) is most important for AChR clustering (Cornish et al., 1999; Gesemann et al., 1995). Indeed, asparagine 1783 (N1783) and isoleucine 1785 (I1785), two residues in the neuron-specific Z8 splice variant at the LG3 domain, are directly involved in the binding to Lrp4. These residues project into the first YWTD beta-propeller domain of Lrp4 (Fig. 12a). Additionally, the LDLa repeats 6-8 and the two EG domains of Lrp4 are required for agrin binding (Zhang et al., 2011). In a next step, this binary agrin-Lrp4 complex dimerizes with another binary agrin-Lrp4 complex forming a tetrameric agrin-Lrp4 supercomplex. This supercomplex is stabilized by an additional interface between agrin and Lrp4 together with an agrin-agrin interface (Fig. 12b; red circles). This

results in a closer association of two Lrp4 molecules, which might promote MuSK dimerization (Zong et al., 2012).

1.7.2 Interaction between the Agrin-Lrp4 Supercomplex and MuSK

In MuSK, the aminoterminal Ig1-2 domains are mainly responsible for agrin-induced AChR clustering (Zong and Jin, 2013). These Ig domains form a semi-rigid rod-like structure, which dimerizes with the Ig1-2 domains of another MuSK molecule (Fig. 12c). Methionin 48 (M48) and leucin 83 (L83) are important hydrophobic residues in the dimer interface and it is likely that they contribute to Lrp4 binding. Another hydrophobic residue isoleucine 96 (I96) located on the opposite of the Ig dimer interface might be required for Lrp4 binding as well (Stiegler et al., 2006; Zong and Jin, 2013). In Lrp4, the LDLa repeats 4-8, the YWTD beta-propeller domains 1-3 and the two EG domains between those propellers are required for MuSK binding (Zhang et al., 2011). Binding of the agrin-Lrp4 supercomplex, containing two Lrp4 molecules, to MuSK results in closer association of two MuSK molecules, leading to their autoactivation.

1.7.3 Interaction between MuSK and Dok-7

The interaction between MuSK and Dok-7 requires MuSK autoactivation and phosphorylation of Y553 in the NPXY motif of the juxtamembrane region (Okada et al., 2006). Phosphorylated Y553 binds to the phosphopeptide-binding groove of the PTB domain of Dok-7 (Fig. 12d). The PH domains of Dok-7 are likely to contribute to the dimerization of two Dok-7 molecules (Bergamin et al., 2010; Zong and Jin, 2013). This results in generation of a tetrameric MuSK-Dok-7 complex, which strengthens MuSK activity.
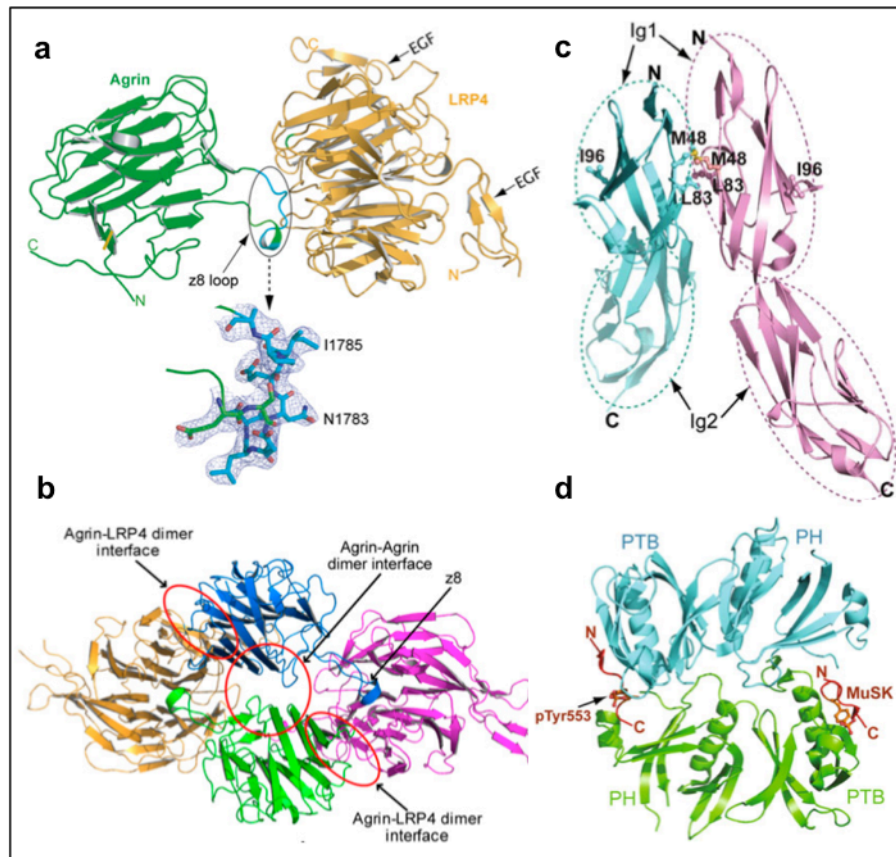
Figure 12 Detailed Structural Interactions between Agrin, LRP4 , MuSK and Dok-7
a. Agrin (green) binds with two residues (N1783 and I1785) of its Z8 splice variant to the first beta-propeller of the Lrp4 protein (Zong et al., 2012). **b.** The arrangement of the tetrameric agrin-Lrp4 supercomplex is stabilized by an interface between agrin and Lrp4 together with an agrin-agrin interface (red circles) (Zong et al., 2012). **c.** Two MuSK molecules dimerize via their aminoterminal Ig1-2 domains. The hydrophobic residues M48, l83 and I96 are likely to contribute to MuSK-Lrp4 binding (Zong and Jin, 2013). **d.** A phosphopeptide-binding groove of the PTB domain of Dok-7 binds phosphorylated Y553 from the MuSK JM domain, while the PH domain is likely to contribute to Dok-7 dimerization (Zong and Jin, 2013).

1.8 Neuromuscular Junction Disorders and Sarcopenia

Impaired function of the NMJ leads to diseases of the muscle, which can be summarized as myasthenic syndromes (Ferraro et al., 2012). The majority of congenital diseases are caused by mutations in AChR subunit genes, which result in structural changes of AChRs and thus in weaker synaptic transmission. However, there are also other targets of mutations ranging from rapsyn and acetylcholinesterase to MuSK (Beeson et al., 2008; Engel and Sine, 2005). Patients suffer from weakness in limb, ocular, bulbar, truncal and respiratory muscles, which becomes even more severe with exertion. Congenital myasthenic syndromes occur worldwide at a frequency of less than 1 in 500000 people (Vincent et al., 1997).

Myasthenic syndromes can also be caused by autoimmune reactions against important NMJ proteins leading to a disease called myasthenia gravis with a frequency of 15 per 100000 people (Ferraro et al., 2012; Robertson et al., 1998). 80% of myasthenia gravis patients produce autoantibodies against AChRs, leading to

a decrease of AChRs at the postsynaptic membrane (Fambrough et al., 1973). Other patients carry autoantibodies against MuSK or Lrp4 (Hoch et al., 2001; Higuchi et al., 2011). In common for all types of myasthenia gravis is a failure in synaptic transmission. This is caused by undeveloped NMJs and damage of the postsynaptic membrane (Fig. 13). Patients suffer from weakness of the head, neck and upper extremity muscles, which becomes more severe with activity (Conti-Fine et al., 2006; Vincent et al., 2006; Vincent et al., 2002). This disease becomes life threatening if respiratory systems are involved.

Sarcopenia is the age-related loss of muscle mass and function (Ferraro et al., 2012). NMJ impairment is likely to play a key role in degeneration over age. Amongst others, alterations of axonal transport due to the loss of trophic factors, denervation of myofibers, mitochondrial dysfunction resulting in disruption of AChR clusters by proteases, are reasons for sarcopenia (Gutmann and Hanzlikova, 1973; Vandervoort, 2002). Calorie restriction might slow down this aging process at the NMJ (Kim et al., 2008a; Opalach et al., 2010).
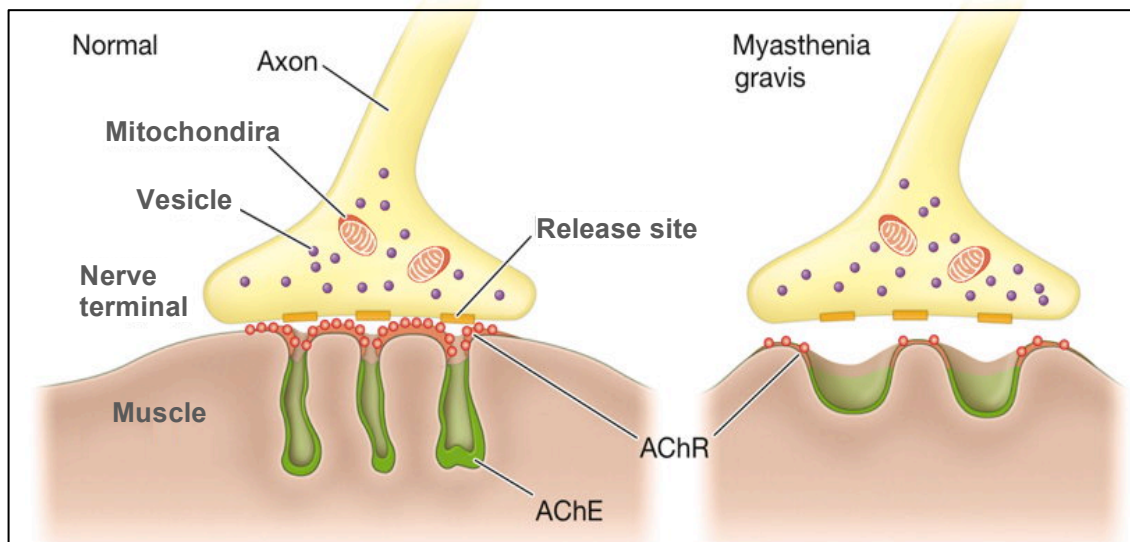
Figure 13 Myasthenia Gravis
Myasthenia gravis is caused by autoantibodies against members of the NMJ, leading to undeveloped NMJs and damage of the postsynaptic membrane (Harrisons Innere Medizin Online).

1.9 Endocytosis and Signaling

MuSK endocytosis and signaling from endosomes upon its activation might play a critical role in NMJ formation and maintenance. Therefore the next chapters will focus on endocytosis.

1.9.1   Types of Endocytosis

Several ways of endocytosis are known, which can be characterized by the type of uptake material, the uptake mechanism and the vesicle size (Fig. 14). Phagocytosis is the uptake of large particles, while the term pinocytosis is used for the uptake of

small soluble particles, membrane bound proteins and fluids. Pinocytosis is further separated into different mechanisms of endocytosis termed macropinocytosis, clathrin-mediated endocytosis (CME), caveolin-mediated endocytosis and clathrin- and caveolin-independent endocytosis (CCIE). Phagocytosis and macropinocytosis depend on actin remodeling of the plasma membrane. CME is based on the coating of an endocytotic vesicle by clathrin and by pinching off the vesicle in a dynamin GTPase dependent manner. The clathrin coat is removed prior to vesicle fusion. Caveolin-mediated endocytosis uses the protein caveolin for coating of plasma membrane invaginations and dynamin for pinching off. The mechanisms for CCIE are poorly understood, but invaginations are likely to form vesicular or tubular intermediates after pinching off by dynamin-dependent or -independent mechanisms and association with lipid rafts. (Mayor and Pagano, 2007; Conner and Schmid, 2003; Le Roy and Wrana, 2005)

Endocytosis typically occurs at sites of the plasma membrane, where specific cargo (e.g. receptor for iron-bound transferrin, low-density lipoprotein receptors and MuSK) associates with adaptors at the plasma membrane and thus causes its uptake by recruitment of accessory proteins. After fission and potential processing of the vesicle, it is transported to its destination inside the cell, which is the early endosome in most cases.
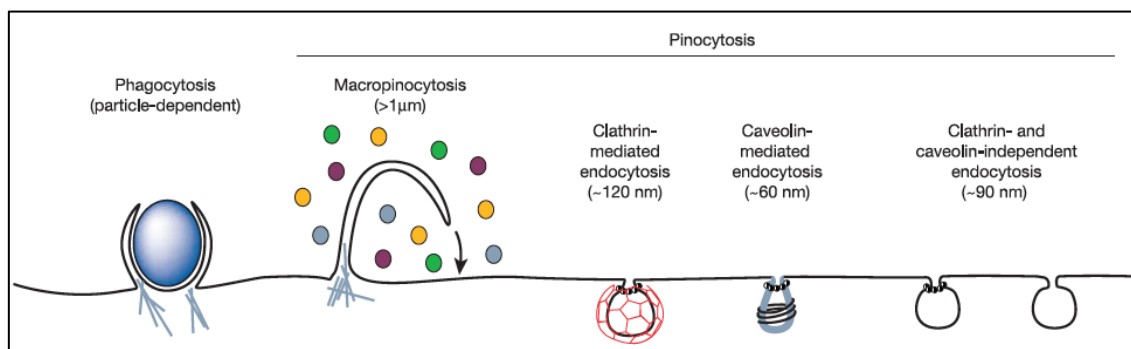
Figure 14 Types of Endocytosis
Endocytosis can be characterized by the type of uptake material, the uptake mechanism and the vesicle size (Conner and Schmid, 2003).

1.9.2   Endocytotic Trafficking Routes

Once material is endocytosed by CME or clathrin-independent endocytosis (CIE) it is usually transported to the early endosome, where the newly formed endosomes fuse with pre-existing ones. The early endosome is a mildly acidic compartment (~pH6.0), where most ligands are released from uptaken receptors (Maxfield and McGraw, 2004). The small GTPase Rab5 and the early endosome antigen 1 (EEA1) are important proteins involved in vesicle fusion (Mills et al., 1999; Woodman, 2000). The early endosome functions as a sorting mechanism for uptaken cargo. For instance, membrane proteins without targeting information will be transported from the early endosome with the bulk of the membrane, while targeting and sorting information is required for a transport into specific compartments (Maxfield and McGraw, 2004). For

transmembrane receptors there are two common final destinations of trafficking known (Fig. 15). They can be recycled back to the plasma membrane or they can undergo degradation. Receptor recycling can be achieved via a rapid or a slow recycling route. Rapid recycling involves Rab4 and Rab35 and is thought to occur directly from early endosomal stages (van der Sluijs et al., 1992; Sato et al., 2008; Grant and Donaldson, 2009). Slow recycling functions via trafficking to endocytotic recycling compartments (ERC) and then back to the plasma membrane. ERCs emerge upon maturation of early endosomes by replacing Rab5 with Rab11 and prevent cargo from being transported to late endosomes and lysosomes by mistake (Sönnichsen et al., 2000; Grant and Donaldson, 2009). Recycling to the plasma membrane is further achieved by several distinct mechanisms including ARF6 or different adaptor proteins (Grant and Donaldson, 2009). Degradation of receptors usually works via maturation of early endosomes to multivesicular bodies (MVB) and late endosomes. Upon receptor activation, ubiquitination often functions as a signal for degradation. The endosomal sorting complex required for transport (ESCRT) is involved in uptake of vesicles (derived from early endosomal compartments) into the lumen of the MVB (Sorkin and von Zastrow, 2009; Raiborg et al., 2002; Babst et al., 2002). The acquisition of Rab7 proteins stands for the maturation into late endosomes, which then fuse with lysosomal compartments. There, proteolytic enzymes and an acidic pH contribute to protein degradation (Sorkin and von Zastrow, 2009).
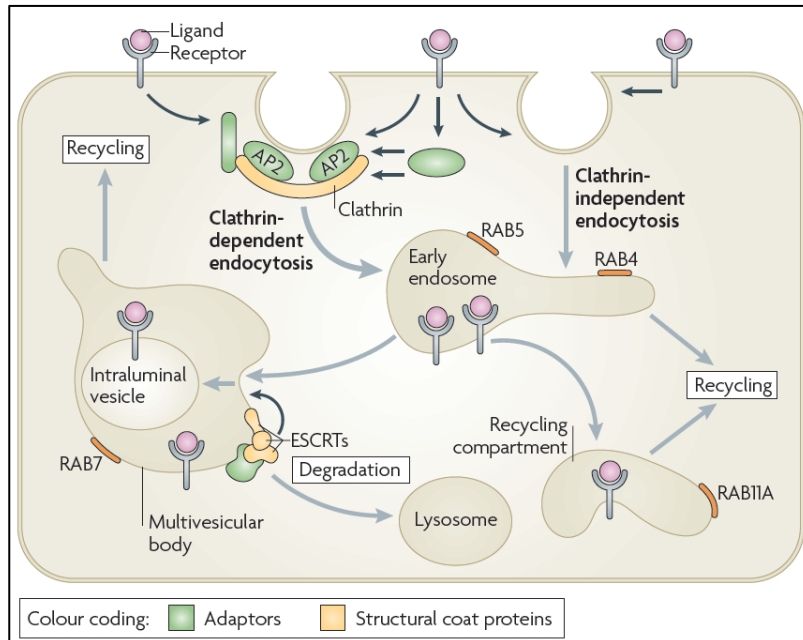
Figure 15 Pathways of Receptor Endocytosis
Endocytosis of transmembrane receptors can function via clathrin-mediated (CME) or clathrin-independent (CIE) endocytosis. After internalization into Rab5 positive early endosomes, receptors can be targeted back to the plasma membrane via fast (Rab4-dependent) or slow (Rab11-dependent) recycling routes. Receptors for degradation are incorporated into intraluminal vesicles in multivesicular bodies (MVB) and Rab7 positive late endosomes, which fuse with lysosomes (Sorkin and von Zastrow, 2009).

1.9.3 Endocytosis of Receptor Tyrosine Kinases and Endosomal Signaling

CME is the major endocytotic pathway of ligand activated RTKs (Goh and Sorkin, 2013). Prominent members of the RTK family such as epidermal growth factor receptor (EGFR), neurotrophic tyrosine kinase receptor type 1 (TrkA) show increased localization with clathrin-coated pits upon ligand activation and internalization is reduced by inhibiting CME (Gorden et al., 1978; Beattie et al., 2000). CIE plays a minor role in RTK endocytosis but increases when CME is saturated (Wiley, 1988). To a great extent, sorting of endocytosed RTKs takes place at the MVB stage, where ubiquitinated RTKs are packed into intraluminal vesicles by ESCRT proteins heading towards degradation (Henne et al., 2011). But also other mechanisms independent of ubiquitination might play a role in RTK degradation (Ying et al., 2010). Recycling plays a minor role for RTKs. However, mechanisms have been discovered for various receptors (EGFR, TrkA, etc.) (Sorkin et al., 1989; Zapf-Colby and Olefsky, 1998). While recycling works via Rab4 and Rab11 positive compartments and also from MVB, unoccupied receptors are recycled faster back to the plasma membrane than ligand-occupied receptors (Goh and Sorkin, 2013; Resat et al., 2003).

As RTKs are predominantly internalized after ligand-dependent activation, sustained signaling in endosomal compartments is a common feature (Polo and Di Fiore, 2006; von Zastrow and Sorkin, 2007; Sorkin and von Zastrow, 2009; Sadowski et al., 2009). Interactions of signaling molecules with activated TrkA were detected in early endosomes (Delcroix et al., 2003). Although receptors transported to intraluminal vesicles stop signaling, receptors in the membrane of MVB or late endosomes still mediate signaling as it was shown for TrkA (Hisata et al., 2007). Also EGFRs remain ligand bound and phosphorylated during even late endosomal stages (Oksvold et al., 2001; Sorkin and von Zastrow, 2002). For other signaling proteins (e.g. H-Ras pathway), recycling compartments were discovered to be sites of sustained signaling (Gomez and Daniotti, 2005). Therefore, endocytosis can be seen as a mechanism to regulate signaling by either terminating receptor activity or by continuing activity in various endosomal compartments.

1.9.4 The Special Role of MuSK and its Endocytosis in Neuromuscular Junction Formation

MuSK holds a special role in the family of RTKs. It is activated by the agrin-induced interaction with Lrp4 and not by direct ligand-binding as in other RTKs like EGFR or TrkA. Additionally, complete MuSK activation is only achieved upon binding of the intracellular protein Dok-7. This leads to a large plasma membrane associated complex, which initiates a downstream signaling cascade regulating NMJ formation. It is an important fact that agrin stimulation of MuSK induces not only AChR clustering but activates MuSK endocytosis as well (Zhu et al., 2008). Moreover, activated MuSK can be a target for ubiquitination, which acts as an internalization and degradation signal (Lu et al., 2007). The NPXY motif, which is also present in the

MuSK JM domain, represents a PTB binding site that is known as clathrin-binding site (Traub, 2009). Additionally, blocking of clathrin- and dynamin-dependent endocytosis reduces MuSK internalization (Luiskandl et al., 2013). In addition, MuSK and caveolin colocalize, suggesting a possible alternative internalization route for MuSK (Luiskandl et al., 2013).

Subsequently after MuSK internalization, the receptor is found in Rab5 and EEA1 positive vesicles. The endocytosed MuSK pool is then divided into portions for degradation via the Rab7 positive late endosomal route and for receptor recycling via Rab4 and Rab11 positive endosomes (Luiskandl et al., 2013).

Despite these findings, information in more detail about agrin-induced MuSK endocytosis and particularly about sustained signaling during endocytosis is still missing. Furthermore, less is known about the endocytotic behavior of MuSK interaction partners Lrp4 and Dok-7 (Luiskandl et al., 2013).

2   Aim of the Master Thesis

MuSK is one of the key players in NMJ signaling. This RTK is responsible for the correct formation and function of NMJs. As it has been implicated in forms of myasthenic syndromes and sarcopenia, more interest on this unrivaled protein has been evoked in the last years. Endocytosis of MuSK, its intracellular trafficking routes for recycling or degradation and the possibility to signal from endosomes remain major topics in the field of NMJ research.

Working with cultured myotubes is more difficult and laborious than working with heterologous cells as for instance fibroblasts. Differentiation of myoblasts into myotubes is a critical event in cell culture and does often induce variability like myotube number and morphology. Morover, it is difficult to track important NMJ proteins with specific antibodies without interfering with their function. Therefore, a heterologous, cell culture based model system expressing the fundamental key players of NMJ formation Lrp4, MuSK and possibly Dok-7 would provide the ability to investigate MuSK endocytosis, trafficking and signaling upon agrin stimulation. The introduction of affinity tags into the proteins of interest, allows visualization by tag-specific antibody/molecule binding without interference with their function.

Considering the above listed advantages, the aim of this thesis was to investigate, whether a heterologous model system of the NMJ can be developed and if MuSK endocytosis can be assessed in this system.

Therefore, the intent was to generate affinity-tagged MuSK and Lrp4 constructs. In a next step, their correct expression and functionality was assessed by immunocytochemistry and biochemical methods. Tagged proteins were stably introduced into fibroblasts and high expressing cells were selected by cell sorting methods. Finally, initial endocytosis assays were aimed to reveal the functionality of the model system and to assess MuSK endocytosis.

3   Results

3.1 Protein Tagging and Tests of Functionality

3.1.1   Tag Selection and Tag Positioning

The generation of recombinant proteins bearing affinity tags has become a widely shared tool in molecular research, as well as in the pharmaceutical industry. It allows specific visualization of the recombinant protein in cell preparations and simple purifications of cell lysates (Terpe, 2003). The potency of affinity tags, the effect on the tertiary structure and the biological activity of the recombinant protein strongly depend on the aminoacid composition and the location in the protein (Bucher et al., 2002).

For the purpose of this project, three affinity tags – haemaglutinin-tag (HA-tag), bungarotoxin binding site-tag (BBS-tag) and FLAG-tag (Tab. 1) – were chosen from a pool of available tags, due to their best binding and detection ability, together with the availability of the tag systems in the lab (Sharma and Höbartner, 2013 unpublished data).

The locations of the affinity tags were chosen to be at the aminoterminal end of the recombinant proteins (Fig. 16). This should enable correct tertiary structure folding of the protein after signal sequence cleavage and insertion into the plasma membran. The affinity tag is accessible to affinity molecules (antibodies, bungarotoxin) in intact cells. Therefore, labeling via the tag can be used for cell surface staining and endocytosis assays. Furthermore, the position of the affinity tags had to be chosen carefully in order not to interfere with protein-protein interactions of agrin, Lrp4 and MuSK. Again, the aminoterminal position offered a favorable option.

As aminoterminal HA-tagged MuSK has been already available in a CMV expression vector, the focus was on generating aminoterminal BBS-tagged MuSK. The advantage of the BBS-tag lies in the number of binding sites of the alpha-bungarotoxin (BGT) molecule and the small size of alpha-BGT as staining molecule (McCann et al., 2005). While an anti-HA antibody can bind two epitopes, one alpha-BGT molecule only binds one BBS-tag, which reduces the possibility of protein crosslinking upon tag-binding. A previously generated BBS-MuSK construct in a pcDNA expression vector was weakly detectable in transfected cells (Sharma, 2013

unpublished data). Therefore, alternative aminoterminal BBS-tagged MuSK constructs were generated. These alternatives included different tandem tags or had different additional linker regions between tandem tags or between the signal sequence and the tag position (Tab. 1). All these variants were generated in order to obtain a MuSK construct with a BBS-tag, which is well expressed and accessible for BGT binding on the aminoterminal extracellular portion of the protein.

Additionally, as aminoterminal FLAG-tagged Lrp4 was available in a pBabe-puro expression vector, the focus for Lrp4 was on generating aminoterminal HA-tagged Lrp4. Therefore, besides HA-Lrp4, different alternative constructs bearing tandem tags were generated (Tab. 1). In contrast to MuSK tagging, possible crosslinking by anti-HA or anti-FLAG antibodies had to be accepted for Lrp4, because it would have been impractical to have BBS-tags introduced in MuSK and Lrp4 at the same time.
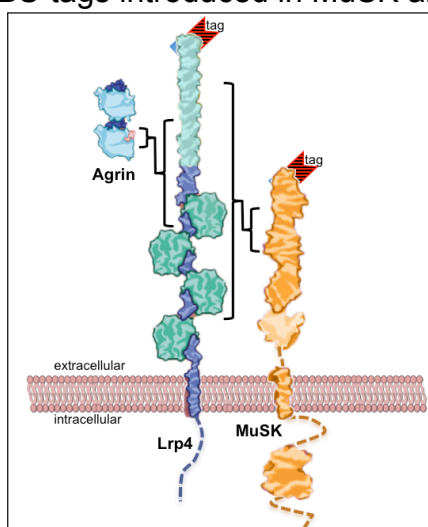

Figure 16 Position of Protein Affinity Tags
The tags were chosen to be introduced at the aminoterminal extracellular portion of the proteins (compare Fig. 11).

Table 1| Affinity Tags and Fusion Proteins

Tag	Sequence	Tag Reference	Protein	#
BBS	WRYYESSLEPYPD	Harel et al., 2001; Sekine-Aizawa and Huganir, 2004; McCann et al., 2005	MuSK	M1
HA	YPYDVPDYA	Wilson et al., 1984	MuSK	M2
BBS-BBS	WRYYESSLEPYPDAAWRYYESSLEPYPD		MuSK	M3
BBS-AADCA	WRYYESSLEPYPD*AADCA*		MuSK	M4
HA-BBS	YPYDVPDYAAAWRYYESSLEPYPD		MuSK	M5
BBS-HA	WRYYESSLEPYPDAAYPYDVPDYA		MuSK	M6
BBS-KASGA-HA	WRYYESSLEPYPD*AKASGA*AYPYDVPDYA		MuSK	M7
BBS-KTARA-HA	WRYYESSLEPYPD*AKTARA*AYPYDVPDYA		MuSK	M8
GG-BBS-HA	*GG*WRYYESSLEPYPDAAYPYDVPDYA		MuSK	M9
DNVP-BBS-KASGA-HA	*DNVP*WRYYESSLEPYPD*AKASGA*AYPYDVPDYA		MuSK	M10
FLAG	DYKDDDK	Einhauer and Jungbauer, 2001; Hopp et al., 1988	Lrp4	L1
HA	YPYDVPDYA	Wilson et al., 1984	Lrp4	L2
FLAG-HA	DYKDDDKAAAYPYDVPDYA		Lrp4	L3
HA-FLAG	YPYDVPDYAGGADYKDDDK		Lrp4	L4

Sequence code: blue, BBS-tag; red, HA-tag; italic, linker; purple, FLAG-tag

3.1.2   Tag   Generation   and   Recombinant   Fusion Protein Cloning

The generation of recombinant fusion constructs was achieved by standard cloning methods. Pre-existing expression vectors containing the proteins MuSK (rat) or Lrp4 (mouse) were used as DNA sequence source. With the help of Q5 site-directed mutagenesis and/or subcloning of existing tag and protein sequences, new recombinant fusion constructs were generated. Tagged MuSK constructs were cloned into pcDNA (or CMV) expression vectors for transient expression in cells. Valuable constructs were further cloned into pBabe-puro and pMX expression vectors for stable expression. Tagged Lrp4 constructs were cloned into pBabe-puro retroviral vectors as well. All generated recombinant fusion protein bearing vectors were analyzed by DNA sequencing for the correct inserts. For a full list of all pre-existing, generated and used vectors bearing protein information see Chapter 5.5, Figure 17 and Table 1.
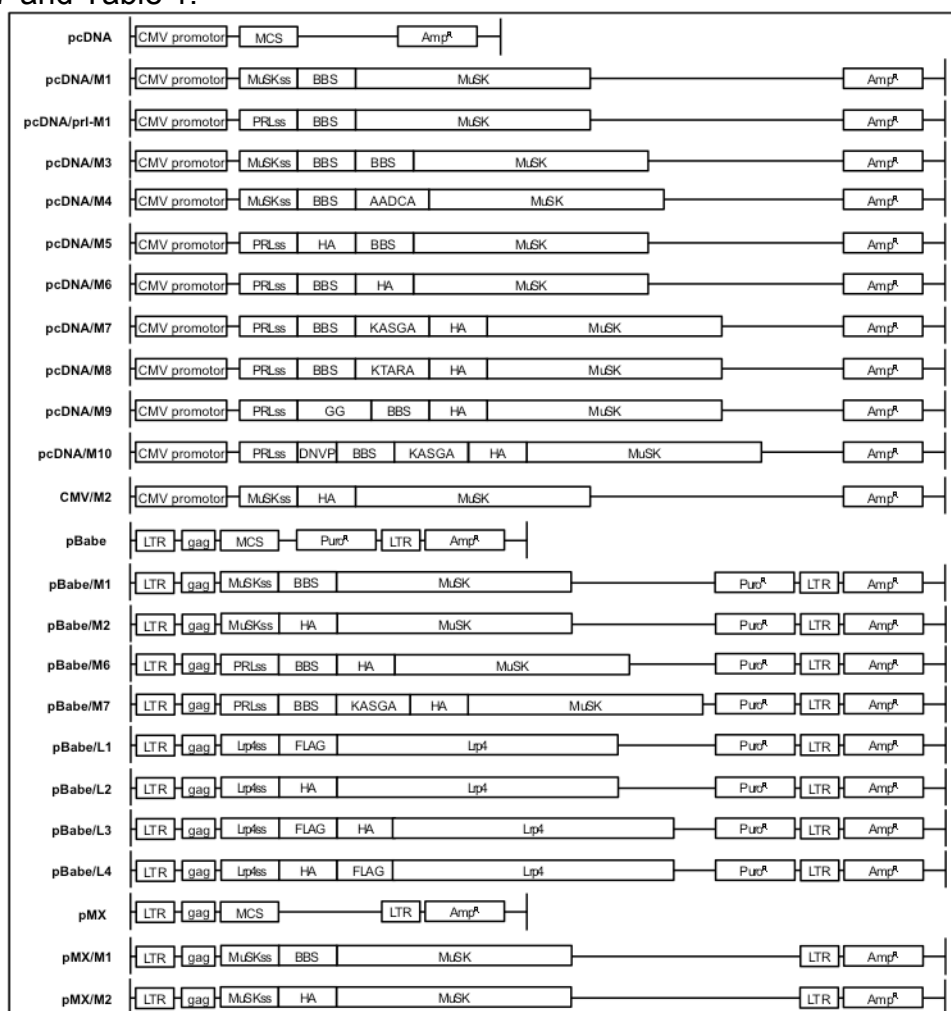
Figure 17 Expression Vectors and Cloned Recombinant Fusion Proteins
Empty expression vectors, as well as generated recombinant expression vectors are shown. CMV, cyto megalo virus; MCS, multiple cloning site; Amp^R, ampicillin resistance; MuSKss, MuSK signal sequence; BBS, BBS-tag; AADCA, AADCA linker; PRLss, prolactin signal sequence; HA, HA-tag; KASGA, KASGA linker; KTARA, KTARA linker; GG, GG linker; DNVP, DNVP linker; pBabe, pBabe-puro; LTR, long terminal repeat; gag, group specific antigen; Puro^R, puromycin resistance; Lrp4ss, Lrp4 signal sequence; FLAG, FLAG-tag.

3.1.3   Tests of Functionality in COS-7 Cells

To assign the functionality of the generated constructs, several criteria have to be fulfilled. It is important that the tagged protein is expressed, is transported to and incorporated into the plasma membrane and that the tag is accessible for its binding molecule for detection. Therefore, all generated tagged MuSK and Lrp4 constructs were tested for their expression level and for the accessibility of their specific affinity tag.

The tests of functionality were performed in COS-7 cells. For biochemical assays, the constructs were transiently expressed in cultured cells. The cells were lysed one day after transfection. From the lysate, immunoprecipitation (IP) and pull-down (PD) experiments were done to selectively enrich MuSK or Lrp4 proteins in the sample. Tagged MuSK proteins were enriched by MuSK IP, HA IP and/or BGT PD. Tagged Lrp4 proteins were enriched by HA IP and by FLAG IP. Proteins were visualized by immunoblotting (IB) with antibodies and binding molecules specific for the protein or the tags. For immunocytochemistry assays, the constructs were transiently expressed in COS-7 cells. One day after transfection the cells were used for cell surface and total protein staining.

3.1.3.1   Functionality of Tagged MuSK Constructs

Figure 18 shows that HA-MuSK (HA) was highest expressed and best detectable by IP with anti-MuSK and anti-HA antibodies compared to any of the tested new tagged MuSK porteins. Introduction of the BBS-tag into MuSK had adverse effects on MuSK expression (Fig. 18a), although MuSK was detectable by IP with anti-MuSK antibodies and by PD with alpha-BGT. Introducing BBS-MuSK into the expression vector pMT21 had no obvious advantageous effect (Fig. 18a,c; compare lanes 3 and 5). Approaches to increase the expression level with the introduction of tandem BBS-tags, HA/BBS-tag combinations or linker sequences for MuSK had no obvious positive effect or even worsened the expression. Introduction of a HA-tag sequence prior to the BBS-tag sequence was thought to foster a better folding of the BBS-tag due to greater distance to the actual MuSK portion. However, a higher expression and detection of this construct was not achieved (Fig. 18a,c; lane 4). Insertions of linker sequences between the BBS- and HA-tag to produce better sterical conditions for BBS-tag folding were not successful (Fig. 18a,c; lane 2). In addition, insertion of a linker region between the signal sequence and the BBS-tag to avoid a possible BBS-tag cleavage did not improve expression (Fig. 18a; lane 1). Several constructs were tested but not shown since fusion proteins were either not detectable (M3, M4, M5) or similary expressed as the proteins in Figure 18 (M8, M9; see Table 1 for construct details). Overall, MuSK proteins carrying a BBS construct were weaker expressed than the MuSK protein carrying a HA-tag only.

Figure 19 shows the visualization of tagged MuSK constructs by surface and intracellular immunostainings. Consistent with the biochemical assays, HA-MuSK revealed the highest expression in total and on the cell surface compared to all other

tested constructs (Fig. 19i). BBS-MuSK was not detectable on the cell surface but was predominantly localized near the nucleus, possibly arrested in the ER, in Golgi or lysosomal compartments (Fig. 19a). BBS-MuSK in pMT21 slightly increased the overall signal and allowed detection via the BBS-tag on the cell surface (Fig. 19b). The introduction of a BBS-HA tag (M6) allowed the independent detection of MuSK by two distinct binding molecules. MuSK was not detected on the cell surface via the BBS-tag (Fig. 19c). Strikingly however, it was possible to stain surface MuSK proteins via the HA-tag to similar extent as the HA-MuSK construct (Fig. 19d). Further insertions of linker sequences (M7, M10) did not enhance the BBS-tag accessibility (Fig. 19e-h). This demonstrates that BBS-HA-MuSK is expressed and incorporated into the cell membrane. The HA-tag is accessible, while the BBS-tag is not.

3.1.3.2 Functionality of Tagged Lrp4 Constructs

The generated constructs of the second protein of interest, Lrp4, were tested the same way as MuSK. Figure 20 shows that tagged Lrp4 was only weakly detectable, while the positive control HA-MuSK always showed a good signal. In detail, IP of single and tandem tagged Lrp4 (L2, L3, L4; see Table 1 for construct details) with anti-HA antibodies failed to detect Lrp4 (Fig. 20; lanes 1, 2 and 3). In contrast, Lrp4 was detectable by IP with anti-FLAG antibodies, although the signal was very weak (Fig. 20; lane 2 and 3).
In immunostainings of transfected COS-7 cells, the cell surface signal of original FLAG-Lrp4 (L1) was always near the detection limit, while intracellular signals were readily detectable (Fig. 21a). FLAG-Lrp4 was located near the nucleus and randomly dispersed over the whole cell. To improve the detection of tagged Lrp4 on the cell surface, the FLAG-tag was exchanged for a HA-tag (L2). Additional constructs containing HA and FLAG tandem tags were also generated (L3, L4). Altogether, it was not possible to detect any of the newly tagged Lrp4 constructs on the cell surface either using anti-MuSK or anti-FLAG antibodies (Fig. 21b-e). Intracellular stainings of tagged Lrp4 were also weaker than original FLAG-Lrp4.

Summing up, it was not possible to achieve an improved detection of tagged MuSK and Lrp4 in immunocytochemical and biochemical experiments for any of the newly generated constructs. It appears that a combination of several factors exists, from tag folding up to basic protein expression levels that contribute to the mentioned difficulties in protein detection. Consequently, the original HA-MuSK (M2), BBS-MuSK (M1) and FLAG-Lrp4 (L1) constructs were then used for heterologous model system development.
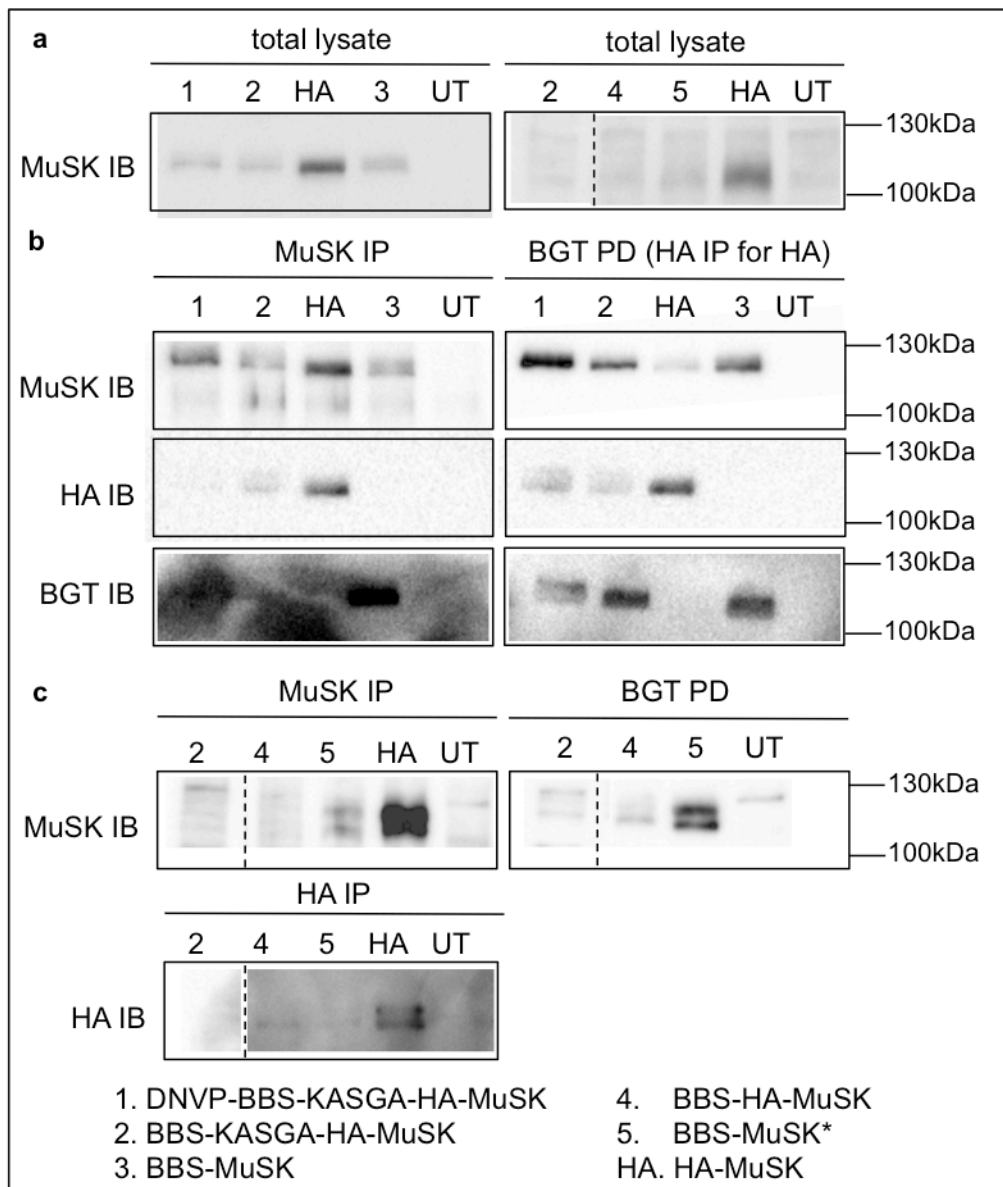
Figure 18 MuSK Detection by Immunoblotting
COS-7 cells were transfected with pEGFP and tagged MuSK constructs. Cells were lysed and IP/PD followed by IB was performed. MuSK was isolated using anti-MuSK antibodies, anti-HA antibodies and biotin-alpha-BGT. MuSK was detected by IB using anti-MuSK H25 antibodies, anti-HA antibodies and biotin-alpha-BGT. **a-c.** HA-MuSK showed the highest overall signal for MuSK between 100-130kDa, while the signals from BBS-tagged MuSK constructs were low. Controls for pEGFP and actin expression are not shown. *, pMT21 vector – others are pcDNA/CMV; UT, untransfected control.
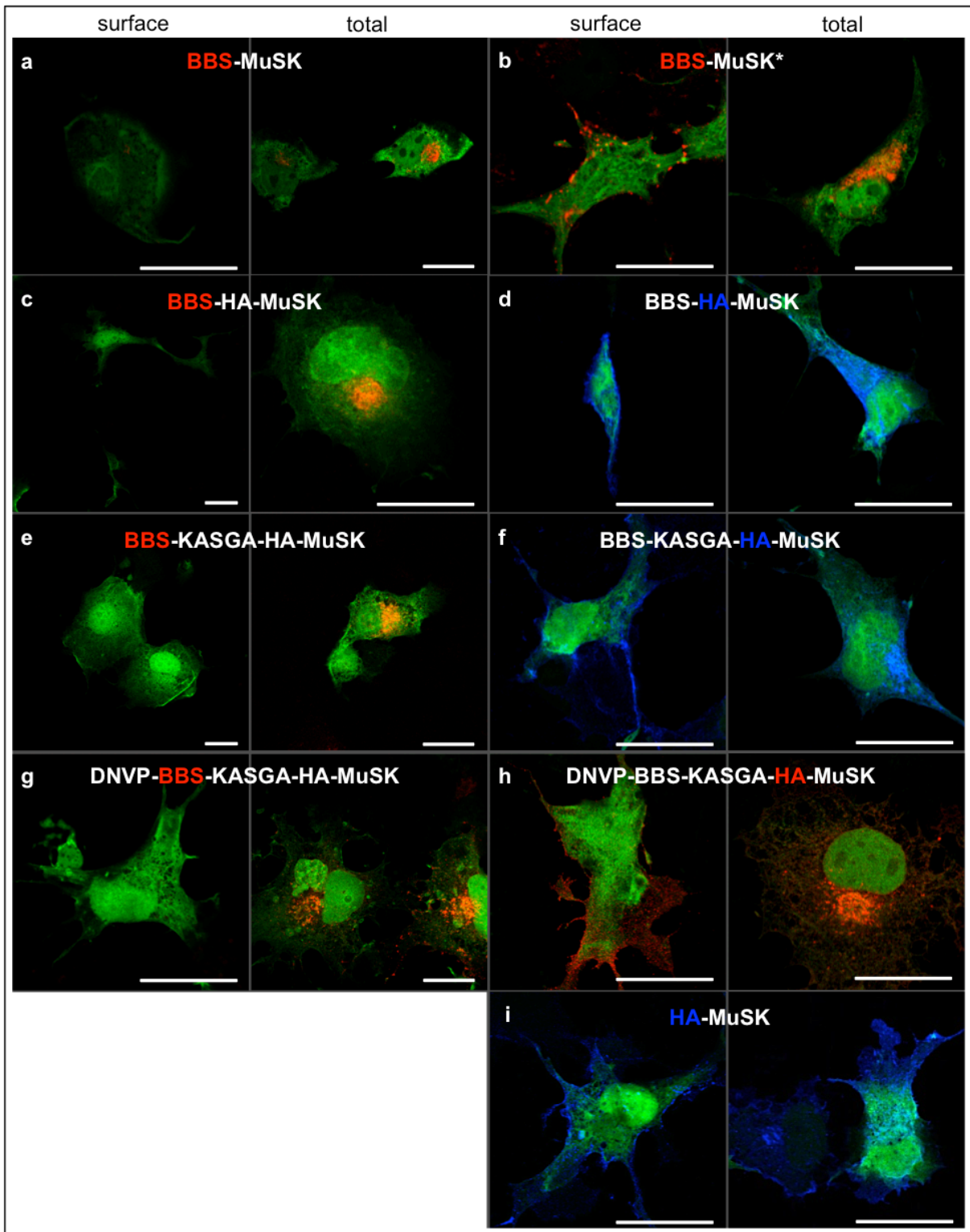
Figure 19 MuSK Detection by Immunocytochemistry
COS-7 cells were transfected with pEGFP and tagged MuSK constructs. Fixed cells were stained for cell surface or total MuSK. The BBS-tag was targeted with biotin-alpha-BGT and streptavidine-Cy3 (red). The HA-tag was targeted with anti-HA antibodies and anti-rabbit-Alexa647 (blue) antibodies or anti-rabbit-Cy3 (red in h.) antibodies. **a,b**. BBS-MUSK was not detectable on the cell surface, but the signal slightly increased by changing the vector from pcDNA into pMT21. **c,d.** Introducing a BBS-HA tandem tag allowed detection of surface MuSK via the HA-tag but not via the BBS-tag. **e-h.** Adding a KASGA linker sequences between the tandem tag and a DNVP linker after the signal sequence had no positive effect. **i.** HA-MuSK showed the highest signal in surface and total stainings. *, pMT21 vector – others are pcDNA/CMV; Scale bars, 25 µm.
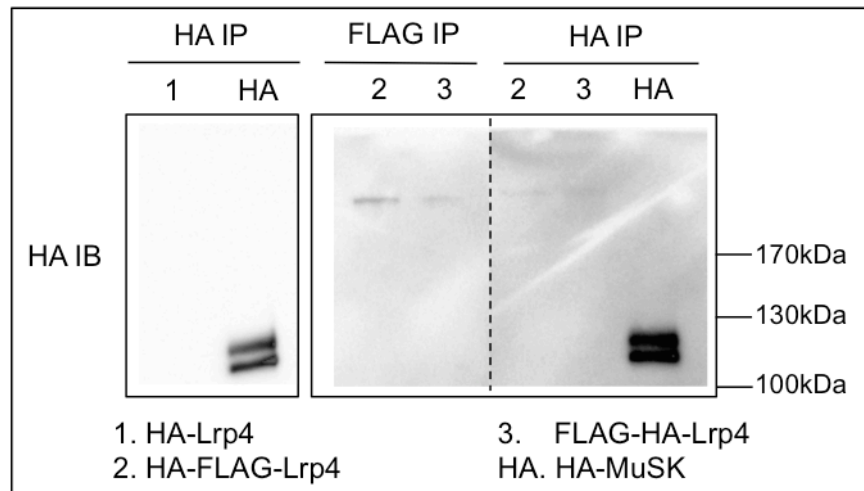
Figure 20 Lrp4 Detection by Immunoblotting
COS-7 cells were transfected with pEGFP and tagged Lrp4 constructs. Cells were lysed and IP followed by IB was performed. Lrp4 was isolated with anti-HA and anti-FLAG antibodies. Lrp4 was detected by IB using anti-HA antibodies. Lrp4 was hardly detectable for all constructs at approximately 200kDa. The HA-MuSK control always showed a strong signal between 100-130kDa. Controls for pEGFP and actin expression are not shown.
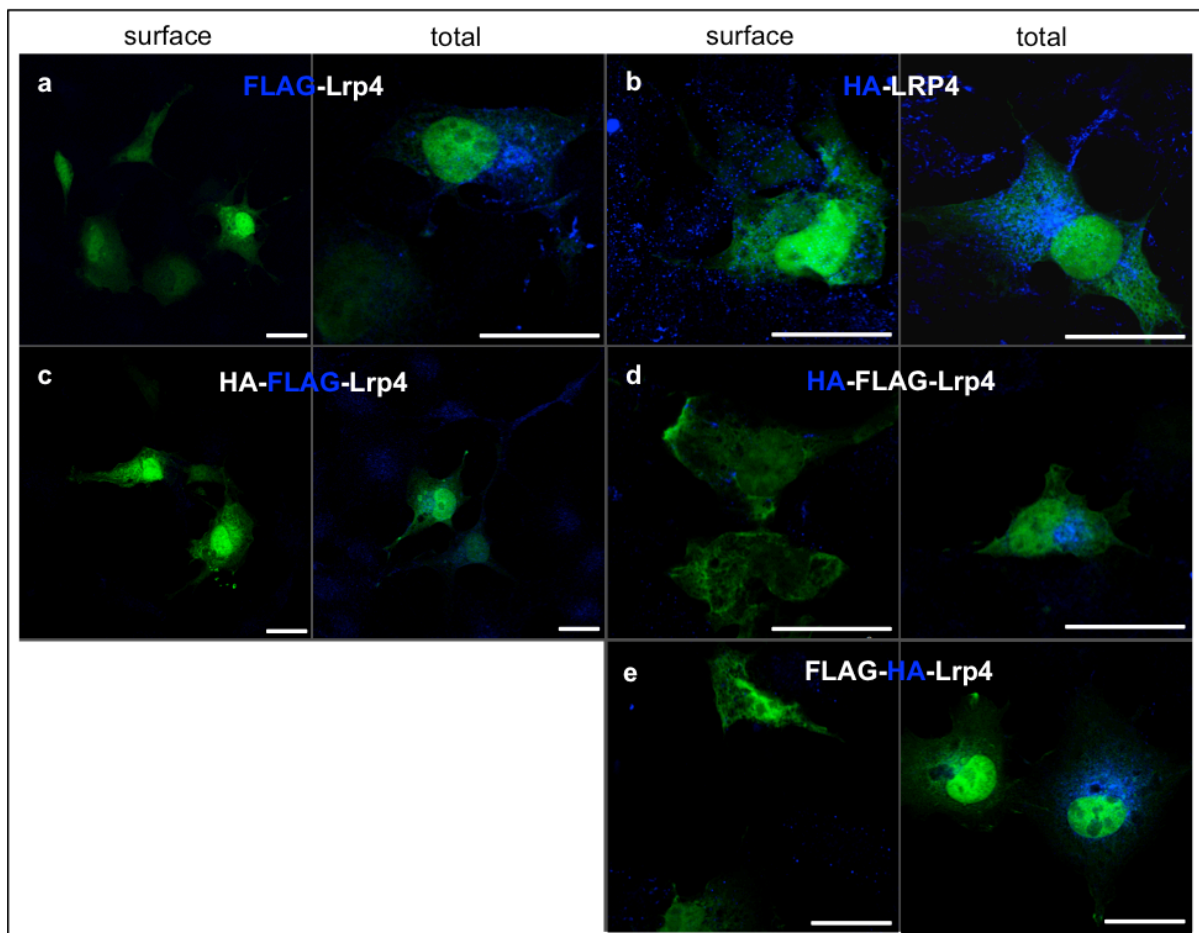

Figure 21 Lrp4 Detection by Immunoprecipitation
COS-7 cells were transfected with pEGFP and tagged Lrp4 constructs. The FLAG-tag was targeted with anti-FLAG and anti-mouse-Alexa647 antibodies (a,c). The HA-tag was targeted with anti-HA and anti-rabbit-Alexa647 antibodies (b,d,e). **a.** FLAG-Lrp4 was not detectable on the cell surface, while the signal from inside the cell was good. **b.** HA-Lrp4 showed unspecific surface signals, while the signal from inside the cell was good. **c,d.** The introduction of a HA-FLAG tandem tag did not result in better surface and total detection. **e.** The introduction of a FLAG-HA tandem tag was also not successful. Scale bars, 25 µm.

27

3.1.4   Tests of Functionality in Myotubes

To determine the biological functionality of tagged MuSK, AChR cluster formation and MuSK phosphorylation in agrin-stimulated myotubes were investigated.

First, MuSK deficient myoblasts were clonally selected for reasonable morphological differentiation into myotubes (Fig. 22a). One positively selected clone was then stably transduced using a retrovial intermediate with either HA-MuSK (M2) or BBS-MuSK (M1). Virus infected myoblasts were selected with puromycin and clonal selection was done after cell recovery. The regained ability of MuSK deficient cell lines expressing M1 or M2 to form AChR clusters was analyzed by alpha-BGT stainings. Myotubes expressing HA-MuSK or BBS-MuSK formed AChR clusters in response to agrin (Fig. 22b). IB analysis of agrin-stimulated myotubes demonstrated and underlined the biological functionality of both HA- and BBS-tagged MuSK constructs (Fig. 22c). HA-MuSK and BBS-MuSK were phosphorylated in response to agrin. Although, HA-MuSK showed higher phosphorylation signals than BBS-MuSK, the functionality tests were positive for both tagged MuSK constructs.
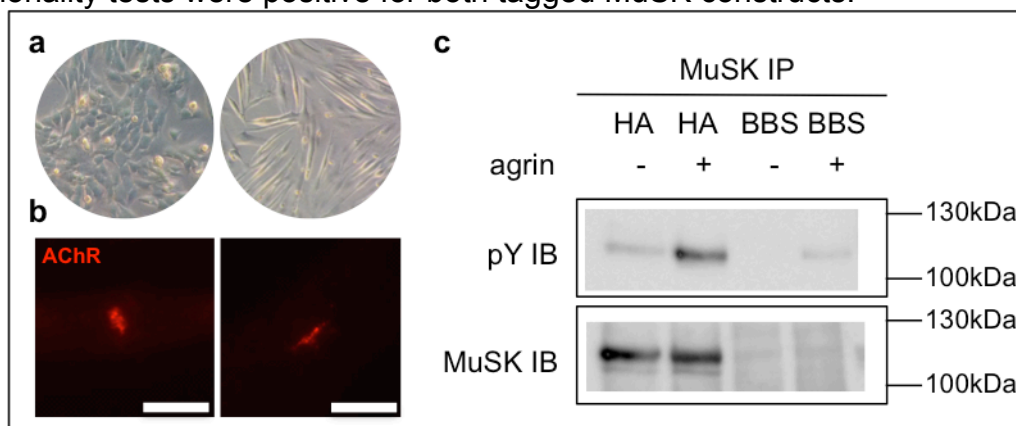

Figure 22 Tests of Functionality of HA-MuSK and BBS-MuSK in Myotubes
a. MuSK deficient muscle cell line before (left) and after (right) differentiation into myotubes. **b.** AChR clusters of HA-MUSK (left) and BBS-MuSK (right) expressing myotubes were stained with alpha-BGT-594. **c.** Myotubes expressing HA-MUSK (HA) and BBS-MuSK (BBS) were lysed and IP followed by IB was performed. MuSK was isolated using anti-MuSK antibodies and detected by IB using anti-MuSK H25 antibodies. Phosphotyrosines (pY) were detected by IB with p99 and p100 antibodies. HA-MuSK expressing myotubes showed highest levels of phosphorylated MuSK with agrin stimulation, while this signal from BBS-MuSK was very weak. MuSK expression was equal within each cell line sample. Scale bars: 10 µm.

3.1.5   Acetylcholine Receptor Clustering in Response
to Tag Binding

An important aspect in studying tagged proteins is the interference of affinity tag binding with biological functions. It is known that antibody binding induces dimerization of RTKs and especially MuSK, which leads to activation and clustering of AChRs on the surface of myotubes (Schlauf, 2011; Herbst and Burden, 2000; Hopf and Hoch, 1998; Spaargaren et al., 1991). Therefore, testing whether HA- and BBS-tagged MuSK were activated by anti-HA antibodies and bungarotoxin respectively, was important. Differentiated myotubes expressing HA- and BBS-tagged MuSK were

treated with antibody or bungarotoxin in presence or absence of agrin and AChR clustering was assessed (Fig. 23a; individual incubation protocols).

Differentiated HA-MuSK (M2) and BBS-MuSK (M1) expressing myotubes were preincubated with anti-HA antibodies or alpha-BGT for 1h at 4°C. Afterwards the myotubes were washed to remove the binding molecules and incubated with or without agrin overnight at 37°C. Controls without preincubation were treated equally. Myotubes were then fixed and AChR clusters were stained and the number of clusters per myotube was counted. The percentages of myotubes forming AChR clusters are shown for each condition. Preincubation with HA specific antibodies caused only a slight increase (+4%) in the number of cluster-positive myotubes compared to unstimulated myotubes (Fig. 23b). Agrin stimulation overnight subsequent to the antibody preincubation induced cluster formation to a similar extent (-2%) as in the control agrin-stimulated myotubes. In BBS-MuSK expressing myotubes, alpha-BGT preincubation resulted in an increase (+7%) in myotubes with clusters (Fig. 23c). Further agrin stimulation overnight resulted in a decrease (-12%) of positive myotubes. These experiments indicate a minimal influence of anti-HA antibodies or alpha-BGT incubation on MuSK activation when cells are exposed to binding molecules for a short time (≤ 1 hour).

To test the effect of MuSK labeling with anti-HA antibodies or bungarotoxin after long-term incubation, the experimental design was modified. First, alpha-BGT does not dimerize by itself and thus it is unlikely to crosslink MuSK. Therefore, preincubations were performed with anti-HA antibodies or biotin-alpha-BGT. Second, the preincubations were performed for periods of 1h and 8h. Third, to prevent a reduction of surface MuSK due to tag binding prior to agrin stimulation, the binding molecule was added to the agrin stimulation solution. An 1h incubation with agrin together with either anti-HA antibodies or biotin-alpha-BGT revealed no strong effect on agrin-induced AChR clustering (Fig. 23d,e). However, a long-term incubation with anti-HA antibodies induced AChR clustering (+5%) compared to unstimulated controls (Fig. 23d). Moreover, long-term incubation of agrin together with anti-HA antibodies interfered with agrin-induced AChR clustering (-8%).

Taken together, these data suggest that the binding of antibody or bungarotoxin to tagged MuSK has an influence on its activation and on AChR cluster formation. Tag specific antibodies might crosslink MuSK and thus activate AChR clustering and on the other hand also might inhibit agrin-induced MuSK activation. Therefore, it cannot be ruled out that labeling MuSK via tag specific molecules for immunocytochemistry assays interferes with native MuSK function.
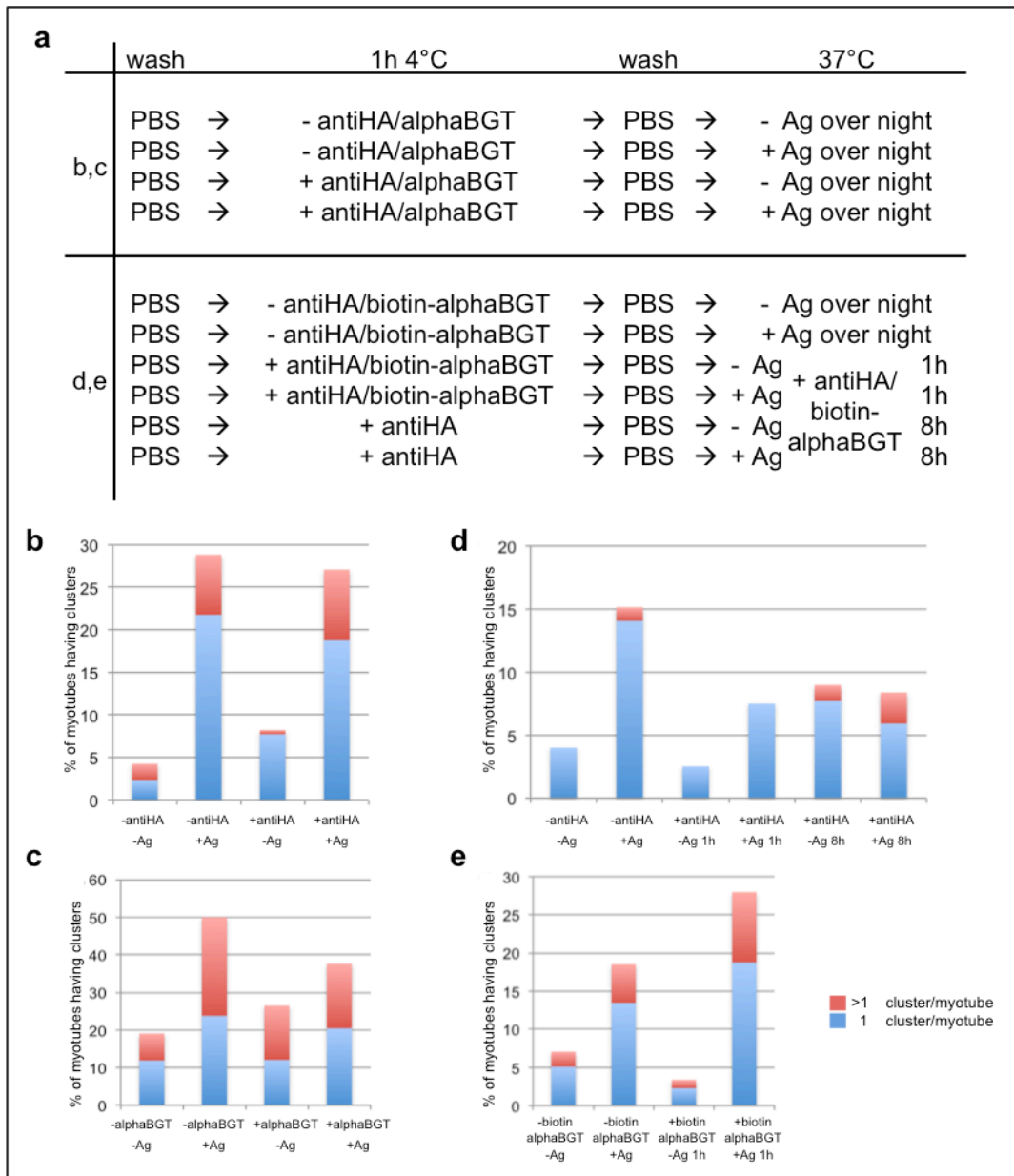
Figure 23 The Effect of Tag Binding on MuSK Activation and AChR Clustering
a. Schema of the preincubation experiments. **b-e.** Myotubes expressing HA-MuSK or BBS-MuSK were treated according to the diagram in (a) and AChR clusters were stained. The number of clusters per tube was counted and the percentages of myotubes forming clusters are plotted. The number of analyzed tubes per sample ranged from 40 to >200. Ag, agrin.

3.2 Generating a Fibroblast Model System for Agrin-Lrp4-MuSK Signaling

3.2.1 Stable Expression of Tagged Lrp4 and MuSK in Mouse Fibroblasts

The generation of several tagged Lrp4 and MuSK variants was the first step towards the development of a new model system for MuSK signaling. We chose a mouse-derived fibroblasts cell system, which was previously used to successfully stably express tagged Lrp4 and MuSK (Bergamin et al., 2010).

NIH3T3 mouse fibroblasts were stably transduced with either tagged Lrp4 or MuSK using a retroviral intermediate. As all constructs were cloned into pBabe-puro expression vectors, the selection of infected cell lines was carried out with puromycin. Additional stable transfections were carried out with pMX expression vectors without puromycin selection. A summary of cell lines expressing alternative tagged proteins is shown in Figure 24a. The used constructs are described in Chapter 3.1. To quantify surface expression of the tagged constructs, living cells were labeled with antibodies against the respective tags and positive labeling was measured by fluorescence activated cell sorting (FACS). Surface FLAG-Lrp4 (L1) was detectable on 13% of the quantified cells, tandem tagged Lrp4 could only be detected on 7% of the cells via the FLAG-tag (Fig. 24a). Among the tagged MuSK constructs, the use of pMX expression vectors exhibited the strongest surface expression with 59% (HA-MuSK M2) and 47% (BBS-MuSK M1) (Fig. 24a).

Lrp4 or MuSK expressing cell lines were selected using a magnetic activated cell sorting (MACS) enrichment method, based on the surface protein labeling. Subsequently, MACS enriched cells were again infected with HA-MuSK, BBS-MuSK or FLAG-Lrp4 respectively, to generate cells expressing tagged Lrp4 and MuSK. Enriched HA-MuSK expressing cells that were infected with FLAG-Lrp4, gained an increase in the surface expression of HA-MuSK from 59% to 90% and good surface expression of FLAG-Lrp4 (31%) (Fig. 24a). As expected from previous experiments in COS-7 cells, BBS-MuSK showed a lower surface expression and enrichment by MACS was not successful.

In further experiments, I used FACS enrichment to simultaneously select cells, which expressed high levels of Lrp4 and MuSK on the cell surface. In Figures 24b and 24d the double positive cell populations, which were selected during the cell sorting, are indicated. For HA-MuSK + FLAG-Lrp4 positive cells (HM cells) it was possible to enrich the amount of Lrp4 expressing cells up to 45% (Fig. 24a,c). Surprisingly, the BBS-MuSK + FLAG-Lrp4 cell line (BM cells) was enriched to ~80% surface expression for both proteins (Fig. 24a,e). Expression of surface MuSK and Lrp4 was assayed by FACS after a period of cell expansion, showing that the expression of MuSK and Lrp4 was not stable. This will be discussed in more detail in the next chapter.

Sorted cells were analyzed for MuSK and Lrp4 expression by immunocytochemistry. While HA-MuSK was highly visible on the cell surface and in intracellular stainings (Fig. 24f), BBS-MuSK was hardly detectable (Fig. 24g). Interestingly, FLAG-Lrp4 was accumulated on the cell surface in randomly distributed patches ranging from 4 to 10µm in length but most of the Lrp4 protein was found intracellularily (Fig. 24f-g).

Although FACS analysis initially faced problems concerning the detection of green fluorescent (Alexa488) binding molecules, which were overcome by using higher concentrations, the generation of double positive cells was convenient. The combination of a stable transduction method based on retroviral infections and two different cell enrichment methods MACS and FACS, yielded two mouse-derived fibroblast cell lines, which expressed tagged Lrp4 and MuSK.


a

NIH3T3	surface (%) FLAG	HA		surface (%) FLAG	HA	BBS
FLAG-Lrp4	**13**	-	→ MACS for FLAG-tag + HA-MuSK*	7	95	-
FLAG-HA-Lrp4	7	11	↗ MACS for FLAG-tag + BBS-MuSK*	8	-	62
HA-FLAG-Lrp4	7	3				
	BBS	HA		FLAG	HA	BBS
HA-MuSK	-	37				
HA-MuSK*	-	**59**	→ MACS for HA-tag + FLAG-Lrp4	31	**90**	-
BBS-MuSK	28	-				
BBS-MuSK*	**47**	-	→ MACS for BBS-tag + FLAG-Lrp4	36	-	**49**
BBS-HA-MuSK	1	15				
BBS-KASGA-HA-MuSK	1	21	AFTER FACS ENRICHMENT	FLAG	HA	BBS
			HM: HA-MuSK* + FLAG-Lrp4	**45**	97	-
			BM: BBS-MuSK* + FLAG-Lrp4	**80**	-	**81**

Figure 24 Generation of a Fibroblast Model System for Agrin-Lrp4-MuSK Signaling
a. Stably transduced NIH3T3 mouse fibroblasts are named corresponding to the stably integrated tagged protein. FACS analysis was performed and the percentages of tag specific positive cells are stated. MACS enrichment was carried out for cell lines with a high number of positive cells (in bold). Enriched cells were again stably transduced with tagged Lrp4 or MuSK. Cell lines expressing HA-MuSK* + FLAG-Lrp4 (HM cells) and BBS-MuSK* + FLAG-Lrp4 (BM cells) were sorted for high Lrp4 and MuSK expression. After these two enrichment steps more than 80% cells were positive for MuSK. The amount of Lrp4 positive cells differed between these two cell lines.

b-c. The FACS plots of unsorted (b) and sorted (c) HM cells are shown. The red area indicates the selected gate for sorting. anti-FLAG antibodies, anti-mouse-Alexa647 antibodies, anti-HA antibodies and anti-rabbit-Alexa488 antibodies were used. **d-e.** The FACS plots of unsorted (d) and sorted (e) BM cells are shown. The red area indicates the selected gate for sorting. anti-FLAG antibodies, anti-mouse-Alexa647 antibodies, biotin-alpha-BGT and streptavidine-Alexa488 were used. **f-g.** Surface and total stainings of sorted HM cells (f) and BM cells (g) are shown. HA-MuSK gives a strong signal, while the BBS-MuSK signal is low. FLAG-Lrp4 is accumulated on the cell surface in patches. anti-FLAG antibodies, anti-mouse-Alexa647 antibodies, anti-HA antibodies, anti-rabbit-Alexa488 antibodies and alpha-BGT-Alexa488 were used. *, pMX vector – others are pBabe-puro; Scalebars, 25 μm.

3.2.2 Stably Transduced Cells Lose Lrp4 Expression during Prolonged Passaging

An issue observed during cell culturing of sorted model system cells was the reduction of cell surface FLAG-Lrp4 over time.

HM cells were kept proliferating for 2.5 weeks. FACS analysis was performed at three time points. While HA-MuSK surface expression was stable over a long period (90%) in the cell line, FLAG-Lrp4 surface expression decreased slowly but continuously (Fig. 25). 46% FLAG-Lrp4 positive cells were detectable after 0.5 weeks, but the amount fell down to 38% and 36% after 1.5 and 2.5 weeks of culturing respectively. Therefore, the estimated double positive cell population decreased from 31% to 27% (Fig. 25; black polygons). The reason for this cell surface Lrp4 reduction is unknown. A possible explanation could be the large size of Lrp4 (~200kDa), which might result in rapid protein removing from the cell surface, difficulties during protein production or ectodomain cleavage.

Summing up, the observed reduction in the cell surface expression of FLAG-Lrp4 over prolonged passaging could cause major problems in experiments with the model system. It is important to work with cell populations of low passage numbers to avoid further reductions in the amount of Lrp4 and MuSK double positive cells.
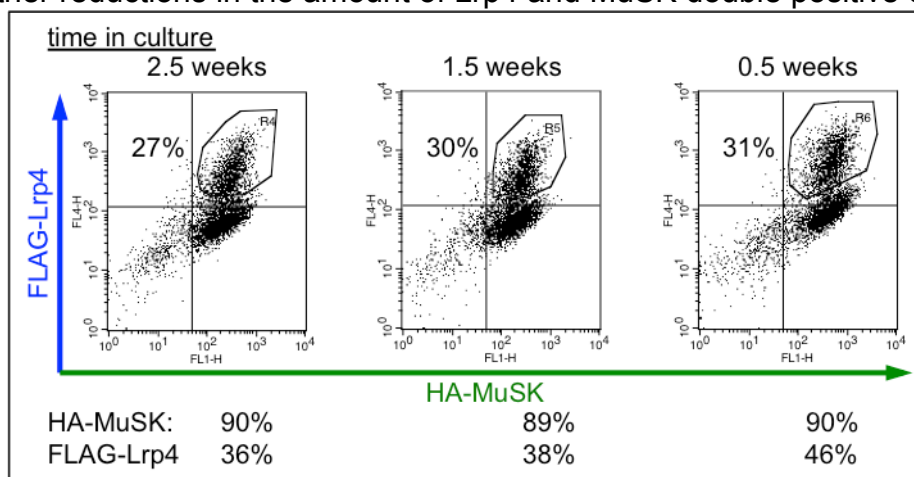

Figure 25 Cell Surface FLAG-Lrp4 is Lost during Cell Passaging
HM mouse fibroblasts were cultured for 2.5 weeks. FACS analysis was performed after 0.5, 1.5 and 2.5 weeks and the corresponding plots are shown. While HA-MuSK surface expression remained stable over the whole period, FLAG-Lrp4 surface expression decreased by 10%. Therefore, the estimated population of double positive cells decreased as well. anti-FLAG antibodies, anti-mouse-Alexa647 antibodies, anti-HA antibodies and anti-rabbit-Alexa488 antibodies were used.

3.2.3 Agrin Stimulation of MuSK and Lrp4 Expressing NIH3T3 Cells Does Not Increase MuSK Phosphorylation

Agrin stimulation of differentiated myotubes induces MuSK phosphorylation and subsequent AChR clustering. Therefore, agrin-induced MuSK phosphorylation represents an important validity criterium for the generated model system.

HM and BM cells were stimulated with agrin for 30min 37°C. MuSK was isolated from lysed cells and the samples were analyzed by IB. Phosphorylated MuSK was detectable for both cell lines (Fig. 26a). However, the strongest phosphotyrosine signals were obtained by IP with anti-HA antibodies. Agrin-induced phosphorylation of MuSK in relation to MuSK expression was quantified (Fig. 26b). While MuSK phosphorylation almost doubled in the HM cell line upon agrin-stimulation in the MuSK IP sample, this was not detectable in the HA IP sample. A clear agrin-dependent change in MuSK phosphorylation was also not visible in the BM cell line.

Taken together, MuSK phosphorylation in response to agrin appears weak and variable in the generated model system cells. Being aware of this major limitation, initial MuSK endocytosis assays were started.
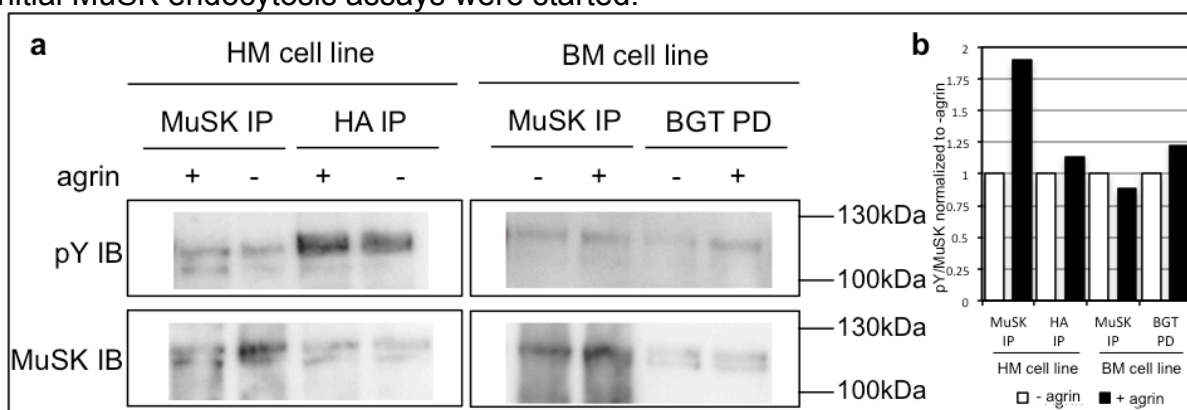
Figure 26 Agrin Stimulation Did Not Increase MuSK Phosphorylation in the NIH Model System
a. HM and BM mouse fibroblasts were stimulated with agrin for 30min at 37°C. After lysis, MuSK was isolated using anti-MuSK antibodies, anti-HA antibodies and biotin-alpha-BGT. Phosphotyrosines (pY) were detected by IB with p99 and p100 antibodies. MuSK was detected by IB using anti-MuSK H25 antibodies. Phosphorylation levels of MuSK are similar between agrin-stimulated and -unstimulated cells. **b.** The signals from the blots in (a) were quantified using ImageLab (BioRad). pY/MuSK intensities from agrin-unstimulated samples were set to 1 and pY/MuSK intensities from agrin-stimulated samples were set into relation. Altough, pY/MuSK signals of MuSK IP samples almost doubled upon agrin stimulation of HM cells, a strong agrin-induced MuSK phosphorylation was not visible in HA IP samples. Agrin-stimulation of BM cells did not provide clear results as well.

3.3 Optimizing Methods for Endocytosis and Live Cell Imaging

3.3.1 Model System Cells Require Special Treatment during Immunocytochemistry Endocytosis Assays

A possible way to assess endocytosis of transmembrane proteins is to fluorescently label the protein of interest while the cell remains at a resting state, followed by enabling endocytosis and detecting internalized labeled proteins. Initial experiments with the newly generated model system demonstrated difficulties in commonly used immunocytochemistry methods. The cells lost their typical morphology during the experiments leading to invalid microscopy images. Therefore, several labeling conditions were evaluated.

According to commonly applied methods for the staining of transmembrane proteins, cells plated on poly-L-lysine (PLL) coated glass coverslips were incubated at 4°C to disable endocytosis. Simulated primary incubations were carried out in PBS supplied with 5% FBS. Afterwards the cells were incubated in a waterbath at 37°C to allow endocytosis for distinct time intervals. Subsequently, primary binding molecules were removed by acidic PBS from proteins that were not internalized. After fixation and permeabilization the cells were incubated with the secondary staining solution. This procedure resulted in round shaped and detached cells, which were impossible to image with the microscope (data not shown).

The strategy to enhance the method involved the changing of the staining buffer and increasing of the resting temperature. As FACS staining methods did not cause great changes in the cell morphology (data not shown), FACS Staining Buffer (FACS-SB) was tested. Additionally, Leibowitz-15 medium (L15), which offers a CO_2 independent cell supply, was used. All buffers were supplied by 5% FBS. However, these buffers did also cause many cells to round up and detach after the primary incubations at 4°C (Fig. 27a). Increasing the temperature to 18°C yielded no success. This morphology changes became even more pronounced after 5 minutes of enabling endocytosis at 37°C.

The successful attempt to solve this issue was to attach the cells of interest at conventional 35mm culture dishes (Greiner), which were coated with gelatin and to perform the endocytosis assay directly on the dish. This change resulted in a sufficient amount of healthy cells after all further steps during the experiment (Fig. 27b). FACS-SB was able to maintain the majority of the cells in perfect morphology.

Concluding, FACS-SB as physiological buffer during surface protein staining on gelatin coated 35mm culture dishes allowed the realization of further endocytosis assays with subsequent cell fixation and imaging.
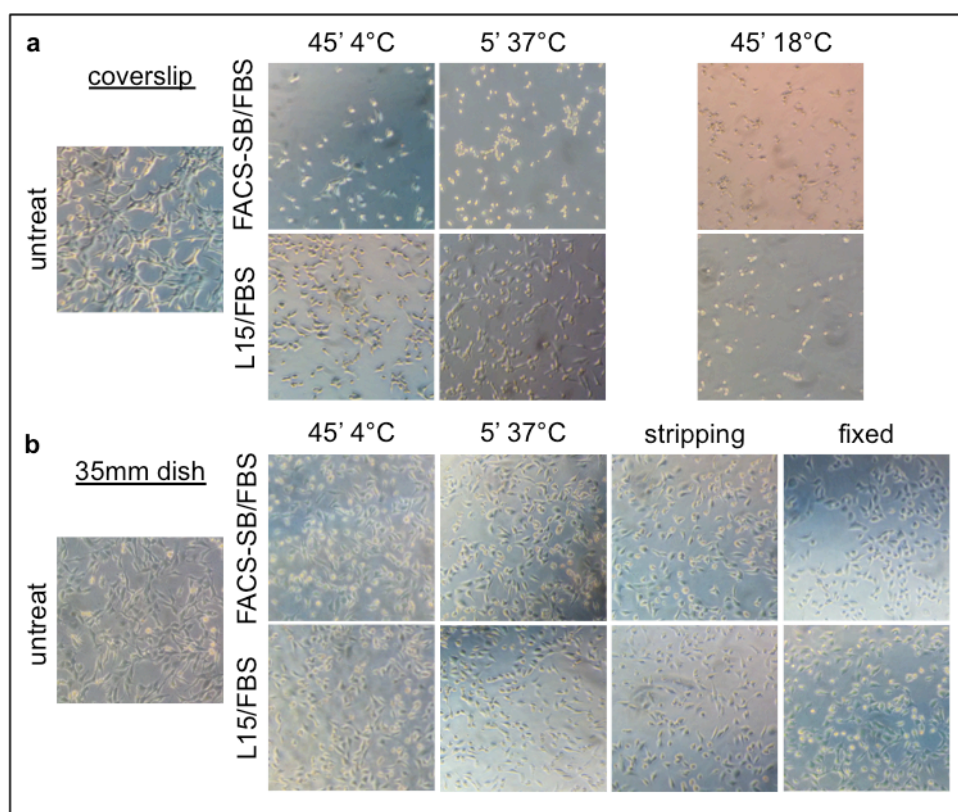
Figure 27 The NIH3T3 Model System Requires Special Treatment
a. HM cells were plated on PLL coated glass coverslips and a surface protein endocytosis assay was simulated. During incubations with primary staining solutions (FACS-SB+5%FBS or L15+5%FBS) for 45min at 4°C the cells become round shaped and detached from the coverslip. Enabling endocytosis in DMEM for 5min at 37°C worsened this effect. Primary incubations carried out at 18°C were without success. **b.** HM cells were seeded on gelatin coated 35mm culture dishes (Greiner). After primary staining incubations in both staining buffers at 4°C and endocytosis at 37°C, the majority of the cells maintained natural morphology. Additionally, after stripping in PBS pH2.6 and after fixation in 4%PFA the cells looked healthy.

3.3.2 The Combination of Ideal Cell Adhesion and Perfect Optical Properties of the Culture Dish Provides the Basis for Live Cell Imaging

Maintaining a stable cell morphology during various staining and imaging procedures is important for acquiring high quality results. As mentioned in the last chapter, a physiological buffer provides a favorable liquid environment for the cell. Live cell imaging was established on Ibidi culture dishes in the Lab, but cell adhesion differed between different dishes and distinct substrates. The substrate composition, however, influenced the quality of the acquired image. Additionally, the differentiation ability of cultured muscle cells was influenced by the substrate. Therefore several combinations were tested for COS-7 cells, C2C12 muscle cells and cultured muscle cells stably expressing HA-MuSK.

Glass has good optical properties for light microscopy, thus a culture dish with a glass bottom is preferred for live cell imaging. This was confirmed with live images of COS-7 cells from an epifluorescence microscope for glass bottom μ-dishes (Ibidi) (Fig. 28). On the contrary, imaging of cells on ibiTreat plastic bottom μ-dishes (Ibidi) produced a spurious fog around the cells. Acquisition with a confocal laser scanning

microscope (Leica), however, yielded sharp and detailed images. These results indicated that the applied epifluorescence live cell imaging set up did not produce high quality images. Moreover, COS-7 cells that were transiently transfected with a Rab5-GFP fusion protein, showed large endosomal aggregations of Rab5 on glass bottom images (Fig. 28). This could be a result of cell stress, which was not visible in transfected cells on plastic bottom dishes. Therefore, ibiTreat plastic bottom μ-dishes were selected for the live cell imaging set up.

An additional focus was live cell imaging of cultured myotubes. Differentiation of myoblasts into myotubes is a very critical step during experiments with muscle cells. HA-MuSK expressing myoblasts only differentiated on gelatin coated ibiTreat μ-Dishes (Fig. 29a). Matrigel or PLL coating interfered with myotube generation. Differentiation of C2C12 muscle cells was tested on different gelatin coated dishes and slides from Ibidi. In reference to the differentiation ability on conventional 35mm culture dishes, the best differentiation status was achieved on μ-dishes with ibiTreat plastic bottom (Fig. 29b). Myotubes on μ-slides with glass or ibiTreat plastic bottom appeared thinner, although this could have resulted from the higher cell density at the beginning.

Summing up, ibiTreat plastic bottom μ-dishes were chosen as best fit for live cell imaging by epifluorescence microscopy. L15 medium was used as physiological buffer during staining and imaging. While NIH3T3 cells were attached on a PLL coat, muscle cells were differentiated preferably on a gelatin coat. COS-7 cells perfectly attached on untreated ibiTreat plastic bottoms.
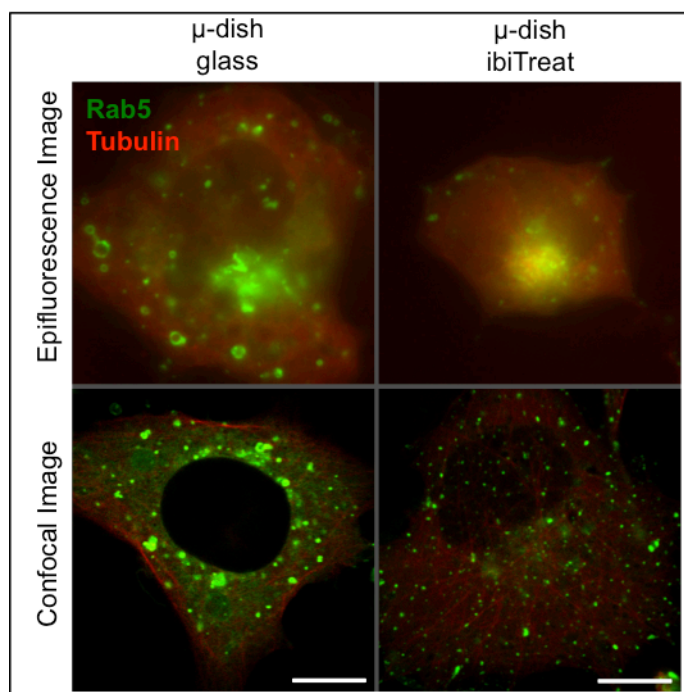
Figure 28 Culture Dishes and Microscopy Methods Influence Image Quality
COS-7 cells were plated on glass and ibiTreat plastic bottom μ-dishes (Ibidi) and were transiently transfected with Rab5-GFP and mCherry-Tubulin. Cells were imaged live with epifluorescence and confocal laser scanning microscopes. Glass bottom dishes yielded better image qualities in epifluorescence microscopy than plastic bottoms. However, the quality of confocal images was never reached. Rab5 accumulations in glass bottom attached cells are a possible evidence for cell stress. Scale bars, 10 μm.
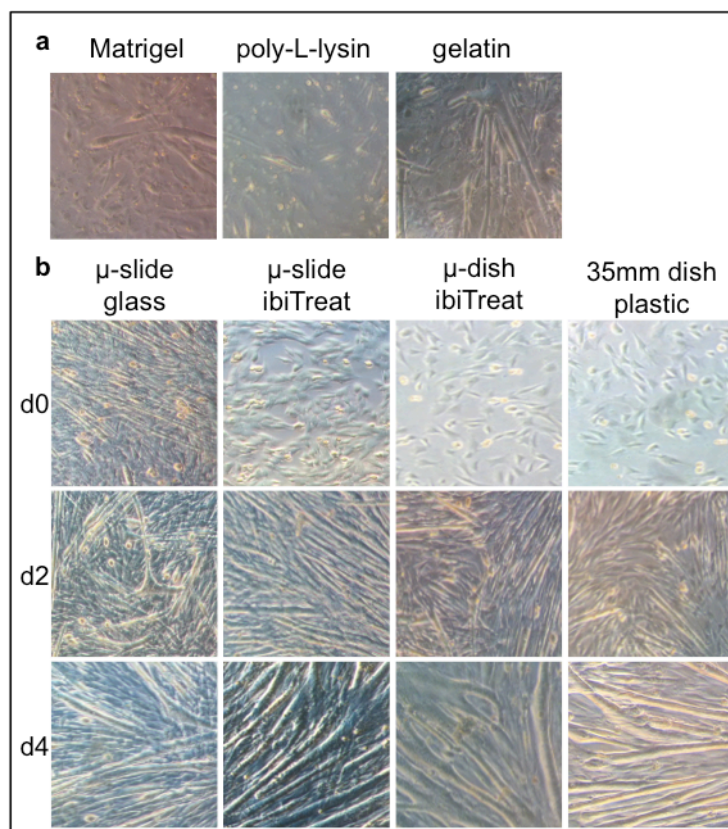
Figure 29 The Substrate for Cell Adhesion Influences the Differentiation of Muscle Cells
a. HA-MuSK expressing myoblasts were plated on Matrigel, PLL or gelatin coated ibiTreat μ-Dishes (Ibidi) and the differentiation status was analyzed 7 days after starting of differentiation. Good shaped myotubes only developed on gelatin coated dishes. **b.** C2C12 myoblasts were seeded on gelatin coated dishes and slides with differently treated surfaces. The best results were achieved on μ-dishes with ibiTreat plastic bottom in reference to conventional 35mm culture dishes after four days of differentiation.

3.4 Endocytosis Assays in the Model System for Agrin-Lrp4-MuSK Signaling

3.4.1 MuSK Colocalizes with Rab5 and Rab7 Positive Compartments

Endocytosis is known as a critical step for RTK signaling. Subsequent trafficking through distinct endosomal compartments is important for sustained receptor activity, receptor recycling and degradation. Initial trafficking experiments for MuSK and Lrp4 were carried out in the newly developed model system.

HM cells were transiently transfected with Rab4-, Rab5-, Rab7- and Rab11-GFP fusion proteins. Colocalization of MuSK, Lrp4 and the endosomal Rab-GFP markers was analyzed. Predominantly, MuSK was found in Rab5 and Rab7 positive compartments (Fig. 30). This indicates that after early endosomal sorting a large amount of MuSK is transported to late endosomes and thus destined for degradation in lysosomes. Consequently, MuSK signaling is likely to be terminated after further trafficking from Rab7 positive compartments. Interestingly, MuSK was not observed

to enter recycling pathways to a great extent. Little colocalization was visible with Rab11 positive compartments, while Rab4 positive vesicles did not contain MuSK (Fig. 30). MuSK trafficking from early endosomes to recycling compartments might be favored instead of a directly Rab4 dependent recycling pathway.

It is still unclear, if MuSK and Lrp4 are endocytosed and trafficked in a di- or tetramerized state through intracellular compartments or if they become separated upon entry in early endosomes due to the intraluminal pH change. Unfortunately, a diffuse staining of Lrp4 did not reveal more detailed information (Fig. 30). It was difficult to exactly define distinct Lrp4 positive vesicles. However, it appeared that there is some colocalization between MuSK and Lrp4, which occurs in Rab5, Rab7 and Rab11 positive compartments. Although, it is possible that MuSK and Lrp4 are transported along the same endosomal pathways, these experiments do not provide any argument about a possible association of these proteins in endosomal compartments and provide no information about the activation status of MuSK.

Summing up, MuSK is likely to be degraded after endocytosis rather than being recycled back to the plasma membrane. This could argue for a prolonged signaling activity during endosomal trafficking until its termination in lysosomes. However, the experimental design does not allow any interpretation on agrin-induced MuSK endocytosis and trafficking, because the cells were not stimulated with agrin. Rather, these experiments resemble baseline background activity and trafficking of MuSK and Lrp4. Additional experiments need to be carried out in order to identify the role of endosomal trafficking upon agrin stimulation and thus to allow an estimation about the processes at a native NMJ.
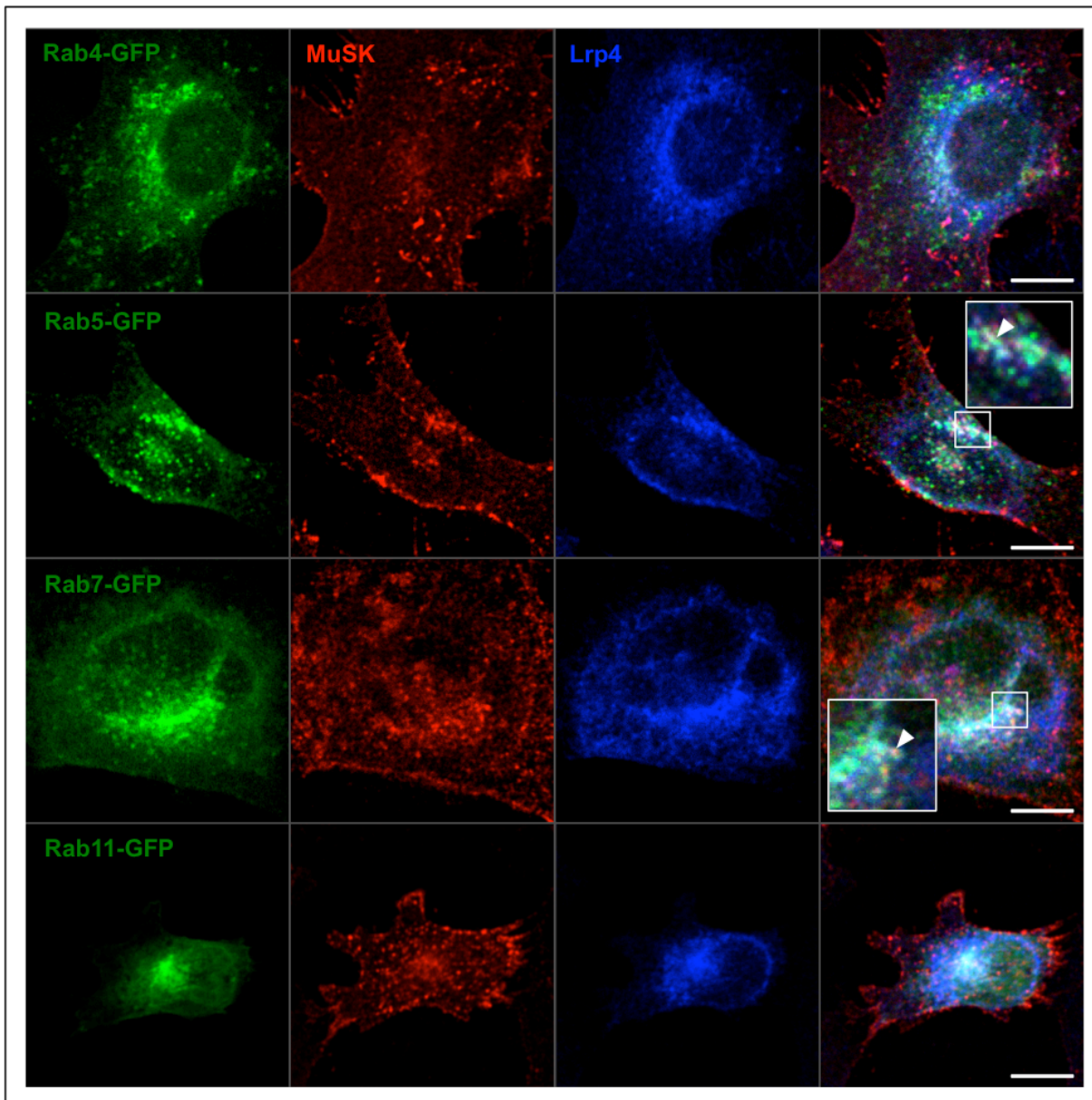
Figure 30 Colocalization Study of MuSK, Lrp4 and Endosomal Compartments
HM cells were plated on PLL coated glass coverslips and were transiently transfected with Rab4-, Rab5-, Rab7- or Rab11-GFP (green). Fixed cells were permeabilized and the total amount of MuSK and Lrp4 was stained. MuSK was visualized via anti-HA antibodies and anti-rabbit-Cy3 antibodies (red) together with the labeling of Lrp4 with anti-FLAG antibodies and anti-mouse-Alexa647 antibodies (blue). The right panel shows overlays of the three corresponding images from the left. MuSK shows less colocalization with Rab4 and Rab11, while MuSK is more often found in Rab5 and Rab7 positive vesicles (white arrowheads e.g.). Although the signal for Lrp4 has bad quality, Lrp4 proteins are contained in all four Rab compartments. Some MuSK and Lrp4 proteins appear colocalized. Scale bars, 10 µm.

3.4.2 The Internalization Process of MuSK Starts within Five Minutes and is Followed by Trafficking to Multivesicular Bodies

An astonishing feature of endocytosis and trafficking of distinct transmembrane proteins is the rapidity in internalization and transport processes. Analyzing how fast MuSK and Lrp4 are internalized and how long they stay in endocytotic compartments might provide insight into their function in signaling at the NMJ.

HM cells were transiently transfected with Rab5- and Rab7-GFP fusion proteins. Surface MuSK and Lrp4 were labeled in living cells via anti-HA and anti-FLAG antibodies, respectively. Cells were put to 37°C to enable endocytosis for several minutes. Subsequently, primary antibodies were removed by acidic PBS from proteins that were not internalized. Labeled proteins that were internalized were specifically visualized with fluorophore coupled secondary antibodies after permeabilization. Fast internalization was detected for Lrp4 (Fig. 31a). Even without endocytotic incubations, Lrp4 was able to internalize into early endosomes and additionally be transported to Rab7 positive compartments. The chosen resting state at 18°C during primary antibody incubation could be a reason for this quick process, as an ideal blocking of endocytosis is achieved at 4°C. However, internalization was not observed for MuSK to such extent. Internalized MuSK was visible in Rab5 positive compartments after 5 minutes of endocytosis, while it was depleted from early endosomes during prolonged endocytosis (Fig. 31a). It is likely that internalized MuSK was transported to Rab7 positive compartments after sorting from early endosomes, as MuSK was detectable in these compartments after 10 minutes of endocytosis. Additional experiments with primary antibody incubations at 4°C confirmed the onset of MuSK internalization between 2 and 5 minutes after enabling endocytosis (Fig. 31b). Expanding endocytosis up to 10 minutes allows internalization of remaining surface proteins and trafficking of already endocytosed proteins.

Summing up, endocytosis of MuSK into early endosomes takes less than 5 minutes and is followed by subsequent transport into late endosomes. Therefore a possible active state for MuSK in endosomal compartments can be ruled out for ~10 minutes or longer. Again, these experiments were carried out without agrin stimulation and thus might only resemble baseline activity of MuSK and Lrp4.
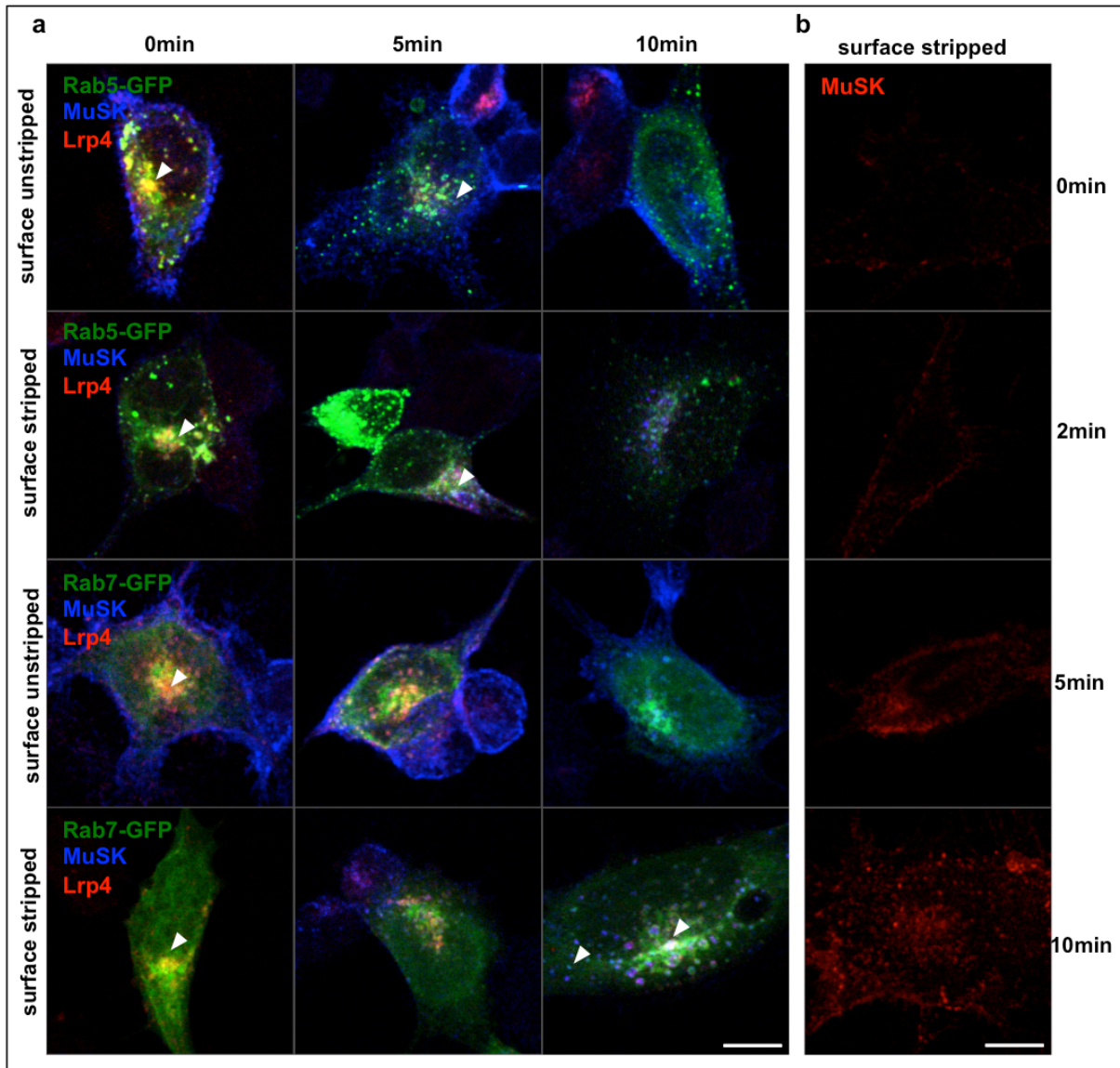
Figure 31 Internalization of MuSK and Lrp4 into Rab5 and Rab7 Positive Vesicles
a. HM cells were plated on PLL coated glass coverslips and were transiently transfected with Rab5- or Rab7-GFP (green). Cells were incubated with primary antibodies against MuSK (anti-HA antibodies) and Lrp4 (anti-FLAG antibodies) in PBS+5%FBS for 45min at 18°C followed by endocytosis in DMEM for defined time intervals at 37°C. Antibodies, which remained on the cell surface were stripped or not stripped. After fixation and permeabilization, MuSK (blue) and Lrp4 (red) were visualized with anti-rabbit-Alexa647 antibodies and anti-mouse-Cy3 antibodies. The internalization process of Lrp4 was strong enough to generate intracellular signals even without enabling endocytosis (0min white arrowheads e.g.). MuSK remained surface located in the first minutes and started to internalize after 5 minutes (5min white arrowheads e.g.) in Rab5 positive vesicles. Upon prolonged endocytosis and trafficking, MuSK was located in Rab7 positive vesicles (10min white arrowheads e.g.). A colocalization of MuSK and Lrp4 was hardly detectable. Lrp4 was localized in Rab7 vesicles rather than in Rab5 vesicles. **b**. HM cells were plated on gelatin coated 35 mm plastic dishes. Cells were incubated with primary antibodies against MuSK (anti-HA antibodies) and Lrp4 (anti-FLAG antibodies) in FACS-SB+5%FBS for 45min at 4°C followed by endocytosis in DMEM for defined time intervals at 37°C. Antibodies, which remained on the cell surface were stripped or not stripped. After fixation and permeabilization, MuSK (red) was visualized with anti-rabbit-Cy3 antibodies. Internalized MuSK can be detected after 5 minutes of endocytosis. Scale bars, 10 µm.

3.4.3   Agrin Stimulation Influences Lrp4 Endocytosis while Internalization of MuSK is Less Affected

Secretion of nerve-derived agrin and subsequent binding to the extracellular domain of Lrp4 initiates MuSK activation. Besides signaling, this might result in enhanced

MuSK endocytosis and trafficking, as it is known for other RTKs. After analyzing MuSK endocytosis in unstimulated model system cells, the next logical step was to perform agrin stimulation.

A similar endocytosis assay as mentioned in the last chapter was carried out for HM cells. Agrin was added during the endocytosis step to reveal its role in endocytosis and trafficking. After 15 minutes of endocytotic activity and stripping off surface attached antibodies, more Lrp4 was internalized in agrin-unstimulated cells compared to stimulated cells (Fig. 32a). During prolonged endocytosis it seems that the amount of endocytosed Lrp4 is reduced in unstimulated cells, indicating a possible degradation of the protein. In agrin-stimulated cells however, the intracellular signal of Lrp4 increased over time, while being weaker as those of unstimulated cells. Further experiments using agrin-stimulated cells with endocytosis intervals of 0-10 minutes and 30-60 minutes should reveal more details on Lrp4 internalization and trafficking.

Unfortunately, the role of agrin on MuSK endocytosis and intracellular trafficking could not be determined in this experiment, as the signal for MuSK was very weak. This could refer to a degradation process, taking place prior to 15 minutes of endocytosis (Fig. 32a). An influence of agrin stimulation on MuSK endocytosis after 15-30 minutes of endocytosis was not detected due to weak immunochemistry signals. Having in mind that agrin stimulation of the generated model system cells did not result in enhanced MuSK phosphorylation (Fig. 26), this outcome is not unexpected.

Comparing the intracellular location of MuSK between agrin-stimulated and -unstimulated model system cells was the next step. HM cells were transiently transfected with Rab5- and Rab7-GFP fusion proteins and stimulated with agrin prior to fluorescently labeling total MuSK and Lrp4 amounts. Early endosomes positive for MuSK were visible only in agrin-stimulated cells, while MuSK was detectable in late endosomes in agrin-stimulated and -unstimulated cells (Fig. 32b).

Summing up, I suggest that agrin can bind to Lrp4 and affect its endocytosis in the model system for agrin-Lrp4-MuSK signaling. However, a subsequent activation of MuSK has not been shown and its endocytosis could not be determined. Future studies with better temporal resolution during endocytosis should produce more valid data.
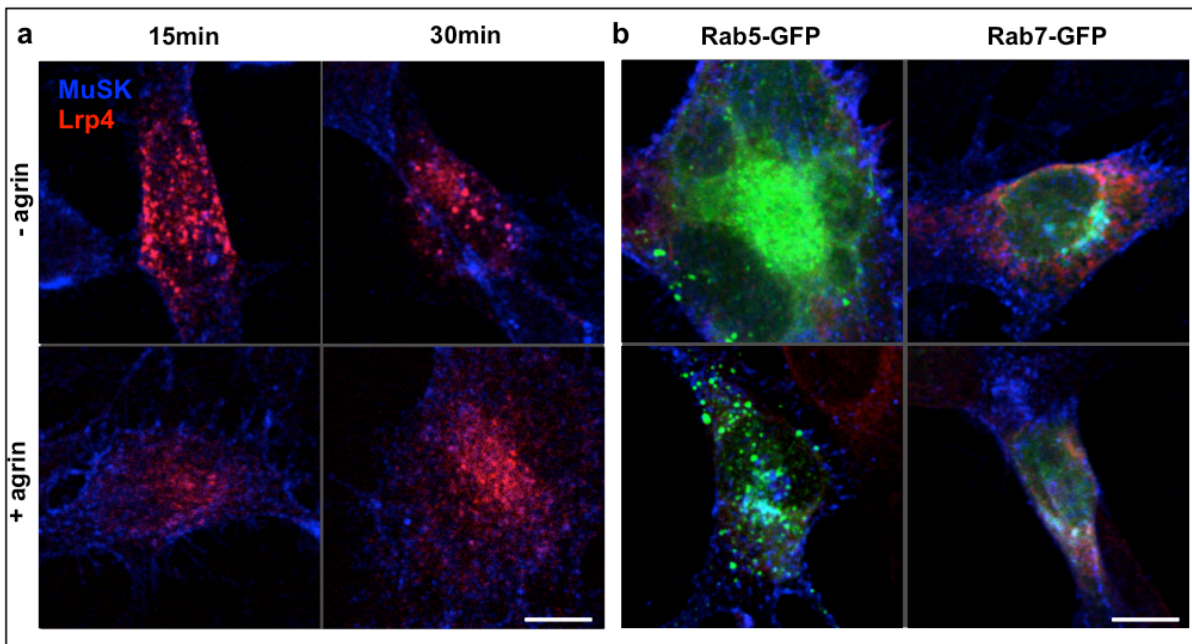
Figure 32 Endocytosis of MuSK and Lrp4 after Agrin Stimulation
a. HM cells were plated on PLL coated glass coverslips. Cells were incubated with primary antibodies against MuSK (anti-HA antibodies) and Lrp4 (anti-FLAG antibodies) in PBS+5%FBS for 45min at 4°C followed by endocytosis in DMEM +/- agrin for defined time intervals at 37°C. Antibodies, which remained on the cell surface were stripped and after fixation and permeabilization endocytosed MuSK (blue) and Lrp4 (red) were visualized with anti-rabbit-Alexa647 antibodies and anti-mouse-Cy3 antibodies. Unstimulated cells show a greater signal for internalized Lrp4 after 15 minutes than stimulated cells. MuSK was weakly detectable in this experiment. **b.** HM cells were plated on PLL coated glass coverslips and were transiently transfected with Rab5- or Rab7-GFP (green). Cells were stimulated with agrin for 2h prior to fixation and staining with the same antibodies used as in (a) was done together with staining of unstimulated controls. When stimulated with agrin, MuSK shows colocalization with Rab5 positive vesicles, while this is reduced in agrin-unstimulated cells. On the contrary, Rab7 positive vesicles contain MuSK in agrin-stimulated and -unstimulated cells. As the Lrp4 signal is too weak, it could not be compared for Rab5 and Rab7 compartments. Scale bars, 10 μm.

3.5 Live Tracking of MuSK

3.5.1 Internalized MuSK is Located in Early Endosomal Structures of Model System Cells for Agrin-Lrp4-MuSK Signaling

The endocytotic routing of MuSK in the model system for agrin-Lrp4-MuSK signaling was investigated by imaging of fixed cells as described in the previous chapter. Another approach focused on live cell imaging. Cell surface located proteins can be labeled by fluorophore coupled binding molecules and their internalization and trafficking can be visualized during imaging of living cells.

HM cells were transiently transfected with a Rab5-GFP fusion protein. Plasma membrane located MuSK was labeled with fluorophore coupled antibodies and was imaged at 37°C. Endocytosed MuSK was visible in Rab5 positive compartments (Fig. 33a). Several MuSK positive early endosomes were tracked in the cell periphery. Additional experiments in transiently transfected COS-7 cells revealed that lately endocytosed MuSK travels along the microtubuli cytoskeleton (Fig. 33b).

Although many limitations and obstacles were faced during setting up live cell imaging, these initial time course experiments confirm MuSK endocytosis into Rab5 positive early endosomes. Future experiments with more valid equipment might allow a deeper insight into this topic.
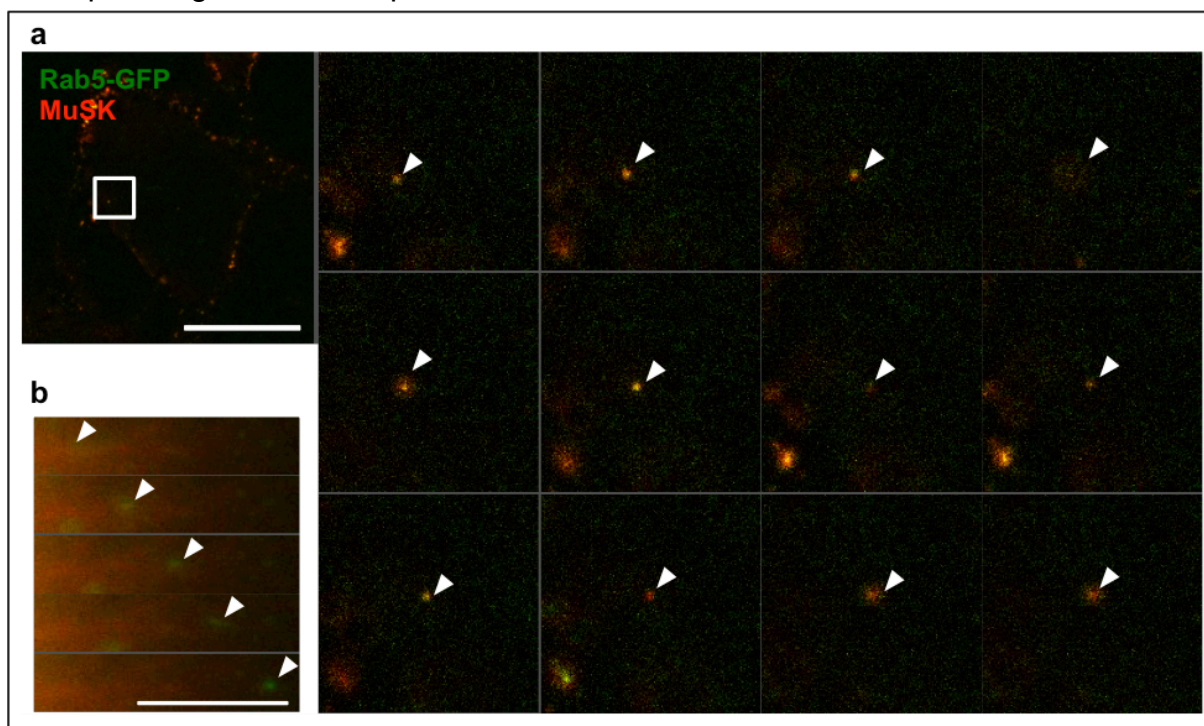
Figure 33 Live Cell Imaging of Model System Cells of Agrin-Lrp4-MuSK Signaling
a. HM cells were plated on PLL coated ibiTreat 35mm dishes (Ibidi) and were transiently transfected with Rab5-GFP (green). Cells were incubated with primary antibodies against MuSK (anti-HA antibodies) in PBS+5%FBS for 45min at 4°C followed by incubation with fluorophore coupled secondary antibodies (anti-rabbit-Cy3 antibodies) in PBS+5%FBS for 45min at 4°C. Subsequently, cells were imaged in prewarmed L15. Images were acquired with filters for GFP and Cy3 every 15 seconds. The shown images focus on a Rab5 and MuSK positive vesicle and represent a time interval (from left to right and top to bottom) of 180 seconds. The indicated vesicle (white arrowhead) is moving slowly until it is out of focus. Scale bar, 20 µm **b.** COS-7 cells were plated on ibiTreat 35mm dishes (Ibidi) and were transiently transfected with MuSK-GFP and mCherry-Tubulin. Images were acquired with filters for GFP and Cy3/mCherry every 5 seconds. The images focus on a MuSK positive vesicle traveling along a microtubule. Scale bar, 10 µm.

4 Discussion and Perspectives

The NMJ is the connection between an alpha motor neuron and a muscle fiber. Correct function of this synapse is of vital importance for the organism. Impairment of characteristic NMJ proteins can cause severe diseases, summarized as myasthenic syndromes. Therefore, the investigation of molecular processes, which contribute to the formation and maintenance of NMJs, is important.

The aim of this master thesis was to generate a heterologous model system for agrin-Lrp4-MuSK signaling and thereby to investigate the endocytotic behavior of the receptor tyrosine kinase MuSK.

4.1 Development of Tagged Proteins

The development of a heterologous model system for agrin-Lrp4-MuSK signaling required tagged MuSK and Lrp4 constructs. The fused affinity tags should permit antibody or bungarotoxin binding to the extracellular domain of these proteins. Subsequently, surface labeled and endocytosed MuSK or Lrp4 can be visualized and tracked during endocytosis. These affinity tags and the generated fusion proteins had to be selected according to important criteria. First, the introduced tag should not interfere with biosynthesis and expression of the fusion protein. Second, the tagged protein has to be correctly incorporated into the plasma membrane. Third, the affinity tag has to be accessible for the corresponding binding molecule. The BBS-tag provides good properties to fulfill these requirements. It was developed to selectively image receptor trafficking by the binding of fluorophore coupled alpha-BGT (Sekina-Aizawa and Huganir, 2004). As the BBS-tag is approximately 10-fold smaller than fluorescent proteins and an alpha-BGT molecule is smaller than antibodies binding to standard tags, the BBS-BGT system is less likely to interfere with the above given criteria (McCann et al., 2005). However, BBS-tagging faced diverse detection problems in COS-7 cells. It was not possible to label BBS-tagged MuSK on the cell surface. Despite of the small size of the BBS-BGT system, a possible explanation could be that the BBS-tag interferes with the tertiary structure of MuSK, which was not observed in previous studies (Sekina-Aizawa and Huganir, 2004). Another explanation could be an overall low protein expression from the introduced vectors.

As MuSK tagged with a haemaglutinin (HA) affinity tag was nicely detectable in immunocytochemistry and immunoblotting assays, the introduction of tandem BBS-HA or HA-BBS tags and linker sequences to separate the BBS-tag from the native protein was assumed to provide a better BBS tagging. Further adoptions included the separation of the signal sequence cleavage site from the BBS-tag, to prevent possible BBS-tag cleavage. However, no improvement in BBS-tagged MuSK detection was yielded. It is most likely that the expression level of BBS-tagged MuSK was insufficient in transfected COS-7 cells compared to HA-tagged MuSK.

The tagging of Lrp4 faced similar problems. As the HA-tag yielded good results in MuSK tagging it was fused with Lrp4, but was not detectable in immunocytochemistry and immunoblotting assays. Better results were obtained by tagging Lrp4 with a FLAG-epitope. The introduction of tandem FLAG-HA or HA-FLAG tags did not improve expression and detection.

4.2 Biological Function of Tagged MuSK

Expression and membrane incorporation of the fusion proteins as well as tag accessibility provide the basic requirements for the application of the developed constructs. Integration of tagged MuSK as a functional protein into its native molecular system at the NMJ is a further challenge. HA-MuSK and BBS-MuSK were expressed in a MuSK deficient muscle cell line, which is incapable of forming AChR clusters upon agrin stimulation. MuSK was immunoprezipitated from myotube lysates and MuSK phosphorylation was increased upon agrin stimulation. Moreover, AChR clusters were formed by agrin-mediated signaling of the tagged MuSK constructs, demonstrating the maintained biological function of HA and BBS tagged MuSK.

A major problem in experimentation with antibody labeling of MuSK and other RTKs has been previously demonstrated in several studies (Hopf and Hoch, 1998; Spaargaren et al., 1991). Antibodies binding MuSK or tagged MuSK induced dimerization of MuSK molecules, resulting in increased MuSK phosphorylation. Moreover, AChR were phosphorylated and accumulated into aggregates upon antibody-mediated MuSK dimerization (Hopf and Hoch, 1998). As expected from these studies, AChR clustering was also altered by HA-specific antibody binding to tagged MuSK, respectively. Incubation with anti-HA antibodies induced AChR cluster formation in HA-MuSK expressing myotubes, while agrin-mediated AChR clustering was reduced. This circumstance is less dominant in the BBS-BGT system, while agrin-mediated AChR clustering was increased during biotin-alpha-BGT incubation of BBS-MuSK expressing myotubes.

Possibilities to overcome this factor are rare but include the application of tag specific Fab fragmented antibodies, which do only bind one epitope. These aspects have to be considered in future projects.

4.3 The Model System for Agrin-Lrp4-MuSK Signaling

Experimentation with muscle cells is laborious and requires differentiation into myotubes, which is a critical but variable step. Having a heterologous model system for agrin-Lrp4-MuSK signaling combines the benefits of a practicable cell system with the advantages of tagged proteins. The NIH3T3 fibroblast model system was ultimately developed with HA-MuSK, BBS-MuSK and FLAG-Lrp4 by retroviral infection. Cells expressing MuSK and Lrp4 in higher amounts were enriched by MACS and FACS. Unfortunately, not all enriched cells expressed both proteins at a similar scale. Lrp4 was far less present at the cell surface. Additionally, the surface located Lrp4 pool was reduced during cell passaging over 2.5 weeks. This could result from a rapid protein removal from the cell surface, while protein production might become stuck. Studies on Lrp4 revealed that the ectodomain is cleaved by metalloproteases in order to modulate signaling processes (Dietrich et al., 2010), which might contribute to the reduction of surface present Lrp4.

In experimentation with the NIH3T3 model system it was demonstrated that agrin stimulation did not increase MuSK phosphorylation. Indeed, this is a prerequisite for a fully functional model of the NMJ, in which agrin binds to Lrp4 and this should be followed by MuSK activation via phosphorylation. Apparently MuSK and Lrp4 proteins are not located in that close proximity at the cell surface, to interact upon agrin binding to Lrp4. Cell surface stainings revealed that Lrp4 is concentrated at distinct regions, while MuSK is more randomly distributed. Therefore it is unlikely that there are enough MuSK and Lrp4 proteins capable of a direct activation cascade for agrin-induced MuSK phosphorylation. Together with possible BBS-tag folding difficulties, low protein expression numbers, interference of the labeling complex with endocytosis, tag-binding-induced MuSK activation and the reduction of Lrp4 expression over time, it remains open if the developed heterologous system represents a good model system for agrin-Lrp4-MuSK signaling.

4.4 Endocytosis of MuSK

Endocytosis of RTKs has been assigned a major role in the regulation of downstream signaling (Goh and Sorkin, 2013). Moreover, MuSK undergoes rapid internalization in response to agrin in muscle cells (Zhu et al., 2008). Initial endocytosis assays in the NIH3T3 model system confirmed that MuSK is endocytosed with and without agrin stimulation. This internalization process took place in approximately 5 minutes, while MuSK was endocytosed and detectable in Rab5 positive early endosomes in unstimulated cells. The results from endocytosis assays with transfected GFP coupled Rab constructs suppose a trafficking route for MuSK from early endosomes to Rab7 positive compartments. This confirms a recent study, which demonstrated MuSK trafficking to lysosomal compartments (Luiskandl et al., 2013). Degradation of MuSK will also represent the end of eventual sustained signaling events of MuSK

after endocytosis. Recycling of MuSK was not detected via the Rab4 positive pathway, while little internalized MuSK protein was colocalized with the Rab11 recycling pathway. However, recycling could have a more crucial role for MuSK, as recent studies revealed MuSK recycling in heterologous cells and a role for AChR pre-patterning in zebrafish (Luiskandl et al., 2013; Gordon et al., 2012). Unfortunately, it was not possible to activate MuSK via the agrin-Lrp4-MuSK pathway in these NIH3T3 model system cells, as MuSK trafficking in response to agrin is a major topic. Endocytosis assays with agrin-stimulated model system cells could not determine MuSK internalization and trafficking. The corresponding agrin-stimulation experiment included endocytosis intervals of more than 15 minutes, but MuSK could have been already internalized and degraded at this time. Therefore, agrin-induced MuSK endocytosis remains unrevealed, as there could be an agrin-mediated effect earlier than 15 minutes. Future agrin stimulation experiments need to be designed for shorter endocytosis times.

4.5 Endocytosis of Lrp4

Endocytosis of Lrp4 was investigated in the NIH3T3 model system in a similar way. Unfortunately, intracellular Lrp4 signals always featured diffused patterns. It was impossible to identify single compartments or vesicles positive for Lrp4. Changes in primary and secondary antibodies and fluorophore variations did not result in better image quality and negative controls did not produce prominent background (data not shown). However, in the acquired images, Lrp4 was located in Rab4, 5, 7 and 11 positive compartments. While the greatest signals were obtained from early and late endosomes, only few Rab4 positive compartments were loaded with internalized Lrp4. In comparison to MuSK, Lrp4 was internalized more rapidly. Again, these data represent baseline activity without agrin stimulation. Stronger signals were detectable for internalized Lrp4 after 15 minutes in agrin-stimulated cells. This could speak for a faster endocytosis process, an accelerated intracellular transport and an accelerated degradation of Lrp4. This hypothesis could explain the detected signal reduction in agrin-stimulated cells. Another possibility is sustained agrin-Lrp4 localization at the plasma membrane, resulting in reduced and slowed endocytosis. Further experiments with shorter and longer endocytosis times need to be designed in order to reveal these issues.

4.6 Perspectives

Recapitulating the discussed results, it has to be mentioned that all conclusions from immunocytochemistry experiments in this master thesis have to be handled with care. Out of many acquired images only representative images were selected for examinations in a qualitative manner. For quantitative assays the amount of reliable images was too low.

Beside conventional cell surface, intracellular and endocytosis staining assays, a focus of this master thesis was on establishing live cell imaging for the NIH3T3 model system and muscle cells. In agrin-unstimulated NIH3T3 model system cells, baseline MuSK endocytosis was confirmed and the uptake into Rab5 positive early endosomes was visible.

It is difficult to give future perspectives regarding the suitability of a heterologous model system for agrin-Lrp4-MuSK signaling. It has to be guaranteed that MuSK and Lrp4 are expressed in detectable levels and that both proteins are evenly distributed over the plasma membrane. The application of a different cell line for the generation of a heterologous cell system could increase the expression level of tagged MuSK and Lrp4. This would be a first step towards agrin-mediated MuSK activation in non-muscle cells. Generating tag specific Fab fragment antibodies and monovalent fluorophore coupled streptavidine would possibly reduce binding molecule induced MuSK activation and additionally decrease the size of the labeling complex, which might interfere with endocytotic processes. It would be of interest, if endocytosis occurs via CME or CIE and therefore colocalization studies with clathrin, caveolin and other markers are essential. An important aspect, which was not addressed in this master thesis, involves sustained MuSK signaling after endocytosis. Colocalization assays with MuSK phosphotyrosine specific antibodies and markers of intracellular compartments would refer to trafficking routes of MuSK in combination with its signaling activity. As live cell imaging of molecular processes is a great tool in natural sciences, further development of the live imaging set up is mandatory. The ultimate goal of these studies is to reproduce and confirm MuSK and Lrp4 trafficking in muscle cells.

5 Materials and Methods

5.1 Consumables

Table 2| Consumables

Type	Source
Cell Strainers	BD Biosciences
Cell Scraper	/
FACS Tubes	BD Biosciences
Microscope Slides Assistent Elka	Karl Hecht
Multipipette Plus	Eppendorf
Rotilabo Folded Filters, Type 600P	Carl Roth
Glass Cap-O-Dest Vials	/
Glass Coverslips (d=18mm, 22x22mm)	Gerhard Menzel
Gloves (nitrile, latex)	various
Immobilion-P PVDF Membrane 0.45µm	EMD Millipore
Parafilm	American National Can
Pasteur Pipettes	Carl Roth
Petri Dishes	Greiner Bio One
Pipette Tips (10µl, 200µl, 1000µl, BeadTips)	Biozym Scientific, Fisherbrand, PeqLab
Rotilab 1.5 Blotting Paper	Carl Roth
Safe-Lock Tubes (PCR, 1.5ml, 2ml)	Eppendorf
Screw Tubes (1.5ml, 15ml, 50ml)	Starlab
Silicone Fat	/
Snap-Cap Tubes (5ml, 10ml)	BD Biosciences
Tissue Culture Steriles (Pipettes, Dishes, Plates, Tubes, Cryovials, ...)	Cellstar, CytoOne, Greiner Bio One, Ibidi, IWAKI, Nunc, Starlab, ThermoFisherScientific

5.2 Chemicals and Reagents

Table 3| Chemicals and Reagents

Type	Source
2-Propanol	Carl Roth
3-(N-morpholino)propanesulfonic acid (MOPS)	Carl Roth
4-(2-hydroxyethyl)-1-piperazineethanesulfonic acid (HEPES)	Carl Roth
Acetic Acid	Carl Roth
Agar Agar	Carl Roth

Agarose	Biozym Scientific
Ammonium Persulfate (APS)	Carl Roth
Ampicillin Sodium Salt (Amp)	Carl Roth
Aprotinin	Carl Roth
beta-Mercaptoethanol	Carl Roth
Bovine Serum Albumine (BSA)	Sigma Aldrich
Bromphenol Blue	Carl Roth
Calcium Chloride ($CaCl_2$)	Carl Roth
Carbon dioxide (CO_2)	/
Chicken Embryo Extract (CEE)	Herbst-Lab
Coomassie Brilliant Blue G250	Carl Roth
Bidistilled Water (ddH_2O)	EMD Millipore
Deoxycholic Acid (DOC)	Carl Roth
Dimethyl Sulfoxide (DMSO)	AppliChem
Deoxy Nucleoside Triphosphates (dNTPs)	Fermentas
DulbecCOS Modified Eagle Medium (DMEM)	Sigma Aldrich
Ethanol	Merck
Ethidium bromide	Carl Roth
Ethylene Glycol Tetraacetic Acid (EGTA)	Amresco
Fetal Bovine Serum (FBS)	Sigma Aldrich
Gelatin	Sigma Aldrich
GeneJet Gel Extraction Kit	Fermentas
GeneRule 1kB DNA Ladder	Fermentas
Gentamycin	Carl Roth
Glycerol	Fisher Chemical
Glycine	Carl Roth
Hank's Balanced Salt Solution (HBSS)	Gibco
Horse Serum (HS)	Gibco
Hydrogen Chloride (HCl)	Carl Roth
Imidazole	Sigma Aldrich
Immersion Oil 518F	Carl Zeiss
Immobilon Western HRP Substrate	EMD Milipore
Interferon Gamma	/
Kanamycine Sulfate (Kan)	Carl Roth
LB-Medium (LB)	Carl Roth
Leibovitz-15 Medium (L15)	Gibco
Leupeptin	Roche
Lumilight Westernblotting Substrate HRP	Roche
Magnesium Chloride ($MgCl_2$)	Fluka
Methanol	Carl Roth
Milk Powder	Carl Roth
GeneJet Plasmid Miniprep Kit	Fermentas
Mowiol-488	Sigma Aldrich
N,N-Bis(2-hydroxyethyl)-2-aminoethanesulphonic Acid sodium salt (BES)	Carl Roth
Neural Agrin 4.8	Herbst and Burden, 2000
Nonyl Phenoxypolyethoxylethanol (NP-40)	Sigma Aldrich
Page Ruler Plus Prestained Protein Ladder	Fermentas
Page Ruler Prestained Protein Ladder	Fermentas
Paraformaldehyde (PFA)	Fluka
Penicillin/Streptomycin (P/S)	Sigma Aldrich
Pepstatin	US Biological
Phenylmethylsulfonyl Fluoride (PMSF)	Carl Roth
Polybrene	Sigma Aldrich
Poly Ethylene Glycol (PEG)	Carl Roth
Poly-L-Lysine (PLL)	Sigma Aldrich
Polyacrylamide 40% (PAA)	Carl Roth

Potassium Chloride (KCl)	Carl Roth
Potassium Dihydrogen Phosphate (KH$_2$PO$_4$)	Carl Roth
Potassium Hydrogen Phosphate (K$_2$HPO$_4$)	Carl Roth
Protein-A-Agarose Beads	Roche
Protein-A-Sepharose Beads	Amersham Biosciences
Protein-G-Agarose Beads	Roche
Q5 Site-Directed Mutagenesis Kit	New England Biolabs
Restriction Enzymes + 10x Buffers	Fermentas, New England Biolabs
Shrimp Akaline Phosphatase (SAP) + 10x Buffer	Fermentas
SOC Outgrowth Medium (SOC)	New England Biolabs
Sodium Acetate Trihydrate (NaOAc)	Carl Roth
Sodium Acide (NaN$_3$)	Carl Roth
Sodium Chloride (NaCl)	Carl Roth
Sodium Dihydrogen Phosphate (NaH$_2$PO$_4$)	Carl Roth
Sodium Dodecyl Sulfate (SDS)	Carl Roth
Sodium Fluoride (NaF)	Fluka
Sodium Hydrogen Phosphate (Na$_2$HPO$_4$)	Carl Roth
Sodium Hydroxide (NaOH)	Carl Roth
Sodium Orthovanadate	Sigma Aldrich
Streptavidine Particles Plus DIM	BDIMag
Streptavidine-Agarose Beads	Novagen
T4-DNA-Ligase + 10x Buffer	Fermentas
Q5 Hot Start High-Fidelity DNA Polymerase	New England Biolabs
Tetramethylethylenediamine (TEMED)	Carl Roth
Triethanolamine (TEA)	Carl Roth
Tris Base	Carl Roth
Tris Hydrochloride (Tris-Cl)	Carl Roth
Triton-X-100	Promega, Roth
Trypsin-EDTA (TE)	Sigma Aldrich
Turbofect	Fermentas
Tween-20	Carl Roth

5.3 Solutions and Buffers

Table 4| 10x Phosphate Buffered Saline (10xPBS)

Reagent	Concentration
NaCl	1.37mM
KCl	27mM
Na$_2$HPO$_4$	43mM
KH$_2$PO$_4$	14mM
ddH$_2$O	
pH	7.3

working solution = 1x in ddH$_2$O; The solution was stored ad RT.

Table 5| 10x Tris-Buffered Saline Tween20 (10xTBS-T)

Reagent	Concentration
1M Tris-Cl pH8	100mM
NaCl	1.5M
Tween-20	0,5%
ddH$_2$O	

working solution = 1x in ddH$_2$O; The solution was stored ad RT.

Table 6| 10x Transferbuffer for Immunoblotting

Reagent	Amount
Tris Base	30.1g
Glycine	144g
ddH$_2$O	ad 1000ml

working solution = 1x in ddH$_2$O with 10% Methanol for transfer of proteins smaller than 100kDa and without Methanol for transfer of proteins larger than 100kDa; The solution was stored ad RT.

Table 7| 2x BES Buffered Saline (2xBBS)

Reagent	Amount
5M NaCl (autoclaved)	5.6ml
1M BES	5.0ml
1M Na$_2$HPO$_4$	150µl
ddH$_2$O (autoclaved)	Ad 100ml

Solution was adjusted to pH 6.95 (+/-0.02 variance) with 10M NaOH. Solution was filtered sterile with 0.2µm filter and aliquots were frozen at -4°C.

Table 8| 4% Paraformaldehyd (4%PFA)

Reagent	Amount
PFA	0.8g
0.5M NaOH	50µl
1x PBS	ad 20ml

The solution was stirred at ~80°C until PFA was completely dissolved. After filtration the solution was stored at -20°C until use. Once thawed the solution was ready to use for not longer than 2 weeks and was kept at 4°C.

Table 9| 4x SDS-PAGE Loading Dye (4xSDS-LD)

Reagent	Concentration
1M Tris-Cl pH6.8	240mM
beta-Mercaptoethanol	8%
20% SDS	8%
Glycerol	40%
ddH$_2$O	
Bromphenol Blue	few

The solution was stored at -20°C.

Table 10| 5x Potassium Calcium Magnesium Buffer (5xKCM)

Reagent	Concentration
KCl	0.5M
CaCl$_2$	0.15M
MgCl$_2$	0.25M
ddH$_2$O	

The solution was stored ad RT.

Table 11| 5x SDS-PAGE Running Buffer (5xSDS-Running Buffer)

Reagent	Concentration
Tris Base	0.12M
Glycine	0.96M
SDS	0.017M
ddH$_2$O	

working solution = 1x in ddH$_2$O; The solution was stored ad RT.

Table 12| 50x Trisbase Aceticacid EDTA Buffer (TAE)

Reagent	Amount

Tris Base	242g
Acetic Acid	57.1ml
0.5M EDTA	100ml
ddH$_2$O	1000ml

working solution = 1x in ddH$_2$O; The solution was stored ad RT.

Table 13| Differentiation Medium for C2C12 Cells (C2DM)

Reagent	Concentration
HS	2%
P/S	1%
DMEM	

The solution was produced under sterile conditions with sterile reagents and stored ad 4°C. The solution was prewarmed in a waterbath at 37°C prior to use.

Table 14| Differentiation Medium for MuSK Deficient Muscle Cells (C3DM)

Reagent	Concentration
FBS	10%
HS	10%
P/S	1%
DMEM	

The solution was produced under sterile conditions with sterile reagents and stored ad 4°C. The solution was prewarmed in a waterbath at 37°C prior to use.

Table 15| 0.2% Gelatin

Reagent	Concentration
Gelatin	0.2%
PBS	

The solution was produced under sterile conditions with sterile reagents and stored ad 4°C.

Table 16| Growth Medium for C2C12 Cells (C2GM)

Reagent	Concentration
FBS	15%
CEE	0.25%
P/S	1%
DMEM	

The solution was produced under sterile conditions with sterile reagents and stored ad 4°C. The solution was prewarmed in a waterbath at 37°C prior to use.

Table 17| Growth Medium for MuSK Deficient Muscle Cells (C3GM)

Reagent	Concentration
FBS	10%
HS	10%
CEE	0.25%
Interferon Gamma	0.2%
P/S	1%
DMEM	

The solution was produced under sterile conditions with sterile reagents and stored ad 4°C. The solution was prewarmed in a waterbath at 37°C prior to use.

Table 18| Growth Medium for COS-7, NIH3T3, Phoenix Cells (GM)

Reagent	Concentration
FBS	10%
P/S	1%
DMEM	

The solution was produced under sterile conditions with sterile reagents and stored ad 4°C. The solution was prewarmed in a waterbath at 37°C prior to use.

Table 19| Growth Medium for C2C12 (C2GM)

Reagent	Concentration
FBS	15%
CEE	0.25%
DMEM	

The solution was produced under sterile conditions with sterile reagents and stored ad 4°C. The solution was prewarmed in a waterbath at 37°C prior to use.

Table 20| Coomassie Staining Solution

Reagent	Amount
Coomassie Brilliant Blue G250	0.25g
Methanol	45ml
Acetic Acid	10ml
ddH_2O	45ml

The solution was stored ad RT.

Table 21| HNTG Lysis Buffer (HNTG)

Reagent	Concentration
HEPES	20mM
NaCl	150mM
Triton X-100	1%
Glycerol	10%
EGTA	1mM
$MgCl_2$	1.5mM
Sodium Orthovanadate	1mM
ddH_2O	

The solution was stored at 4°C.

Table 22| LB Medium (LB)

Reagent	Amount
LB	25g
ddH_2O	ad 1000ml

The solution was stirred at RT until most of the LB was dissolved. After autoclaving the solution was cooled to ~40°C and antibiotics (50µg/ml ampicillin or 25µg/ml kanamycin) was added. The solution were stored at 4°C.

Table 23| LB Petri Dishes

Reagent	Amount
LB	25g
Agar Agar	15g
ddH_2O	ad 1000ml

The solution was stirred at RT until most of the LB was dissolved. After autoclaving the solution was cooled to ~40°C and antibiotics (100µg/ml ampicillin or 50µg/ml kanamycin) were added. The solution was poured into Petri Dishes and incubated at RT for 2 days. Dishes were stored at 4°C.

Table 24| Lysis Buffer plus Inhibitors

Reagent	Dilution Factor
Pepstatin 0.5mg/ml (Etanol)	1:500
Leupeptin 1.0mg/ml (ddH_2O)	1:1000
Aprotinin 1.0mg/ml (ddH_2O)	1:1000
Sodium Orthovanadate 200mM (ddH_2O)	1:200

PMSF 100mM (Etanol)	1:500
Lysis Buffer (HNTG, NP-40 or RIPA)	

Inhibitors (stored at -20 and -80°C) were thawed and added to cold lysis buffer. PMSF was added last into the cap of the tube followed by inverting the tube. The solution was immediatley used at 4°C.

Table 25| Magnetic Activated Cell Sorting Buffer (MACS Buffer)

Reagent	Concentration
FBS	3%
PBS	

The solution was produced under sterile conditions with sterile reagents freshly and was put on ice.

Table 26| Mowiol

Reagent	Amount
Mowiol 4-88	2.4g
Glycerol	6.0g
ddH$_2$O	6.0ml
0.2M Tris-HCl	12ml

Glycerol and Mowiol were mixed and dissolved by frequent agitation at RT for 1h. ddH$_2$O was added and stirred at RT for 1h. Tris-HCl was added and incubated at 50°C for 2h while stirring every 20min for 2min. Solution was centrifuged at 5000 g-force for 15min. The supernatant was aliquoted into 1.5ml tubes, frozen and stored at -20°C. For embedding, an aliquot was thawed on ice and kept at 4°C until used.

Table 27| NP-40 Lysis Buffer (NP-40)

Reagent	Concentration
NP-40	1%
EGTA	5mM
NaCl	50mM
TEA pH7.5	30mM
NaF	50mM
ddH$_2$O	

The solution was stored at 4°C.

Table 28| Radioimmunoprecipitation Assay Lysis Buffer (RIPA)

Reagent	Concentration
HEPES	20mM
NaCl	150mM
SDS	0.1%
DOC	0.5%
Triton X-100	1%
NaF	5mM
EDTA	2.5mM
ddH$_2$O	

The solution was stored at 4°C.

Table 29| SDS-PAGE Running Gels

Reagent	Amount for one 1.5mm Gel		
	6% PAA	7.5% PAA	10%PAA
40% Acrylamide	1.5ml	1.88ml	2.5ml
SDS-PAGE Running Gel Buffer	2.5ml	2.5ml	2.5ml
ddH$_2$O	5.84ml	5.4ml	4.84ml
10% SDS	100µl	100µl	100µl
10% APS	50µl	50µl	50µl

TEMED	10µl	10µl	10µl

The solution was immediately used.

Table 30| SDS-PAGE Stacking Gels

Reagent	Amount for one 1.5mm Gel 5%PAA
40% Acrylamide	0.625ml
SDS-PAGE Running Gel Buffer	1.25ml
ddH$_2$O	3.025ml
10% SDS	50µl
10% APS	50µl
TEMED	5µl

The solution was immediately used.

Table 31| SDS-PAGE Running Gel Buffer

Reagent	Amount
Tris Base	90.8g
HCl	10.9g
ddH$_2$O	ad 500ml
pH	8.5

The solution was stored at RT.

Table 32| SDS-PAGE Stacking Gel Buffer

Reagent	Amount
Tris Base	0.24g
Tris-Cl	7.56g
ddH$_2$O	100ml
pH	6.8

The solution was stored at RT.

Table 33| FACS Staining Buffer (FACS-SB)

Reagent	Concentration
Tris Base	0.24g
Tris-Cl	7.56g
ddH$_2$O	100ml
pH	6.8

The solution was stored at RT.

Table 34| Transformation Storage Buffer (TSB)

Reagent	Concentration
PEG	10%
DMSO	5%
MgCl$_2$	10mM
MgSO$_4$	10mM
LB	

The solution was used icecold.

5.4 Equipment and Software

Table 35| Equipment and Software

Type	Source
4°C Room, 4°C Refrigerators, -20°C Freezers	various
Analytical Balance ABS	Kern
Axiovert-200 Microscope for Live Cell Imaging + 100x PlanNeoFluar 1.30Oil Ph3 Objective + additional Equipment + Metamorph Software	Carl Zeiss, EMBL, Lambda, VisitronSystems, Ludl Electronic Products Ltd., Molecular Devices
Cell Count Chamber	Neubauer
Cell Culture Incubator	Binder
Centrifuge 5010	Eppendorf
ChemiDoc XRS+ and ImageLab	Bio Rad
DM IL TC Microscope	Leica
Dri-Block Heater DB-2A	Techne
DM IRB Epifluorescence Microscope + 63x HCX PL APO 1.40-0.60 Oil Objective + additional Equipment + Metamorph Software	Leica, VisitronSystems, Molecular Devices
FACSCalibur Cell Analyzer + CellQuestPro Software	BD Biosciences
Ice Machine	/
ImageJ	National Institutes of Health
Incubation Shaker Unitron	Infors HAT
Laboratory Shaker 3016	GFL
Laminar Flow	Holten
LSRII Flow Cytometer	BD Biosciences
Magnet for 5ml Snap-Cap Tubes	/
Magnetic Stirring Hotplate 3001	Heidolph
Microcentrifuge 5415D	Eppendorf
Microcentrifuge 5417R	Eppendorf
Microcentrifuge 5424	Eppendorf
MZ 16F Microscope + IM1000	Leica
N_2 Dewar	KGW Isotherm
Nanodrop 2000	PeqLab
Pipette Boys	various
Pipettes	Gilson, Eppendorf
Photoshop 7.2	Adobe
Power Pac 200 / HC	Bio Rad
Rotator	VWR
SDS-PAGE and Agarose-GE Equipment	various
SP5 Confocal Laser Scanning Microscope + LAS-AF + LAS-AF-Lite	Leica
Thermal Cycler C1000	Bio Rad
Thermomixer	PeqLab, Eppendorf
Trans Blot Turbo	Bio Rad
Ultra Turrax	IKA
Universal 32 Centrifuge	Hettich
UV-Lamp, Camera and Printer	PeqLab
Vacuum Pumps	various
Varifuge 3.0R	Heraeus
various Foreceps	various
Vortexer	VWR, IKA
Waterbaths (37°C, 56°C)	GFL

5.5 Plasmids

Table 36| Plasmids

Name (Vector/Gene)	Source	Resistance	Construct
BS/HA-MuSK	unknown	Amp^R	M2
BS/LRP4	S. Burden	Amp^R	
BS/MuSK	R. Herbst	Amp^R	
CMV/HA-MuSK	R. Herbst	Amp^R	M2
pBabe-puro/BBS-HA-MuSK	R. Herbst, A. Höbartner	Amp^R	M6
pBabe-puro/BBS-KASGA-HA-MuSK	R. Herbst, A. Höbartner	Amp^R	M7
pBabe-puro/BBS-MuSK	R. Herbst, M. Sharma	Amp^R	M1
pBabe-puro/Dok7-HA	S. Burden	Amp^R	
pBabe-puro/FLAG-HA-LRP4	R. Herbst, A. Höbartner	Amp^R	L3
pBabe-puro/FLAG-LRP4	unknown	Amp^R	L1
pBabe-puro/FLAG-LRP4-mCherry	unknown	Amp^R	
pBabe-puro/FLAG-LRP4-mCherry	unknown	Amp^R	
pBabe-puro/GFP-LRP4	unknown	Amp^R	
pBabe-puro/HA-FLAG-LRP4	R. Herbst, A. Höbartner	Amp^R	L4
pBabe-puro/HA-LRP4	R. Herbst, A. Höbartner	Amp^R	L2
pBabe-puro/HA-MuSK	R. Herbst, M. Sharma	Amp^R	M2
pBabe-puro/LRP4	S. Burden	Amp^R	
pBabe-puro/MuSK	unknown	Amp^R	
pBabe-puro/MuSK-GFP	unknown	Amp^R	
pcDNA/BBS-BBS-MuSK	R. Herbst	Amp^R	M3
pcDNA/BBS-AADCA-MuSK	R. Herbst	Amp^R	M4
pcDNA/DNVP-BBS-KASGA-HA-MuSK	A. Höbartner	Amp^R	M10
pcDNA/BBS-HA-MuSK	R. Herbst, A. Höbartner	Amp^R	M6
pcDNA/BBS-KASGA-HA-MuSK	R. Herbst, A. Höbartner	Amp^R	M7
pcDNA/BBS-KTARA-HA-MuSK	R. Herbst, A. Höbartner	Amp^R	M8
pcDNA/BBS-MuSK	R. Herbst, M. Sharma	Amp^R	M1
pcDNA/BBS1-MuSK	R. Herbst, A. Höbartner	Amp^R	M1
pcDNA/GG-BBS-HA-MuSK	R. Herbst	Amp^R	M9
pcDNA/HA-BBS-MuSK	R. Herbst, A. Höbartner	Amp^R	M5
pcDNA/prl-BBS-MuSK	R. Herbst	Amp^R	M1
pCDNA3	unknown	Amp^R	
pEGFP C1	B. Murray	Kan^R	
pEGFP/Rab11	H. Sitte/R.Lodge	Kan^R	
pEGFP/Rab4	H. Sitte/R.Lodge	Kan^R	
pEGFP/Rab5	H. Sitte/R.Lodge	Kan^R	
pEGFP/Rab7	H. Sitte/R.Lodge	Kan^R	
pMT21	B. Murray	Amp^R	
pMT21/BBS-MuSK	B. Woller, S. Parzer	Amp^R	M1
pMX/BBS-MuSK	A. Höbartner	Amp^R	M1
pMX/FLAG-LRP4-mCherry	unknown	Amp^R	
pMX/HA-MuSK	A. Höbartner	Amp^R	M2
unknown/tubulin-mCherry	G. Vendra	Kan^R	

All generated and preexisting plasmids are written. Not all were needed for the discussed experiments. The work on tag generation and cloning was done in tight collaboration with R. Herbst, B. Woller, S. Parzer and M. Sharma.

5.6 Oligonucleotides

Table 37| Oligonucleotides

Name	Sequence 5'-3'
DNVP1-Forward	GTACCATGGCGGTACTACGAGAG
DNVP1-Reverse	GTAATCGGAAACTACTCCTTGGCAC
DNVP-Forward	GTTCCATGGCGGTACTACGAGAG
DNVP-Reverse	GTTATCGGAAACTACTCCTTGGCAC
Lrp4-HA-Forward	GATTATGCGGGGGGGVGVTTGTGCSTGTGGTCGGAGC
Lrp4-HA-Reverse	CGGCACATCATACGGATACTCCAGACTGCTGGCTATTC
Lrp4-AatlI-Forward	GTCGCATGTGCATGTGGTCGGAGC
Lrp4-AatlI-Reverse	GTCCAGACTGCTGGCTATTC

All oligonucleotides were produced by Sigma. Only oligonucleotides used by A.Höbartner are shown.

5.7 Antibodies and Bungarotoxins

Table 38| Antibodies and Bungarotoxins

Name	Source	Short Name	Dilution
alpha-bungarotoxin	Sigma	alpha-BGT	ICC: 1:500
alpha-bungarotoxin Alexa 488	Invitrogen	alpha-BGT-488	ICC/FACS: 1:500
alpha-bungarotoxin Alexa 594	Invitrogen	alpha-BGT-594	ICC: 1:500
alpha-bungarotoxin biotinylated	Molecular Probes	biotin-alpha-BGT	ICC/FACS/PD: 1:500 WB: 1:250
choleratoin FITC	Sigma		ICC: 1:200
donkey anti mouse Alexa Fluor 488 conjugate	JIR	anti-mouse-Alexa488	ICC/FACS: 1:1000
donkey anti mouse Alexa Fluor 647 conjugate	JIR	anti-mouse-Alexa647	ICC/FACS: 1:1000
donkey anti mouse Cy3	JIR	anti-mouse-Cy3	ICC: 1:1000
goat anti clathrin HC (C-20)	Santa Cruz	anit-clathrin	ICC: 1:200; 1:100
goat anti mouse HRP conjugate	JIR	anti-mouse-HRP	WB: 1:5000
goat anti rabbit Alexa Fluor 488 conjugate	JIR	anti-rabbit-Alexa488	ICC/FACS: 1:1000
goat anti rabbit Alexa Fluor 647 conjugate	JIR	anti-rabbit-Alexa647	ICC/FACS: 1:1000
goat anti rabbit Cy3	JIR	anti-rabbit-Cy3	ICC: 1:1000
goat anti rabbit HRP conjugate	JIR	anti-rabbit-HRP	WB: 1:5000
mouse anti acetylcholine receptor alpha	BD Biosciences	anti-AchRalpha	ICC/WB: 1:200
mouse anti actin AC-40	Sigma Aldrich	anti-actin	WB: 1:1000
mouse anti caveoliln-1	BD Biosciences	anti-caveolin	ICC: 1:100; 1:50
mouse anti early endosome antigen 1	BD Biosciences	anti-EEA1	ICC: 1:100; 1:50
mouse anti FLAG tag (M2)	Sigma Aldrich	anti-FLAG	ICC/WB: 1:400
mouse anti GFP	Santa Cruz	anti-GFP	WB: 1:1000
mouse anti goat Alexa Fluor 647 conjugate	JIR	anti-Goat-Alexa647	ICC: 1:800
mouse anti HA tag Alexa Fluor 647 conjugate	Cell Signaling	anti-HA-Alexa647	ICC/FACS: 1:400
mouse anti rab-5	BD Biosciences	m-anti-Rab5	ICC: 1:200
p100: pTyr 9411	Cell Signaling	p100	WB: 1:2000

p99: p-Tyr SC 7020	Santa Cruz	p99	WB: 1:1000
rabbit anti FLAG tag Alexa Fluor 647 conjugate	Cell Signaling	anti-FLAG-Alexa647	ICC/FACS: 1:100
rabbit anti FLAG tag biotinylated	Cell Signaling	biotin-anti-FLAG	ICC/FACS: 1:100
rabbit anti HA tag	Sigma Aldrich	anti-HA	ICC/FACS: 1:400; IP: 1:1000
rabbit anti HA tag biotinylated	Cell Signaling	biotin-anti-HA	ICC/FACS: 1:400
rabbit anti MuSK (H25) serum	Diederichs and Herbst, 2007	anti-MuSK H25	WB: 1:250
rabbit anti c-term MuSK 94277+94279	Herbst and Burden, 2000	anti-MuSK	IP: 1:1000
rabbit anti rab-5	Cell Signaling	r-anti-Rab5	ICC: 1:100
streptavidine 450	unknown	streptavidine 450	FACS: 1:250
streptavidine 605	unknown	streptavidine 605	FACS: 1:250
streptavidine FITC	unknown	streptavidine FITC	FACS: 1:250
streptavidine PE-Cy7	unknown	streptavidine PE-Cy7	FACS: 1:250
streptavidine Alexa Fluor 488 conjugate	JIR	streptavidine-Alexa488	ICC/FACS: 1:1000; 1:250
streptavidine Alexa Fluor 647 conjugate	JIR	streptavidine-Alexa647	ICC/FACS: 1:1000
streptavidine Cy3 conjugate	JIR	streptavidine-Cy3	ICC/FACS: 1:1000
streptavidine HRP conjugate	Cell Signaling	streptavidine-HRP	WB: 1:2000

All used antibodies and bungarotoxins are written. Not all were needed for the discussed experiments.

5.8 Cell Lines and Bacterial Strains

Table 39| Original Cell Lines

Name	Source	Information
C2C12	Herbst-Lab	various passages
MuSK$^{-/-}$ mouse muscle cell	Herbst-Lab	various passages
COS-7	Herbst-Lab	various passages
NIH3T3	Herbst-Lab	used for stable transduction
NIH3T3	M. Kunze	used for stable transduction
Phoenix	Herbst-Lab	used for stable transduction
Phoenix	Ellmeier-Lab	used for stable transduction

Table 40| Bacterial Strains

Name	Source	Information
E.Coli	Herbst-Lab	chemically competent
E.Coli #C2987	New England Biolabs	5-alpha competent

5.9 Molecular Biology Methods

5.9.1   Preparation of Competent *E.Coli* Bacteria

From a dilution streak of competent *E.Coli*, one colony was inoculated into 4ml LB and incubated on a shaker (220rpm) at 37°C overnight. From this overnight culture 1ml was added to 100ml of prewarmed LB and incubated on a shaker (220rpm) at 37°C until an OD_{600} value of 0.3 – 0.6 was reached. Then the bacterial culture was set on ice (4°C) and centrifuged at 5000rpm for 5min in 50ml tubes. After discharging the supernatant, the bacterial pellet was resuspended in icecold TSB immediately and aliquots were frozen and stored at -80°C.

5.9.2   Enzymatic DNA Restriction

For enzymatic restrictions of DNA, enzymes and buffers supplied by Fermentas or New England Biolabs were used. Buffer/Enzyme combinations for double digests and concentrations of buffer ingredients for sequential double digests were used according to the manufacturers' protocols. Control digests were mostly done in a 20µl volume containing 1µl DNA solution, 0.5-1µl restriction enzyme, buffer and ddH_2O. Digests for cloning were done in 30µl or 40µl volumes, containing proper DNA amounts (3µg e.g.), 1µl restriction enzyme, buffer and ddH_2O. Digests were vortexed, spinned and incubated at 37°C for 1-2h.

5.9.3   Agarose Gel Electrophoresis

To analyze DNA strands and fragments, agarose gels with agarose percentages corresponding to DNA length were poured (0.8% agarose in 50ml TAE e.g.) and loaded with 5µl DNA ladder and a DNA sample, which was premixed with 5x DNA loading dye. Agarose gels were run at 100V in TAE until desired separation of DNA bands was reached. Gels and buffers were supplied by total 5µl Etidium bromide. Visualization and imaging was done using UV light.

5.9.4   Agarose Gel Extraction

To purify DNA from agarose gels, the desired band was cut out and DNA was extracted with GeneJet Gel Extraction Kit according to its protocol. By running 1µl elution on an agarose gel and comparing the bands intensity to 5µl DNA ladder bands, the concentration of the eluted DNA samples was estimated.

5.9.5   DNA Dephosphorylation

To dephosphorylate linear DNA fragment ends produced by enzymatic restrictions and to prevent re-ligation, shrimp alkaline phosphatase and its corresponding buffer supplied by Fermentas were used. The reaction was mostly done in a 10.5µl volume containing 9µl of digest, 1µl 10xSAP Buffer and 0.5µl SAP Enzyme. After incubation at 37°C for 30min, heat inactivation was done at 65°C for 15min. The reaction was then used for ligation.

5.9.6   DNA Ligation

For the ligation of two DNA fragments (vector and insert) T4-DNA-ligase and its buffer supplied by Fermentas were used. Vector and Insert were digested with restriction enzymes producing compatible ends. Vector and insert DNA were mostly applied at a molar ratio 1:5. Vector to insert calculations were carried out with the following equation:

$$\frac{Vector\,[ng] * Insert\,[kb]}{Vector\,[kb]} * molar\,Ratio\left[\frac{Insert}{Vector}\right] = Insert\,[ng]$$

The reaction was done in a 20µl volume containing vector and insert DNA, 1µl T4-DNA-ligase, 2µl 10x T4-DNA-ligase buffer and ddH$_2$O. After incubation at RT for 2-4h, the ligation was used for transformation into competent bacteria.

5.9.7   Transformation of Competent Bacteria with DNA Ligations

For the transformation of ligated DNA fragments the full ligation reaction volume was supplied with 20µl 5x KCM, 60µl ddH$_2$O and 100µl recently thawed chemical competent bacteria (*E.Coli*). After an initial incubation on ice for 30min, a heat shock was applied at 42°C for 2min and the reaction was put back on ice. 900µl LB were added and the reaction was incubated at 37°C for 30min. After centrifugation at full speed for 1min, the pellet was resuspended in 100-150µl of the supernatant and plated on LB dishes with selection medium. The dishes were incubated at 37°C overnight. A control transformation without insert DNA was always carried out as described above.

5.9.8   Transformation of Competent Bacteria with Plasmid DNA

For the transformation of plasmids 1µl DNA, 10µl 5x KCM, 40µl ddH$_2$O and 50µl recently thawed chemical competent bacteria (*E.Coli*) were mixed and incubated on ice for 15min. A heat shock was applied at 42°C for 2min and the reaction was put back on ice. 900µl LB were added and the reaction was incubated at 37°C for 15min.

100µl of the reaction was plated on LB dishes with selection medium and dishes were incubated at 37°C overnight.

5.9.9   Bacterial Overnight Cultures

To obtain an overnight culture of a single bacterial colony, one colony was picked from a culture dish with a tip and was inoculated into 5ml LB supplied by selection medium.
For a high volume overnight culture, 50µl of a bacterial culture were inoculated into up to 20ml LB supplied by selection medium.
To obtain an overnight culture from a glycerol stock culture, a small amount of the glycerol stock culture was scraped off with a tip and inoculated into 5ml (or more) of LB supplied by selection medium.
The cultures were then incubated on a shaker (220rpm) at 37°C overnight.

5.9.10   Plasmid Mini Preparation

To obtain pure plasmid DNA from a bacterial overnight culture, GeneJet Plasmid Miniprep Kit from Fermentas was used according to the manufacturers' protocols.

5.9.11   DNA Sequencing

Microsynth AG carried out sequencing of Plasmid DNA sections to confirm correct ligations/mutations. Therefore a 15µl volume containing 1.2µg DNA in ddH$_2$O was sent to Microsynth AG to perform a Barcode Economy Run Service with selected standard primers. To run sequencing with premixed primers, the desired primer was added to the reaction at a 2µM concentration. Results were obtained by email at the next day.

5.9.12   Q5 Site-Directed Mutagenesis Kit

The Q5 Site-Directed Mutagenesis Kit supplied by New England Biolabs was used to insert new DNA sequences into existing protein coding DNA open reading frames. This procedure required several following working steps:
  Primer Design
      This step was accomplished using the online tool NEBaseChanger v1.1 from New England Biolabs.
  Primer Ordering
      Calculated oligonucleotides were ordered from and supplied by Sigma Aldrich.
  Polymerase Chain Reaction
      For this step the following reaction schemes were used:

Table 41| Q5 PCR Reaction Scheme

Reagent	Concentration
Q5 Hot Start High-Fidelity 2x Master Mix	1x
10µM Forward Primer	0.5µM
10µM Reverse Primer	0.5µM
Template DNA (10ng/µl)	10ng
ddH$_2$O	

Table 42| Q5 PCR Custom Reaction Scheme I

Reagent	Concentration
Q5 5x Reaction Buffer	1x
10µM Forward Primer	0.5µM
10µM Reverse Primer	0.5µM
Template DNA (10ng/µl)	10ng
Hot Start T4 DNA Polymerase	1U/40µl
ddH$_2$O	

Table 43| Q5 PCR Custom Reaction Scheme II

Reagent	Concentration
High Fidelity 5x DNA Polymerase Buffer	1x
10µM Forward Primer	0.5µM
10µM Reverse Primer	0.5µM
Template DNA (10ng/µl)	10ng
Hot Start High Fidelity DNA Polymerase	1U/40µl
100mM dNTPs	10mM
ddH$_2$O	

The reaction volumes were set to 12.5µl, 25µl or 40µl and divided to 3, 6 or 8 single reactions, respectively.

Following cycling conditions were used:

Table 44| Q5 PCR Cycling Conditions

Step	Temperature	Time
Initial Denaturation	98°C	30sec
	98°C	10sec
30 Cycles	Annealing	30sec
	72°C	2.5min
Final Extension	72°C	2min
Hold	4°C	forever

The annealing temperature was chosen according to the primer sequence and was usually used as a gradient.

PCR Agarose Gel Electrophoresis

4µl of the PCR product were analyzed on an agarose gel. The correct band was eluted from the agarose gel and DNA concentration was measured.

Kinase Ligase DpnI Reaction

For this 5µl volume reaction, ~30ng eluted PCR product were used, supplied by 2x KLD Reaction Buffer, 10x KLD Enzyme Mix and ddH$_2$O. The reaction was incubated at RT for 10-15min.

Transformation

To 2.5µl KLD reaction 25µl chemically competent *E.Coli* or C2987 *E.Coli* were added and incubated on ice for 30min. After heat shock at 42°C for 30sec and a following incubation at RT for 5min, 950µl of LB or SOC Outgrowth Medium was added and gently shaken at 37°C for 1h. 100µl of this reaction were plated on LB dishes with selection medium and dishes were incubated at 37°C overnight.

5.10 Cell Culture Methods

5.10.1 Thawing Cells

Cells frozen at -80°C or in liquid nitrogen were thawed by incubating the cryovial with the cell suspension in a waterbath at 37°C. After the suspension was thawed, it was transferred into a 15ml tube under (from now on) sterile conditions, immediately. Approximately 5ml of growth medium were added drop-wise and were carefully resuspended. The suspension was centrifuged at 1500rpm for 5min and the supernatant was discarded. The cell pellet was resuspended in fresh prewarmed growth medium and plated in desired concentrations.

5.10.2 Freezing Cells

Cells growing on a culture dish were trypsinized and pelleted. The cell pellet was resuspended in 1ml freezing medium, transferred into a cryovial and frozen and stored at -80°C. Normal growth medium supplied by 20% serum and 10% DMSO was used as freezing medium.

5.10.3 Trypsinizing Cells

To detach adherent cells from the culture dish, all medium was discarded and cells were incubated in 1ml prewarmed TE at 37°C for maximum 5min (muscle cells were incubated at 33°C for ~3min). Cells were resuspended in the culture dish with 5ml growth medium and transferred into a 15ml tube. Cells were centrifuged at 1500rpm for 5min and the supernatant was discarded. The cell pellet was resuspended in fresh medium for further use.

5.10.4 Counting Cells

To count the cell number in a suspension, 10µl of the suspension were put into a cell count chamber by Neubauer. Under the tissue culture microscope cells were counted

and averaged from 4 big quadrants (1mm x 1mm), each consisting of 16 small quadrants (0.25mm x 0.25mm). This value approximates the cell number in 0.1µl of suspension.

5.10.5 C2C12 Cell Line

The mouse C2C12 myoblast cell line was originally obtained by Yaffe and Saxel in 1977. Reaching confluent state, under serum decrement these cells can differentiate into myotubes. C2C12 myoblasts were grown in C2GM at 37°C and 5%CO_2 atmosphere. Cells were split every 2 to 3 days at ~80% confluence. For differentiation into myotubes cells were plated on gelatin coated culture dishes. After reaching 90-100% confluence differentiation was started by changing the medium to C2DM. Medium was changed every 24h until myotube formation was complete after 4 days.

5.10.6 MuSK$^{-/-}$ Mouse Muscle Cell Line

The MuSK deficient myogenic cell line was originally obtained from MuSK knockout mice by Mazhar and Herbst in 2012. These cells contain a temperature-sensitive SV40 large T antigen.
Thus, at 33°C and the presence of interferon gamma differentiation is inhibited and the cells are proliferating. At 37°C and absence of interferon gamma the cells start to differentiate into myotubes. Myoblasts were grown in C3GM at 33°C and 6%CO_2 atmosphere. Cells were split every 2 to 3 days at ~80% confluence. For differentiation into myotubes cells were usually plated on gelatin coated culture dishes. After reaching 90-100% confluence, differentiation was started by changing the medium to C3DM and transferring cells to 37°C and 5%CO_2. Medium was changed every 24h until myotube formation was started after 3 days. Then medium was changed to C2DM until myotube formation was complete after another 3 to 4 days.

5.10.7 COS-7, NIH3T3 and Phoenix Cell Lines

The COS-7 fibroblast cell line was originally obtained from *Cercopithecus aethiops* kidney tissue by Gulzman in 1981. It contains DNA sequences for expression of SV40 T antigen. The NIH3T3 fibroblast cell line was originally obtained from *Mus musculus* embryonic tissue by Todaro and Green in 1962. The Phoenix cell line was constructed via integrating gag-pol and env constructs for ecotropic and amphotropic viruses into the HEK293T cell line (human embryonic kidney tissue), by Kinsella and Nolan in 1996. COS-7, NIH3T3 and Phoenix Cell were grown in GM at 37°C and 5%CO_2 atmosphere. Cells were split every 2 to 3 days at ~80% confluence.

5.10.8   Culture Dish and Cover Slip Coating

Gelatin Coating of Culture Dishes

The bottom of the culture dish was covered with 0.2% gelatin and incubated at RT for ~15min. For coating of Ibidi 35mm dishes 400µl of coating solution were used. The solution was discarded and the culture dish was washed with PBS prior to cell seeding.

Poly-L Lysine Coating of Ibidi 35mm Culture Dishes

The bottom of the culture dish was covered with 400µl 0.1% PLL and incubated at RT for 1h. The solution was discarded and the culture dish was washed with PBS prior to cell seeding.

Poly-L Lysine Coating of Ibidi 35mm Culture Dishes

The bottom of the culture dish was covered with 400µl 0.1% PLL and incubated at RT for 1h. The solution was discarded and the culture dish was washed with PBS prior to cell seeding.

Matrigel Coating of Ibidi 35mm Culture Dishes

20µl of Matrigel were applied to the center of the culture dish and evenly distributed with a custom made glass Drigalski-spattle. The solution was dried at RT and cells were directly seeded.

Poly-L Lysine Coating of Glass Coverslips

Coverslips were washed in 70% Ethanol, dried and incubated in 0.1% PLL at RT for 5min. Coverslips were drained and PLL was hardened at 60°C for 1h. Prior to cell seeding, coated coverslips were sterilized under UV for 5min.

5.10.9   Calcium-Phosphate Transfection Method

Day before Transfection

Cells were seeded on 6 well plates with $3.0*10^5$ cells per 2ml per one well.

Day of Transfection

2xBBS and 0.25M $CaCl_2$ (sterile filtrated 0.2µm) were quick thawed and placed at RT. DNA for transfection was prepared into sterile, round bottom, polystyrene tubes. For transfection of one well of a 6well plate 4-5µg DNA were mixed with 175µl 0.25M $CaCl_2$. 175µl 2xBBS were added slowly and drop-wise while vortexing. After 13min the solution was added gently and drop-wise on top of the cells. Cells were incubated at 37°C and 5%CO_2 atmosphere.

Day 1 after Transfection

Medium was replaced with fresh medium ~15h after transfection.

Day 2 after Transfection

Cells and supernatant were ready to use for further procedures.

5.10.10 Turbofect Transfection Method

Day before Transfection

Cells were seeded according to Table 45.

Day of Transfection

DNA was prepared in sterile, round bottom, polystyrene tubes. DMEM was added and briefly mixed with DNA by resuspending. Turbofect was added and the solution was vortexed for 10sec. Volumes are given in Table 45. After incubation at RT for 15-20min the solution was added gently and drop-wise on top of the cells. Cells were incubated at 37°C and 5% CO_2 atmosphere.

Day 1 after Transfection

Cells were ready to use for further procedures.

Table 45| Turbofect Transfection Method

Dish Size / GM Volume	Cell Number	Total DNA	GFP	DMEM	Turbofect
1well of 24well plate / 0.5ml	~$8.0*10^4$	0.5µg	25ng	50µl	1µl
1well of 12well plate (+/- coverslip) / 1ml	~$1.0*10^5$	1µg	50ng	100µl	2µl
3.5cm Ibidi dish / 2ml	~$3.5*10^5$	3µg	/	200µl	4µl
6cm dish / 5ml	~$6.0*10^5$	5µg	200ng	500µl	10µl

5.10.11 Stable Transduction Method

For the stable transduction retroviral vector systems were used. pBabe-puro and pMX vectors containing desired DNA constructs were first transfected with calcium-phosphate method into Phoenix cells capable of producing Group-specific antigen (gag), reverse transcriptase (pol) and envelope protein (env) to generate viral particles containing desired DNA. Virus particles were then delivered to target cells for infection and stable integration of the viral genome (containing desired DNA) into the target cells' genome. Following procedure was accomplished:

Day 1

Phoenix cells were seeded according to calcium-phosphate method.

Day 2

Phoenix cells were transfected with calcium-phosphate method.

Day 3

Medium was changed on transfected Phoenix cells.

Day 4

Target cells were seeded for stable transfection at $1*10^5$ cells per one 6well in 2ml medium.

Day 5

The viral supernatant of Phoenix cells was collected and centrifuged at 3000rpm for 10min. The supernatant was transferred into sterile, round bottom, polystyrene tubes and mixed with Polybrene for a 5ng/ml final concentration. This solution was then added on top of aspirated target cells

and incubated for 4h or overnight at cell corresponding environment. Afterwards the solution was changed to normal cell corresponding GM.

Day 6

The day after infection cells were split in a 1:8 ratio. If antibiotic selection was desired for pBabe-puro vector infections, puromycin was added to GM at 2µg/ml, 3µg/ml or 6µg/ml concentrations.

Following Days

GM +/- puromycin was changed every 2 days. Selected cells were ready to use for further procedures after complete negative selection on control plates, or directly after splitting without selection. Selected cells were cultivated with decreased puromycin concentrations.

5.10.12 Clonal Selection of Muscle Cells

To generate a cell population originating from one single cell clone the following procedure was done. Myoblasts, which were derived from MuSK deficient muscle cells, were seeded on 10cm dishes with 100, 200 and 500 cells per dish and cultivated without splitting until single separated colonies were visible, ~1 week after seeding. At that point single colonies were marked on the bottom of the dish with a waterproof marker by looking against a light source. After aspirating the medium and washing with PBS, autoclaved cut pipette tips were coated with silicon fat and set on top of the single colonies. 50µl prewarmed TE were put onto the colony into the tip and incubated at 33°C and 6%CO_2 atmosphere for ~5min. In the meantime 1ml of prewarmed C3GM was aliquoted into 12well plates and labeled. For each colony, 100µl C3GM from the corresponding well were added to the tip, resuspended and transferred into the well. The cells were then cultivated without splitting until the well was 80% confluent. Then each colony was split 1/3 to a 6cm dish for further cultivation and 2/3 to a gelatin coated 3.5cm dish for differentiation. Differentiated cells were stained for acetylcholine receptor clusters or were used for MuSK immunoprecipitation. Ideal clones were further cultivated from the 6cm dish and early passages were frozen.

5.10.13 Agrin 4.8 Preparation

Agrin 4.8 was already available in the lab and had not to be produced for this master thesis. The following procedure explains the preparation of agrin 4.8. 1*10^6 HEK293T cells were plated on a 10cm dish (37°C and 5%CO_2 atmosphere) for calcium phosphate transfection with plasmid DNA containing the carboxyterminal half of agrin on the next day. 15h after transfection the medium was changed to DMEM supplied by 1%P/S and 10%FBS and the cells were incubated at 37°C and 5%CO_2 atmosphere for 48h. The medium was transferred into a 15ml tube and centrifuged at 1500rpm for 5min. The supernatant was tested for the optimal concentration used for

stimulation of myotubes by biochemical methods. The supernatant was stored at 4°C and used at optimal concentrations.

5.10.14 Agrin Stimulation

For acetylcholine receptor cluster assays of differentiated myotubes (3.5cm dish) cells were washed with PBS once and incubated in 2ml DMEM supplied by 12µl agrin solution per ml DMEM at 37°C and 5%CO_2 atmosphere overnight.

For immunoprecipitation assays of differentiated myotubes (3,5cm or 10cm dish) cells were washed with PBS once and incubated in 2ml or 4ml DMEM, respectively at 37°C and 5%CO_2 atmosphere for 2h. Then DMEM was changed to 2ml or 4ml DMEM supplied by 15µl agrin solution per ml DMEM and was incubated at 37°C and 5%CO_2 atmosphere for 0.5h to 1h.

5.10.15 Chicken Embryo Extract Preparation

Fertilized chicken eggs were bred for 13 days at 38°C with continuously tilting and turning three times a day. Eggs were opened under sterile conditions, embryos were removed from eggs and polled. Eyes were taken out and embryos were transferred to an equal volume of icecold HBSS. Embryos were then homogenized in HBSS by an ultra turrax on ice. The homogenate was then centrifuged at 3000rpm for 10min. The supernatant was transferred to fresh tubes and was agin centrifuged at 9000rpm for 20min. The supernatant was aliquoted, frozen and stored at -80°C. Aliquots were thawed at room temperature and refrozen at -20°C for soon consumption.

5.10.16 Bungarotoxin and Antibody Preincubation of Myotubes

To stimulate differentiated myotubes for acetylcholine receptor cluster assays with alpha-BGT, biotin-alpha-BGT or anti-HA antibodies on 3.5cm dishes, cells were washed with PBS once and incubated in 2ml DMEM supplied by alpha-BGT (1:500), biotin-alpha-BGT (1:500) or anti-HA antibodies (1:400) at 4°C for 1h. Afterwards, cells were washed with PBS and incubated with or without agrin stimulation at 37°C and 5%CO_2 atmosphere for specific time intervals.

5.10.17 Magnetic Activated Cell Sorting Cell Enrichment

To enrich cells expressing desired surface proteins Magnetic Activated Cell Sorting (MACS) was used. For a single sort two 10cm dishes of a cell line with 80-90% confluence were washed and trypsinized using 1ml prewarmed TE each. All cells were collected into one 15ml tube with total 5ml PBS. After centrifugation with

1500rpm for 5min the supernatant was discarded and the cell pellet was resuspended in 0.5ml staining solution. The staining solution contained biotin-anti-HA antibodies (1:250) or biotin-alpha-BGT (1:500) or biotin-anti-FLAG antibodies (1:250) in MACS Buffer. After incubation on ice for 15min with regular gentle shaking, 10ml icecold MACS Buffer were added and resuspended. The suspension was centrifuged with 1500rpm at 4°C for 5min and the supernatant was discarded and this washing step was repeated once. Then the cell pellet was resuspended in 250µl MACS Beads and was incubated on ice for 15min with regular gentle shaking. Then 3ml MACS Buffer were added, resuspended and the cell solution transferred into a sterile, round bottom, polystyrene tube. Immediately, the tube was put onto the MACS magnet for 5min. Magnetic bead bound cells were pulled on the tube wall towards the magnet and the supernatant was transferred into another tube, which was again put onto the magnet. This was repeated for in total 3 magnetic incubations. Quickly, the bead bound cells from the three tubes were transferred into a new tube with GM and plated on a culture dish for further cultivation. During cell proliferation the beads were detached from the cell surface.

5.11 Immunocytochemistry Methods

5.11.1 Surface Protein and Total Protein Staining

This method was used for transiently transfected COS-7 and NIH3T3 cells, as well as for stably transduced NIH3T3 cells. Surface protein staining specifically labeled proteins, whose binding sequence for the used binding molecule (antibody or bungarotoxin) was exposed to the outside of the plasma membrane of a cell. In contrast, total protein staining specifically labeled all proteins present at a cell, which showed a binding sequence for the used binding molecule (antibody or bungarotoxin).

On glass coverslips transfected or stable cells were starved in DMEM at 37°C and 5%CO_2 atmosphere for 0.5-2h. Then 12well plates containing the coverslips were out on ice and cells were washed once with icecold PBS for 5min, followed by fixation with 4%PFA (~500µl/well) at RT for 10min. Cells were washed with PBS three times and were permeabilized with 0.1%Triton-X-100/PBS at RT for 5min for total staining. For surface staining this step was skipped. Again cells were washed with PBS three times and blocked in 5%FBS/PBS while gently shaking at RT for 30min. A darkened, humidified chamber with a Parafilm covered bottom was prepared and 50µl of primary staining solution were pipetted as drop on the Parafilm. The coverslips were transferred upside down onto the drop with a forceps and incubated at RT for 1h. Then the coverslips were transferred back into the 12well plate and were washed with PBS for three times. Then 200-300µl secondary staining solution were put into an aspirated well and was incubated darkened, gently shaking at RT for 1h. Cells

were washed with PBS three times prior to embedding the coverslip in Mowiol on a microscopy slide. The slides were incubated at RT for 2-4h and stored at -4°C.

As staining buffer 5%FBS/PBS was used and supplied by primary and secondary binding molecules to obtain the staining solution. Aquired images were processed in Photoshop 7.2 and ImageJ.

5.11.2   Surface Protein Endocytosis Assay

This method was used to label surface proteins that were endocytosed into intracellular compartments after distinct times of endocytosis in stably transduced and transiently transfected NIH3T3 cells, as well as in stably transduced NIH3T3 cells. Several staining conditions were analyzed to optimize the best procedure, including different staining temperatures, different staining buffers and staining on PLL coated coverslips or gelatin coated 3.5cm dishes. Each condition was carried out with and without removing binding molecules that remained on the surface after endocytosis by stripping with PBS pH2.6.

Cells, prepared on PLL coated glass coverslips (in 12well plate) and on gelatin coated 3.5cm dishes, were starved in DMEM at 37°C and 5%CO_2 atmosphere for 0.5h. Coverslips were transferred into 12well plates and the growth area on 3.5cm dishes was divided into 2 or 4 staining areas with a grease pencil and put on ice. Cells were washed with icecold PBS once. Coverslips were put upside up into a humidified chamber with a Parafilm covered bottom and 50µl of primary staining solution (in different staining buffers) were applied on top of the coverslip. For the 3.5cm dishes, 20µl primary staining solution (in different staining buffers) were applied on top of the staining areas. Cells were incubated at different temperatures (4°C, 18°C or RT) for 45min. Afterwards coverslips were put back into the 12well plate and all cells were washed with icecold PBS three times and prewarmed DMEM was applied onto the cells. Endocytosis was allowed to occur by putting dishes and plates into a 37°C waterbath for different time intervals (0, 2, 5, 10, 15, 30, 60min). Subsequently, cells were washed with icecold PBS once. For stripping conditions cells were incubated two times with icecold PBS pH2.6 on ice for 2min each with icecold PBS washing steps in between and after stripping. Afterwards cells were fixed with 4%PFA at RT for 10min and cells were permeabilized with 0.1%Triton-X-100/PBS at RT for 5min after washing with PBS once. Cells were then incubated with secondary staining solution at RT for 45min, followed by PBS washing for three times. Some assays needed incubation with a third staining solution at RT for 45min, followed by PBS washing for three times. Afterwards, coverslips were embedded with Mowiol on microscopy slides and a coverslip was applied with Mowiol on 3.5cm dishes. The slides and dishes were incubated at RT for 2-4h and stored at -4°C.

As staining buffers 5%FBS/PBS, 5%FBS/FACS-SB or 5%FBS/L15 was used and supplied by primary and secondary binding molecules to obtain the staining solutions. Aquired images were processed in Photoshop 7.2 and ImageJ.

5.11.3   Acetylcholine Receptor Cluster Assay

This method was used to stain acetylcholine receptor clusters on differentiated and agrin-stimulated myotubes.

Cells, prepared on gelatin coated 3.5cm dishes, were washed with PBS once and fixed with 4%PFA at RT for 10min. After washing with PBS for three times cells were incubated in PBS supplied by alpha-BGT-594 darkened at RT for 1h. Cells were washed with PBS for three times and embedded with a coverslip in Mowiol. The dishes were incubated at RT for 2-4h and stored at -4°C. Aquired images were processed in Photoshop 7.2 and ImageJ.

5.12 Live Cell Imaging Methods

As live cell imaging was not established in the laboratory until this master thesis, the methods used were very basic approaches to start with live cell imaging. The first images were obtained with the help of G. Vendra and B. Woller. All equipments from microscope to culture dish had to be adapted and improved during all imaging events. Imaging was realized by using an Axiovert-200 epifluorescence microscope for live cell imaging from Zeiss, together with supporting equipment. Images were acquired with a 100x objective for a given number of images during a given time interval with two colors at each time point. Aquired images were processed in Photoshop 7.2 and ImageJ.

5.12.1   Live Tracking of Visualizable Proteins

This method was used to track movements of proteins in transiently transfected COS-7 and stably transduced NIH3T3 cells.

Cells were plated on 3.5cm ibiTreat μ-Dishes for Turbofect transfection with plasmids containing information for fluorophore tagged proteins and/or for live cell staining with binding molecules. If fluorophore tagged proteins were visualized without any staining of further proteins, cells were washed and put into prewarmed HBSS or L15 one day after transfection. If staining of further proteins was desired, cells were washed with icecold PBS once and incubated in primary staining solution at 4°C for 45min-1h. After washing with icecold PBS for three times, secondary staining solution was applied and incubated at 4°C for 45min-1h. Cells were washed with icecold PBS three times and prewarmed HBSS or L15 was applied onto the cells. Live cell imaging was then performed in a 37°C imaging chamber with or without 5%CO_2 atmosphere immediatley.

As staining buffer 5%FBS/PBS, 5%FBS/FACS-SB or 5%FBS/L15 was used and supplied by primary and secondary binding molecules to obtain the staining solutions.

5.12.2   Live Endocytosis of Visualizable Proteins

This method was used to track endocytosis of proteins in stably transduced NIH3T3 and stably transduced MuSK deficient muscle cells.

Differentiated myotubes and NIH3T3 cells on 3.5cm ibiTreat µ-Dishes were used for live cell staining with binding molecules. Cells were either stimulated with agrin overnight prior to live cell imaging, stimulated with agrin right before staining and imaging or not at all. For staining, cells were washed with icecold PBS once and incubated in primary staining solution at 4°C for 45min-1h. After washing with icecold PBS for three times, secondary staining solution was applied and incubated at 4°C for 45min-1h if required. Cells were washed with icecold PBS three times and prewarmed L15 was applied onto the cells. Live cell imaging was then performed in a 37°C imaging chamber without 5%CO_2 atmosphere immediatley.

As staining buffer 5%FBS/PBS, 5%FBS/FACS-SB or 5%FBS/L15 was used and supplied by primary and secondary binding molecules to obtain the staining solutions.

5.13 Biochemical Methods

For biochemical analysis transiently transfected COS-7 and stably transduced NIH3T3 cells, as well as fully differentiated myotubes were used. Cells were either lysed directly or after stimulation with agrin and/or bungarotoxin and/or antibody.

5.13.1   Cell Lysis

Cells were put on ice and washed with icecold PBS once. For 3.5cm dishes 100µl, for 6cm dishes 500µl and for 10cm dishes 1ml lysis buffer with inhibitors were added on ice. The dishes were incubated on a shaker at 4°C for 20min. Cells were scraped off and cell suspension was transferred into a cold 1.5ml tube. The suspension was centrifuged at full speed and 4°C for 10min. The supernatant (lysate) was then directly used for immunoprecipitation and pull down experiments, or was frozen in liquid nitrogen and stored at -80°C until used. Always, an aliquot of the supernatant (usually 10% of the total volume) was frozen as total lysate together with 4xSDS-LD at -20°C.

5.13.2   Immunoprecipitation and Pull Down

Cell lysates were kept on ice and supplied by antibodies (immunoprecipitation) or bungarotoxins (pull down). The reactions were incubated rotating in 1.5ml tubes at 4°C overnight. Then protein A (15µl; if antibody source was rabbit), protein G (20µl; if antibody source was mouse), streptavidine (20µl; if antibody/bungarotoxin was biotinylated) agarose beads or protein A sepharose beads (15µl; if antibody source

was rabbit) were added and incubated rotating in 1.5ml tubes at 4°C for 2h. Then tubes were centrifuged with full speed at 4°C for 1min and the supernatant except ~100µl was discarded. The pellet was washed with ~800µl icecold lysis buffer three times, by always incubating the pellet while rotating at 4°C for 5min followed by centrifugation with full speed at 4°C for 1min. After aspirating the supernatant to the 100µl mark, additional ~60µl of supernatant were taken off with a pipette, while being careful not to disturb the pellet. Then the pellet was resuspended with 4xSDS-LD and directly used for gel electrophoresis or frozen and stored at -20°C.

5.13.3 Denaturating Poly Acrylamid Gel Electrophoresis

Running and stacking gels were prepared, the slots were cleaned and gels were put into gel tray with 1xSDS-Running Buffer. Samples from immunoprecipitation, pull down and total lysates that were premixed with 4xSDS-LD were boiled at 95°C for 5min, followed by centrifugation at full speed for 4min. Denaturated samples were loaded onto the polyacrylamide gel together with 3µl or 6µl prestained protein ladder. Gels were run at 100V until single marker bands were visible in the running gel, then the voltage was increased up to 145V until all bands were separated as desired.

5.13.4 Western Blot Analysis

After SDS-PAGE, gels were put into 1x transfer buffer for immunoblotting and incubated shaking at RT for ~10min. A PVDF-membrane was activated in absolute methanol for a few seconds, rinsed with ddH$_2$O and incubated in 1x transfer buffer shaking RT for ~10min. Then the PVDF-membranes and the gels were assembled between two transfer buffer drained blotting papers in the blotting tray. The gels were blotted using the standard program for BioRad mini or midi gels for 30min. After transfer, the membranes were put into TBS-T shaking at RT for some minutes. For primary antibody incubation the membranes had to be blocked in 5%Milkpowder/TBS-T (for most antibodies) or in 5%BSA/TBS-T (for anti phosphotyrosine antibodies) shaking at RT for 2h or at 4°C overnight. Blocking solution was quickly washed out with TBS-T and primary antibody solution was incubated shaking at RT for 2h or at 4°C overnight on top of the membranes. The antibody solution was put back and stored at 4°C for reuse. Membranes were washed three times with TBS-T shaking at RT for 5min. Secondary antibody solution was added and incubated shaking at RT for 2h or at 4°C overnight. Membranes were again washed three times with TBS-T shaking at RT for 5min. Then membranes were incubated with HRP-substrate at RT for up to 5min and the signal was visualized by a Fluorimager. Afterwards, membranes were stripped in 10% acetic acid while shaking at RT for 2h, followed by washing with TBS-T. Now membranes were ready to reprope, starting with blocking solution.

Primary antibodies were diluted in 5%BSA/TBS-T supplied by 0.1% NaN$_3$ and reused for several times.

Secondary antibodies were diluted in 5%BSA/TBS-T and were immediately used once.

Quantification of IBs was done with ImageLab (BioRad).

5.14 Flow Cytometry Methods

5.14.1 Fluorescence Activated Cell Sorting for Counting Cell Populations

This method was used to analyze expression levels of proteins present at the plasma membrane of cells, with the binding sequence for the used binding molecule (antibody or bungarotoxin) exposed to cell surface.

COS-7 cells were prepared on 24well or 12well plates and transiently transfected with the desired DNA. Stably transduced NIH3T3 cells were prepared on gelatin coated 12well plates (1*10^5 cells/well). On the day after transfection or cell seeding plates were put on ice and cells were washed with icecold PBS three times. Primary staining solution (200-300µl/one 12well and 150µ/one 24well) was added and incubated shaking darkened at 4°C for 1h. Cells were washed with icecold PBS three times and incubated in secondary staining solution (200-300µl/one 12well and 250µ/one 24well) shaking darkened at 4°C for 1h. Cells were washed again with icecold PBS three times and incubated with clear icecold TE (50µl/one 12well and 40µ/one 24well) shaking darkened at 4°C for 20min. Trypsinized cells were resuspended in 3%FBS/PBS (150µl/one 12well and 120µ/one 24well) and transferred into cold FACS tubes. Cells were kept on ice and counted at the FACSCalibur Cell Analyzer.

FACS-SB was used as staining buffer with 3%BSA for primary and 5%BSA for secondary staining solution and was supplied by primary and secondary binding molecules.

FACS measurements were done at the Division and Institute of Immunology of the Medical University of Vienna under the help of Univ.-Prof. Mag. Dr. Wilfried Ellmeier and Lisa Göschl.

5.14.2 Fluorescence Activated Cell Sorting for Selection of Cell Populations

This method was used to select cell populations for their expression levels of proteins present at the plasma membrane of cells, with the binding sequence for the used binding molecule (antibody or bungarotoxin) exposed to cell surface. Selected cells were sorted and further cultivated.

Stably transduced NIH3T3 cells were prepared on gelatin coated 6cm and 10cm dishes for ~90% confluence at the day of sorting. Cells were starved in prewarmed DMEM at 37°C and 5%CO_2 atmosphere for 30min. Then cells were put on ice and washed with icecold sterile PBS once. Primary staining solution was added on top of the cells (3ml/one 10cm and 1ml/one 6cm) and incubated darkened and shaking at 4°C for 1h. Cells were washed with icecold sterile PBS two times and secondary staining solution (3ml/one 10cm and 1ml/one 6cm) was incubated on top of the cells darkened and shaking at 4°C for 1h. After washing with icecold sterile PBS for two times, 1ml clear icecold TE was added to the cells and was shaking darkened at 4°C for 20min. Cells were resuspended in 5ml icecold sterile PBS and pooled in 15ml tubes if required. After centrifugation with 1500rpm at 4°C for 5min the supernatant was discarded and the pellet was resuspended in 500µl icecold sterile PBS. To obtain a single cell solution, cells were filtered by a cell strainer two to three times prior to sorting. Sorted cells were collected in GM and cultivated at 37°C and 5%CO_2 atmosphere.

Sterile FACS-SB was used as staining buffer with 3%BSA for primary and 5%BSA for secondary staining solution and was supplied by primary and secondary binding molecules.

Cell sorting was done in cooperation with the Core Facility Flow Cytometry of the Medical University of Vienna under supervision of Ao. Univ. Prof. Dr. Andreas Spittler.

6 Abbreviations

°C	centigrade		V	volt
~	approximately		WB	Western Blot
cm	centimeter		x	times
E.Coli	Escherichia Coli		µg	microgram
e.g.	example given		µl	microliter
g	gram		µm	micrometer
h	hour			
HRP	horseradish peroxidase			
ICC	immunocytochemistry			
kb	kilobase			
M	Molar			
min	minute			
ml	milliliter			
mM	milli Molar			
mm	millimeter			
ng	nanogram			
OD_{600}	optical density at 600nm			
PCR	polymerase chain reaction			
pH	pH value			
rpm	rounds per minute			
RT	room temperature			
sec	seconds			
UV	ultraviolet light			

7 References

Alaynick, W.A., Jessell, T.M., Pfaff, S.L. (2011). SnapShot: Spinal Cord Development. Cell. 146, 178-178.

Alberts, B., Johnson, A., Lewis, J., Raff, M., Roberts, K., Walter, P. (2008). Molecular Biology of the Cell. Fifth Edition.

Anderson, M.J., Cohen, M.W. (1977). Nerve-induced and spontaneous redistribution of acetylcholine receptors on cultured muscle cells. J Physiol. 267, 757-773.

Babst, M., Katzmann, D.J., Snyder, W.B., Wendland, B., Emr, S.D. (2002). Endosome-associated complex, ESCRT-II, recruits transport machinery for protein sorting at the multivesicular body. Dev Cell. 3. 283-289.

Balice-Gordon, R.J., Breedlove, S.M., Bernstein, S., Lichtman, J.W. (1990). Neuromuscular junctions shrink and expand as muscle fiber size is manipulated: in vivo observations in the androgen-sensitive bulbocavernosus muscle of mice. J Neurosci. 10, 2660-2671.

Balice-Gordon, R.J., Lichtman, J.W. (1993). In vivo observations of pre- and postsynaptic changes during the transition from multiple to single innervation at developing neuromuscular junctions. J Neurosci. 13, 834-855.

Beattie, E.C., Howe, C.L., Wilde, A., Brodsky, F.M., Mobley. W.C. (2000). NGF signals through TrkA to increase clathrin at the plasma membrane and enhance clathrin-mediated membrane trafficking. J Neurosci. 20, 7325-7333.

Beeson, D., Webster, R., COSsins, J., Lashley, D., Spearman, H., Maxwell, S., Slater, C.R., Newsom-Davis, J., Palace, J., Vincent, A. (2008). Congenital myasthenic syndromes and the formation of the neuromuscular junction. Ann N Y Acad Sci. 1132, 99-103.

Bergamin, E., Hallock, P.T., Burden, S.J., Hubbard, S.R. (2010). The cytoplasmic adaptor protein Dok7 activates the receptor tyrosine kinase MuSK via dimerization. Mol Cell. 39, 100-109.

Bevan, S., Steinbach, J.H. (1977). The distribution of alpha-bungarotoxin binding sites of mammalian skeletal muscle developing in vivo. J Physiol. 267, 195-213.

Bezakova, G., Helm, J.P., Francolini, M., Lømo T. (2001). Effects of purified recombinant neural and muscle agrin on skeletal muscle fibers in vivo. J Cell Biol. 153, 1441-1452.

References

Bezakova, G., Ruegg, M.A. (2003). New insights into the roles of agrin. Nat Rev Mol Cell Biol. 4, 295-308.

Braithwaite, A.W., Harris, A.J. (1979). Neural influence on acetylcholine receptor clusters in embryoniy development of ekeletal muscles. Nature. 279, 549-551.

Bridges, T.M., LeBois, E.P., Hopkins, C.R., Wood, M.R., Jones, C.K., Conn, P.J., Lindsley, C.W. (2010).The antipsychotic potential of muscarinic allosteric modulation. Drug News Perspect. 23, 229-240.

Bucher, M.H., Evdokimov, A.G., Waugh, D.S. (2002). Differential effects of short affinity tags on the crystallization of Pyrococcus furiosus maltodextrin-binding protein. Acta Crystallogr D Biol Crystallogr. 58, 392-397.

Burden, S.J. (2000). Wnts as retrograde signals for axon and grwoth cone differentiation. Cell. 100, 495-497.

Burden, S.J. (2011). SnapShot: neuromuscular junction. Cell. 144, 826.

Burden, S.J., Yumoto, N., Zhang, W. (2013). The role of MuSK in synapse formation and neuromuscular disease. Cold Spring Harb Perspect Biol. 5.

Burgess, R.W., Nguyen, Q.T., Son, Y.J., Lichtman, J.W., Sanes, J.R. (1999). Alternatively spliced isoforms of nerve- and muscle-derived agrin: their roles at the neuromuscular junction. Neuron. 23, 33-44.

Caldwell, J.H. (2000). Clustering of sodium channels at the neuromuscular junction. Microsc Res Tech. 49, 84-89.

Clague, M.J. (1999). Membrane transport: Take your fusion partners. Curr Biol. 9, 258-260.

Conner, S.D., Schmid, S.L. (2003). Regulated portals of entry into the cell. Nature. 442, 37-44

Conti-Fine, B.M., Milani, M., Kaminski, H.J. (2006). Myasthenia gravis: past, present, and future. J Clin Invest. 116, 2843-2854.

Cornish, T., Chi, J., Johnson, S., Lu, Y., Campanelli, J.T. (1999). Globular domains of agrin are functional units that collaborate to induce acetylcholine receptor clustering. J Cell Sci. 112, 1213-1223.

DeChiara, T.M., Bowen, D.C., Valenzuela, D.M., Simmons, M.V., Poueymirou, W.T., Thomas, S., Kinetz, E., Compton, D.L., Rojas, E., Park, J.S., Smith, C., DiStefano, P.S. Glass, D.J., Burden, S.J., Yancopoulos, G.D. (1996). The Receptor Tyrosine Kinase MuSK Is Required for Neuromuscular Junction Formation In Vivo. Cell 85, 501-512.

Delcroix, J.D., Valletta, J.S., Wu, C., Hunt, S.J., Kowal, A.S., Mobley, W.C. (2003). NGF signaling in sensory neurons: evidence that early endosomes carry NGF retrograde signals. Neuron 39, 69-84.

Dietrich, M.F., van der Weyden, L., Prosser, H.M., Bradley, A., Herz, J., Adams, D.J. (2010). Ectodomains of the LDL Receptor-Related Proteins LRP1b and LRP4 Have Anchorage Independent Functions In Vivo. PLoS One. 5, e9960

Doyle, D.A. (2004). Structural changes during ion channel gating. Trends Neurosci. 27, 298-302.

Duclert, A., Changeux, J. P. (1995). Acetylcholine receptor gene expression at the developing neuromuscular junction. Physiol Rev. 75, 339-368.

Dürnberger, G., Camurdanoglu, B.Z., Tomschik, M., Schutzbier, M., Roitinger, E., Hudecz, O., Mechtler, K., Herbst, R. (2014). Global analysis of muscle-specific kinase signaling by quantitative phosphoproteomics. Mol Cell Proteomics. 13, 1993-2003.

Einhauer, A., Jungbauer, A. (2001). The FLAG peptide, a versatile fusion tag for the purification of recombinant proteins. J Biochem Biophys Methods. 49, 455-465.

Engel, A.G., Sine, S.M. (2005). Current understanding of congenital myasthenic syndromes. Curr Opin Pharmacol. 5, 308-321.

Fambrough, D.M. (1979). Control of acetylcholine receptors in skeletal muscle. Physiol Rev. 59, 165-227.

Fambrough, D.M., Drachman, D.B, Satyamurti, S. (1973). Neuromuscular junction in myasthenia gravis: decreased acetylcholine receptors. Science. 182, 293-295.

Ferns, M.J., Campanelli, J.T., Hoch, W., Scheller, R.H., Hall, Z. (1993). The ability of agrin to cluster AChRs depends on alternative splicing and on cell surface proteoglycans. Neuron. 11, 491-502.

Ferraro, E., Molinari, F., Berghella, L. (2012). Molecular control of neuromuscular junction development. J Cachexia Sarcopenia Muscle. 3, 13-23.

Flucher, B.E., Daniels, M.P. (1989). Distribution of Na+ channels and ankyrin in neuromuscular junctions is complementary to that of acetylcholine receptors and the 43 kd protein.Cell. 3, 163-175.

Frank, E., Fischbach, G.D. (1979). Early events in neuromuscular junction formation in vitro: induction of acetycholine receptor clusters in the postsynaptic membarne and morphology of newly formed synapses. J Cell Biol. 83,143-158.

Freeman, W.H. and Company. (2008). Molecular Cell Biology. Sixth Edition.

Gautam, M., Noakes, P.G., MosCOSo, L., Rupp, F., Scheller, R.H., Merlie, J.P., Sanes, J.R. (1996). Defective neuromuscular synaptogenesis in agrin-deficient mutant mice. Cell. 85, 525-535.

Gesemann, M., Cavall, V., Denzer, A.J., Branaccio, A., Schumacher, B., Ruegg, M.A. (1996). Alternative splicing of agrin alters its binding to heparin, dystroglycan, and the putative agrin receptor. Neuron. 16, 755-767.

Gesemann, M., Denzer, A.J., Ruegg, M.A. (1995). Acetylcholine receptor-aggregating activity of agrin isoforms and mapping of the active site. J Cell Biol. 128, 625-636.

Ghazanfari, N., Fernandez, K.J., Murata, Y., Morsch, M., Ngo, S.T., Reddel, S.W., Noakes, P.G., Phillips, W.D. (2010). Muscle specific kinase: organiser of synaptic membrane domains. Int J Biochem Cell Biol. 43, 295-298.

Goh, L.K., Sorkin, A. (2013). Endocytosis of receptor tyrosine kinases. Cold Spring Harb Perspect Biol. 5.

Gomez, G.A., Daniotti, J.L. (2005). H-Ras dynamically interacts with recycling endosomes in CHO-K1 cells: involvement of Rab5 and Rab11 in the trafficking of H-Ras to this pericentriolar endocytic compartment. J Biol Chem. 280, 34997-35010.

References

Gorden, P., Carpentier, J. L., Cohen, S., Orci, L. (1978). Epidermal growth factor: morphological demonstration of binding, internalization, and lysosomal association in human fibroblasts. Proc Natl Acad Sci U S A. 75, 5025-5029.

Gordon, L.R., Gribble, K.D., Syrett, C.M., Granato M. (2012). Initiation of synapse formation by Wnt-induced MuSK endocytosis. Development. 139, 1023-1033.

Grant, B.D., Donaldson, J.G. (2009). Pathways and mechanisms of endocytic recycling. Nat Rev Mol Cell Biol. 10, 597-608.

Gulzman, Y. (1981). SV40-transformed simian cells support the replication of early SV40 mutants. Cell. 23, 175-182.

Gutmann, E., Hanzlíková, V. (1973). Basic mechanisms of aging in the neuromuscular system. Mech Ageing Dev. 1, 327-349.

Hamuro, J., Higuchi, O., Okada, K., Ueno, M., Iemura, S., Natsume, T., Spearman, H., Beeson, D., Yamanashi. Y. (2008). Mutations causing DOK7 congenital myasthenia ablate functional motifs in Dok-7. J Biol. Chem. 283, 5518-5524.

Harel, M., Kasher, R., Nicolas, A., Guss, J.M., Balass. M., Fridkin. M., Smit, A.B., Brejc, K., Sixma, T.K., Katchalski-Katzir, E., Sussman, J.L., Fuchs, S. (2001). The binding site of acetylcholine receptor as visualized in the X-Ray structure of a complex between alpha-bungarotoxin and a mimotope peptide. Neuron. 32, 265-275.

Harrisons Innere Medizin Online, 18. Auflage, Abbildung 386-1, Copyright: ABW Wissenschaftsverlag GmbH

Hartline, D. K., Maynard, D. M. (1975). Motor patterns in the stomatogastric ganglion of the lobster, Panulirus argus. J. Exp. Biol. 62, 405-420.

Henne, W.M, Buchkovich, N. J., Emr, S.D. (2011). The ESCRT pathway. Dev Cell. 21, 77-91.

Herbst, R., Burden, S.J. (2000). The juxtamembrane region of MuSK has a critical role in agrin-mediated signaling. EMBO J. 19,67-77.

Herz, J. (2001). The LDL Receptor Gene Family: Review (Un)Expected Signal Transducers in the Brain. Neuron. 29, 571-581.

Higuchi, O., Hamuro, J., Motomura, M., Yamanashi, Y. (2011). Autoantibodies to low-density lipoprotein receptor-related protein 4 in myasthenia gravis. Ann Neurol. 69, 418-422.

Hirota, S.A. (2001). A quick guide to muscarinic acetylcholine receptors. Bio Pharm. J. 5, 6–8.

Hisata, S., Sakisaka, T., Baba, T., Yamada, T., Aoki, K., Matsuda, M., Takai, Y. (2007). Rap1-PDZ-GEF1 interacts with a neurotrophin receptor at late endosomes, leading to sustained activation of Rap1 and ERK and neurite outgrowth. J Cell Biol. 178, 843-860.

Hoch, W., Campanelli, J.T., Harrison, S., Scheller, R.H. (1994). Structural domains of agrin required for clustering of nicotinic acetylcholine receptors. EMBO J. 13, 2814-2821.

Hoch, W., McConville, J., Helms, S., Newsom-Davis, J., Melms, A., Vincent, A. (2001). Auto-antibodies to the receptor tyrosine kinase MuSK in patients with myasthenia gravis without acetylcholine receptor antibodies. Nat Med. 7, 365-368.

Hopf, C., Hoch, W. (1998). Dimerization of the muscle specific kinase induces tyrosine phosphorylation of acetylcholine receptors and their aggregation on the surface of myotubes. J Biol Chem 273, 64676473

Hopp, T.P, Gallis, B., Prickett, K.S. (1988). A short polypeptide marker sequence useful for recombinant protein identification and purification. Bior Technology. 6, 1204-1210.

http://antranik.org/synaptic-transmission-by-somatic-motorneurons/ 2014-10-09 11:42am

Hubbard, S.R. (2004). Juxtamembrane autoinhibition in receptor tyrosine kinases. Nat Rev Mol Cell Biol. 5, 464-471.

Inoue, A., Setoguchi, K., Matsubara, Y., Okada, K., Sato, N., Iwakura, Y., Higuchi, O., Yamanashi, Y. (2009). Dok-7 activates the muscle receptor kinase MuSK and shapes synapse formation. Sci Signal. 2.

Kim, J.H., Kwak, H.B., Leeuwenburgh, C., Lawler, J.M. (2008a). Lifelong exercise and mild (8%) caloric restriction attenuate age-induced alterations in plantaris muscle morphology, oxidative stress and IGF-1 in the Fischer-344 rat. Exp Gerontol. 43, 317-349.

Kim, N., Stiegler, A.L., Cameron, T.O., Hallock, P.T., Gomez, A.M., Huang, J.H., Hubbard, S.R., Dustin, M.L., Burden, S.J. (2008b). Lrp4 is a receptor for Agrin and forms a complex with MuSK. Cell. 135, 334-342.

Kinsella, T.M., Nolan, G.P. (1996). Episomal vectors rapidly and stably produce high-titer recombinant retrovirus. Hum Gene Ther. 7, 1405-1413

Koo, S.J., Pfaff, S. L. (2002). Fine-Tuning Motor Neuron Properties: Minireview Signaling from the Periphery, Neuron. 35, 823-826.

Kummer, T.T., Misgeld, T., Sanes, J.R. (2006). Assembly of the postsynaptic membrane at the neuromuscular junction: paradigm lost. Curr Opin Neurobiology. 16, 74-82.

Le Roy, C., Wrana, J.L. (2005). Clathrin- and non-clathrin-mediated endocytic regulation of cell signalling. Nat Rev Mol Cell Biol. 6, 112-126.

Lemmon, M.A., Schlessinger, J. (2010).Cell signaling by receptor tyrosine kinases. Cell. 141, 1117-1134 .

Lin, W., Burgess, R.W., Dominguez, B., Pfaff, S.L., Sanes, J.R., Lee, K.F. (2001). Dinstinct roles of nerve and muscle in postsynaptic differentiation of the neuromuscular synapse. Nature. 410, 1057-1064.

Lu, Z., Je, H.S., Young, P., Gross, J., Lu, B., Feng, G. (2007). Regulation of synaptic growth and maturation by a synapse-associated E3 ubiquitin ligase at the neuromuscular junction. J Cell Biol. 177, 1077-1089.

Luiskandl, S., Woller, B., Schlauf, M., Schmid, J.A., Herbst, R. (2013) Endosomal trafficking of the receptor tyrosine kinase MuSK proceeds via clathrin-dependent pathways, Arf6 and actin. FEBS J. 280, 3281-3297

Luo, Z., Wang, Q., Zhou, J., Wang, J., Liu, M., He, X., Wynshaw-Boris, A., Xiong, W., Lu, B. and Mei, L. (2002). Regulation of AChR Clustering by Dishevelled Interacting with MuSK and PAK1. Neuron. 35, 489-505.

References

Marder, E., Calabrese, R.M. (1996). Principles of rhythmic motor pattern generation. Physiol. Rev. 76, 687-717.

Marques, M.J., Conchello, J.A., Lichtman, J.W. (2000). From plaque to pretzel: fold formation and acetylcholine receptor loss at the developing neuromuscular junction. J Neurosci. 20, 3663-3675.

Maxfield, F.R., McGraw, T.E. (2004). Endocytic recycling. Nature Reviews Molecular Biology. 5, 121-132.

Mayor, S., Pagano, R.E. (2007). Pathways of clathrin-independent endocytosis. Nature Rev Mol Cell Biol. 8, 603-612.

Mazhar, S. Herbst, R. (2012). The formation of complex acetylcholine receptor clusters requires MuSK kinase activity and structural information from the MuSK extracellular domain. Mol Cell Neurosci. 49, 475-786.

McCann, C.M., Bareyre, F.M., Lichtman, J.W., Sanes, J.R. (2005). Peptide tags for labeling membrane proteins in live cells with multiple fluorophores. Biotechniques. 38, 945-952.

McMahan, U.J. (1990). The agrin hypothesis. Cold Spting Harb Symp Quant Biol. 55, 407-418.

Millar, N.S. (2009). A review of experimental techniques used for the heterologous expression of nicotinic acetylcholine receptors. Biochem Pharmacol. 78, 766-776.

Mills, I.G., Jones, A.T., Clague, M.J. (1999). Regulation of endosome fusion. Mol Membr Biol. 16, 73-79.

Miyazawa, A., Fujiyoshi, Y., Unwin, N. (2003). Structure and gating mechanism of the acetylcholine receptor pore. Nature. 423, 949-955.

Nissen, C., Nofzinger, E.A., Feige, B., Waldheim, B., Radoisa, M.P., Riemann, D., Berger, M. (2006). Neuropsychopharmacology. 31, 1294-1300.

Nitkin, R.M., Smith, M.A., Magill, C., Fallon, J.R., Yao, Y.M., Wallace, B.G., McMahan, U.J. (1987). Identification of agrin, a synaptic organizing protein from Torpedo electric organ. J Cell Biol. 105, 2471-2478.

Nykjaer, A., Willnow, T.E. (2002). The low-density lipoprotein receptor gene family: a cellular Swiss army knife? Trends Cell. Biol. 12, 273-280.

Okada, K., Inoue, A., Okada, M., Murata, Y., Kakuta, S., Jigami, T., Kubo, S., Shiraishi, H., Eguchi, K., Motomura, M., Akiyama, T., Iwakura, Y., Higuchi, O., Yamanashi, Y. (2006). The muscle protein Dok-7 is essential for neuromuscular synaptogenesis. Science. 312, 1802-1805.

Oksvold, M.P., Skarpen, E., Wierød, L., Paulsen, R.E., Huitfeldt, H.S. (2001). Re-localization of activated EGF receptor and its signal transducers to multivesicular compartments downstream of early endosomes in response to EGF. Euro J Cell Biol. 80, 285-294.

Ontell, M., Kozeka, K. (1984). Organogenesis of the mouse etensor digitorum logus muscle: a quantitative study. Am J Anat. 171, 149-161

Opalach, K., Rangaraju, S., Madorsky, I., Leeuwenburgh, C., Notterpek, L. (2010). Lifelong calorie restriction alleviates age-related oxidative damage in peripheral nerves. Rejuvenation Res. 13, 65-74.

Polo, S., Di Fiore, P.P. (2006). Endocytosis conducts the cell signaling orchestra. Cell, 124, 897-900.

Raiborg, C., Bache, K.G., Gillooly D.J., Madshus, I.H., Stang, E., Stenmark, H. (2002). Hrs sorts ubiquitinated proteins into clathrin-coated microdomains of early endosomes. Nat Cell Biol. 4, 394-398.

Resat, H., Ewald, J.A., Dixon, D.A., Wiley, H.S. (2003). An integrated model of epidermal growth factor receptor trafficking and signal transduction. Biophys J. 85, 730-743.

Robertson, N.P., Deans, J., Compston, D.A.S. (1998). Myasthenia gravis: a population based epidemiological study in Cambridgeshire, England. 65, 492-496.

Ruegg, M,.A., Bixby, J. L. (1998). Agrin orchestrates synaptic differentiation at the vertebrate neuromuscular junction. Trends Neurosci. 22-27.

Sadowski, L., Pilecka, I. , Miaczynska, M. (2009). Signaling from endosomes: location makes a difference. Exp Cell Res. 315, 1601-1609.

Sanes, J. R. , Lichtman, J. W. (2001). Induction, assembly, maturation and maintenance of a postsynaptic apparatus. Nat. Rev. Neurosci. 11, 791-805

Sanes, J. R., Lichtman, J. W. (1999). Development of the vertebrate neuromuscular junction. Annu. Rev. Neurosci. 22, 389–442.

Sato, M., Sato, K., Liou, W., Pant, S., Harada, A., Grant, B.D. (2008). Regulation of endocytic recycling by C. elegans Rab35 and its regulator RME-4, a coated-pit protein. EMBO J. 27, 1183-1196.

Schlauf, M. (2011). The Role of Posttranslational Modifications in the Endocytosis of Muscle-Specific Kinase. Diplomarbeit, University of Vienna

Sekine-Aizawa, Y., Huganir, R.L. (2004). Imaging of receptor trafficking by using alpha-bungarotoxin-binding-site-tagged receptors. Proc Natl Acad Sci U S A. 101, 17114-17119.

Selverston, A.I., Russel, D.F., Miller, J.P. (1976). The stomatogastric nervous system: Structure and function of a small neural network. Progress in Neurobiology. 7, 215-290.

Sharma, M. (2012). Internship Herbstlab, unpublished

Sharma, M., Höbartner, A. (2012). Internship Herbstlab, unpublished

Shi, L,. Fu, A.K., Ip, N.Y. (2012). Molecular mechanisms underlying maturation and maintenance of the vertebrate neuromuscular junction. Trends Neurosci. 35, 441-453.

Shi, L., Fu, A.K., Ip, N.Y. (2012). Molecular mechanisms underlying maturation and maintenance of the vertebrate neuromuscular junction. Trends Neurosci. 35, 441-453.

Slater, C.R. (1982). Postnatal maturation of nerve-muscle junctions in hindlimb muscles of the mouse. Dev Biol. 94, 11-22.

Sönnichsen, B., De Renzis, S., Nielsen, E., Rietdorf, J., Zerial, M. (2000). Distinct membrane domains on endosomes in the recycling pathway visualized by multicolor imaging of Rab4, Rab5, and Rab11. J Cell Biol. 149, 901-914.

Sorkin, A., Kornilova, E., Teslenko, L., Sorokin, A., Nikolsky, N. (1989). Recycling of epidermal growth factor-receptor complexes in A431 cells. Biochim Biophys Acta. 1011, 88-96.

References

Sorkin, A., von Zastrow, M. (2002). Signal transduction and endocytosis: close encounters of many kinds. Nat Rev Mol Cell Biol. 3, 600-614.

Sorkin, A., von Zastrow, M. (2009). Endocytosis and signalling: intertwining molecular networks. Nature Reviews Molecular Cell Biology. 10, 609-622.

Spaargaren, M., Defize, L.H., Boonstra, J., De Laat, S.W. (1991). Antibody-induced dimerization activates the epidermal growth factor receptor tyrosine kinase. The Journal of Biology Chemistry. 166, 1733-1739.

Steinbach, J.H. (1981). Developmental changes in acetylcholine receptor aggregates at rat skeletal neuromuscular junctions. Development Biology. 84, 267-276.

Stiegler, A.L., Burden, S.J., Hubbard, S.R. (2006). Crystal structure of the agrin-responsive immunoglobulin-like domains 1 and 2 of the receptor tyrosine kinase MuSK. J Mol Biol. 364, 424-433.

Sugiyama, J.E., Glass, D.J., Yancopouls, G.D., Hall, Z.W. (1997). Laminin-induced Acetylcholine Receptor Clustering: An Alternative Pathway. J Cell Biol. 139, 181-191.

Terpe, K. (2003). Overview of tag protein fusions: from molecular and biochemical fundamentals to commercial systems. Appl Microbiol Biotechnol. 60, 523-533.

Till, J.H., Becerra, M., Watty, A., Lu, Y., Ma, Y., Neubert, T.A., Burden, S.J., Hubbard, S.R. (2002). Crystal structure of the MuSK tyrosine kinase: insights into receptor autoregulation. Structure. 10, 1187-1196.

Todaro, G.J., Green, H. (1963). Quantitative studies of the growth of mouse embryo cells in culture and their development into established lines. J. Cell Biol. 17, 299-313.

Traub, L.M. (2009). Tickets to ride: selecting cargo for clathrin-regulated internalization. Nature Reviews Molecular Cell Biology 10, 583-596.

Tsen, G., Halfter, W., Kröger, S., Cole, G.J. (1995). Agrin is a heparan sulfate proteoglycan. J Biol Chem. 270, 3392-3399.

Unwin, N. (2005). Refined structure of the nicotinic acetylcholine receptor at 4A resolution. J Mol Biol. 346, 967-989.

Valenzuela, D.M., Stitt, T.N., DiStefano, P.S., Rojas, E., Mattsson, K., Compton, D.L., Nuñez, L,. Park, J.S., Stark, J.L., Gies, D.R. (1995). Receptor tyrosine kinase specific for the skeletal muscle lineage: expression in embryonic muscle, at the neuromuscular junction, and after injury. Neuron. 15, 573-584.

van der Sluijs, P., Hull, M., Webster, P., Mâle, P., Goud, B., Mellman, I. (1992). The small GTP-binding protein rab4 controls an early sorting event on the endocytic pathway. Cell. 70, 729-740.

Vandervoort, A. (2002). Aging of the human neuromuscular system. Muscle Nerve. 25, 17-25.

Villaroel, A., Sakmann, B. (1996). Calcium permeability increase of endplate channels in rat muscle during postnatal development.J Physiol. 496, 331-338.

Vincent, A. (2002). TIMELINE: Unravelling the pathogenesis of myasthenia gravis. Nature Reviews Immunology. 2, 797-804.

Vincent, A., Lang, B., Kleopa, K.A. (2006). Autoimmune channelopathies and related neurological disorders. Neuron, 52, 123-138.

Vincent, A., Newland, C., Croxen, R., Beeson, D. (1997). Genes at the junction--candidates for congenital myasthenic syndromes. Trends Neurosci. 20, 15-22.

von Zastrow, M., Sorkin, A. (2007). Signaling on the endocytic pathway. Curr Opin Cell Biol. 19, 436-445.

Watty, A., Neubauer, G., Dreger, M., Zimmer, M., Wilm, M., Burden, S.J. (2000) The in vitro and in vivo phosphotyrosine map of activated MuSK. Proc Natl Acad Sci USA. 97, 4585-4590

Weatherbee, S.D., Anderson, K.V., Niswander, L.A. (2006). LDL-receptor-related protein 4 is crucial for formation of the neuromuscular junction. Development. 133, 4993-5000.

Wiley, H.S. (1988). Anomalous binding of epidermal growth factor to A431 cells is due to the effect of high receptor densities and a saturable endocytic system. J Cell Biol. 107, 801-810.

Wilson, I.A., Niman, H.L., Houghten, R.A., Cherenson, A.R., Connolly, M.L., Lerner, R.A. (1984). The structure of an antigenic determinant in a protein. Cell. 37, 767-778.

Witzemann, V. (2006). Development of the neuromuscular junction. Cell Tissue Res. 326, 263-271.

Woodman, P.G. (2000). Biogenesis of the sorting endosome: the role of Rab5. Traffic. 1, 695-701.

Wu, H., Xiong, W.C., Mei, L. (2010). To build a synapse: signaling pathways in neuromuscular junction assembly. Development. 137, 1017-1033.

Yaffe, D., Saxel, O. (1977). "Serial passaging and differentiation of myogenic cells isolated from dystrophic mouse muscle. Nature. 270, 725-727.

Yang, X., Arber, S., William, C., Li, L., Tanabe, Y., Jessell, T.M., Birchmeier, C., Burden, S.J. (2001). Patterning of muscle acetylcholine receptor gene expression in the abscene of motor innervation. Neuron. 30, 399-410.

Yang, X., Li, W., Prescott, E.D., Burden, S.J., Wang, J.C. (2000): DANN topoisomerase II beta and neural development. Science. 287, 131-134.

Ying, H., Zheng, H., Scott, K., Wiedemeyer, R., Yan, H., Lim, C., Huang, J., Dhakal, S., Ivanova, E., Xiao, Y., Zhang, H., Hu, J., Stommel, J.M., Lee. M.A., Chen. A.J., Paik. J.H., Segatto. O., Brennan. C., Elferink. L.A., Wang. Y.A., Chin. L., DePinho. R.A. (2010). Mig-6 controls EGFR trafficking and suppresses gliomagenesis. Proc Natl Acad Sci U S A. 107, 6912-6917.

Young, S. H., Poo, M.M. (1983). Spontaneous release of transmitter from growth cones o embryonic neurons. Nature. 305, 634-637.

Yumoto, N., Kim, N., Burden, S.J. (2012). Lrp4 is a retrograde signal for presynaptic differentiation at neuromuscular synapses. Nature. 489, 438-442.

Zapf-Colby, A., Olefsky, J.M. (1998). Nerve growth factor processing and trafficking events following TrkA-mediated endocytosis. Endocrinology. 139, 3232-3240.

Zhang, B., Luo, S., Wang, Q., Suzuki, T., Xiong, W.C., Mei, L. (2008). LRP4 serves as a coreceptor of agrin. Neuron. 60, 285-297.

Zhang, W., Coldefy, A.S., Hubbard, S.R., Burden, S.J. (2011). Agrin binds to the N-terminal region of Lrp4 protein and stimulates association between Lrp4 and the first immunoglobulin-like domain in muscle-specific kinase (MuSK). J Biol Chem. 286, 40624-40630.

Zhu, D., Yang, Z., Luo, S., Xiong, W.C., Mei, L. (2008). Muscle-specific receptor tyrosine kinase endocytosis in acetylcholine receptor clustering in response to agrin. J Neurosci. 28, 1688-1696.

Ziskind-Conhaim, L., Bennett, J.I. (1982). The effects of electrical inactivity and denervation on the distribution of acetylcholine receptors in developing rat muscle. Dev. Biol. 90, 185-197.

Zong, Y., Jin, R. (2013). Structural mechanisms of the agrin-LRP4-MuSK signaling pathway in neuromuscular junction differentiation. Cell Mol Life Sci. 70, 3077-3088.

Zong, Y., Zhang, B., Gu, S., Lee, K., Zhou, J., Yao, G., Figueiredo, D., Perry, K., Mei, L., Jin, R. (2012). Structural basis of agrin-LRP4-MuSK signaling. Genes Dev. 23, 247-258.

Section for Synapse Formation, Center for Brain Research, Medical University of Vienna, Ass.-Prof. Priv.-Doz. Dr. Ruth Herbst

Division of Immunobiology, Institute of Immunology, Medical University of Vienna, Univ.-Prof. Mag. Dr. Wilfried Ellmeier

Core Facility Flow Cytometry, Medical University of Vienna, Ao. Univ. Prof. Dr. Andreas Spittler

8   Appendix

8.1 Acknowledgements

8.2 Abstract

The neuromuscular junction (NMJ) is the connection between an alpha motor neuron and a muscle fiber. This cholinergic synapse is formed during embryonic and early postnatal development and is characterized by the high postsynaptic enrichment of acetylcholine receptors (AChRs). Upon action potential arrival at the motor end plate, acetylcholine is released by the nerve and binds to AChRs at the muscle membrane, leading to subsequent contraction. NMJ derived diseases are summarized as myasthenic syndromes and symptoms range from muscle weakness to respiratory failure.

Formation and maintenance of this highly specialized structure are based on signaling events, primarily initiated by the receptor tyrosine kinase 'muscle-specific kinase' (MuSK). Upon nerve innervation, pre-patterned AChR clusters are strengthened via secretion of nerve-derived agrin. Agrin binds to the postsynaptic located 'low density lipoprotein receptor related protein 4' (Lrp4), which in turn induces autophosphorylation of the MuSK kinase domain and subsequent AChR clustering. Furthermore, MuSK activation is thought to act as signal for endocytosis. As recent studies revealed sustained signaling events of other receptor tyrosine kinases in endosomal compartments, investigation of MuSK internalization and trafficking is of particular interest.

At first, this master thesis was aimed on the development of a heterologous model system for agrin-Lrp4-MuSK signaling, because experimentation with differentiated muscle cells is complex. Affinity tagged MuSK and Lrp4 fusion proteins were generated via basic molecular biology cloning methods. Tags located in the extracellular portions of these proteins should allow specific protein detection in biochemical and immunocytochemistry analysis. Although protein tagging interfered

with detection and expression levels, the biological functionality of fusion proteins was confirmed since they are able to rescue AChR clustering. Subsequently, mouse fibroblasts were modified via retroviral infection to stably express tagged MuSK and Lrp4 proteins. Promising cell populations were enriched via magnetic activated and fluorescence activated cell sorting.

The second aim of this master thesis was to assess MuSK endocytosis in the newly developed model system. Endocytosis assays revealed a baseline MuSK internalization taking place within 5 minutes. MuSK was taken up into early endosomes and was predominantly trafficked to multivesicular bodies, while recycling only played a minor role. Lrp4 showed a similar baseline endocytosis but endocytosis was faster and recycling via Rab11 compartments was increased compared to MuSK.

Binding of antibody or ligand to the respective affinity tag in MuSK was discovered to interfere with AChR clustering in agrin-stimulated myotubes. Furthermore, agrin stimulation of model system cells failed to clearly increased MuSK phosphorylation. Corresponding endocytosis assays did not reveal a major influence on MuSK internalization and trafficking upon agrin stimulation. These major limitations necessitate questioning of the functionality of the newly developed model system and demand further optimization.

8.3 Zusammenfassung

Die Neuromuskuläre Junction (NMJ) stellt die Verbindung zwischen einem Alpha Motorneuron und einem Muskel dar. Diese cholinerge Synapse wird während der Embryonal- und frühen Postnatalentwicklung gebildet und ist durch die hohe Anreicherung von Acetylcholinrezeptoren (AChR) charakterisiert. Erreicht ein Aktionspotential die Motorendplatte, wird Acetylcholin vom Nerv ausgeschüttet und bindet an AChR an der Muskelmembran, wodurch eine Muskelkontraktion ausgelöst wird. Erkrankungen der NMJ werden als myasthenische Syndrome beschrieben und reichen von Muskelschwäche bis hin zur Atemlähmung.

Die Bildung und Aufrechterhaltung dieser hoch spezialisierten Struktur basiert auf Signalkaskaden, welche vorwiegend von der "muskel-spezifischen Kinase" (MuSK) initiiert werden. Während der Innervierung wird Agrin vom Nerv ausgeschüttet, wodurch vorgeformte AChR-Cluster gestärkt werden. Agrin bindet an "low density lipoprotein receptor related protein 4" (Lrp4) in der Muskelmembran, induziert dadurch die Autophosphorylierung der Kinase-Domäne von MuSK und somit die Aggregierung von AChR. Außerdem wird die Aktivierung von MuSK als Signal für Endozytose gewertet. Studien belegen, dass verwandte Rezeptor Tyrosin Kinasen auch nach Endozytose weiter aktiv sind. Daher sind Mechanismen, welche Internalisierung und Sortierung von MuSK kontrollieren von besonderem Interesse.

Das erste Ziel dieser Masterarbeit war die Entwicklung eines heterologen Modelsystems des Agrin-Lrp4-MuSK Signalweges, da Versuche an differenzierten

Muskelzellen durchaus komplex sind. MuSK und Lrp4 Proteine wurden unter der Verwendung von molekularbiologischen Methoden mit Tag-Sequenzen an deren extrazellulären Domänen fusioniert. Dadurch sollte eine spezifische Proteindetektion in biochemischen und immunzytochemischen Analysen ermöglicht werden. Obwohl dieses sogenannte „Tagging" die Expression und Detektion der Proteine negativ beeinflusste, konnte die biologische Funktionalität bestätigt werden, da diese Fusionsproteine AChR-Clustering in Muskelzellen induzierten. Darauffolgend wurden Maus-Fibroblastenzellen mit einer retroviralen Methode dahingehend modifiziert, dass sie MuSK und Lrp4 Fusionsproteine stabil exprimieren. Zellpopulationen mit hoher Proteinexpression wurden mit magnet-aktivierter und fluoreszenz-aktivierter Zellsortierung angereichert.

Das zweite Ziel dieser Masterarbeit bezog sich auf die Analyse von MuSK-Endozytose im neu entwickelten Modelsystem. Endoztyose-Experimente zeigten, dass MuSK in einer Grundaktivität innerhalb von 5 Minuten internalisiert wird. MuSK wurde in frühe Endosomen aufgenommen und vorwiegend in multivesikuläre Körper sortiert, während Recycling eine geringere Rolle spielte. Lrp4 wies eine ähnliche Grundaktivität auf, wobei aber die Endozytosegeschwindigkeit erhöht und das Recycling über den Rab11 positiven Weg im Vergleich zu MuSK verstärkt wurde.

In Kontrollexperimenten konnte ich feststellen, dass die Bindung von Antikörper beziehungsweise Ligand an deren Tag-Sequenzen in MuSK mit der AChR Aggregierung in Agrin-stimulierten Muskelzellen interferiert. Außerdem konnte im Modelsystem keine durch Agrin hervorgerufene und verstärkte Phosphorylierung von MuSK nachgewiesen werden. Diese schwerwiegenden Einschränkungen stellen die Funktionalität des neu entwickelten Modelsystems in Frage und machen zusätzliche Tests und Optimierung notwending.

8.4 Curriculum Vitae

Andreas Höbartner, BSc

Citizen:	Austria
Date of Birth:	July, 1989

Scientific career

09. 2013 – 01. 2015	Master Thesis at the Center of Brain Research Vienna, at the Section for Synapse Formation, Ass.-Prof. Priv.-Doz. Dr. Ruth Herbst
07. 2013	Lab Rotation at the European Neuroscience Institute Göttingen, at the group STED Microscopy of Synaptic Function, Prof. Dr. Silvio O. Rizzoli
03. 2012 –	Master Program Molecular Biology at the University of Vienna with specialization in Neurosciences
09. 2011	Internship at the Institute of Pathology at the Hospital Krems/Donau at the Department of Microbiology
10. 2008 – 03. 2012	Bachelor Program Biology at the University of Vienna with specialization in Molecular Biology, with a degree as Bachelor of Science
08. 1999 – 06. 2007	Secondary school BG/BRG Piaristengasse Krems/Donau, final examination with distinction

8.5 Declarations

Ich habe mich bemüht, alle nicht von mir stammenden, wissenschaftlichen Inhalte und Bildmaterialien ausreichend zu kennzeichnen und sie in den References zusammenzufassen. Sollte dennoch eine Verletzung geistigen Eigentums oder des Urheberrechts bekannt werden, ersuche ich um Meldung bei mir.